博士論文

Stability and Redox Reactivity of Gas-phase Cerium Oxide Clusters

（気相セリウム酸化物クラスターの安定性と酸化還元反応性）

永田　利明

Contents

Chapter 1

General Introduction

1.1. Heterogeneous catalyst

Catalysis is one of the most important concepts to realize the sustainable development, to which much attention has been paid. A heterogeneous catalyst is a form of catalyst, existing in a different phase from the catalyzed reactants. This is opposite to a homogeneous catalyst, where the catalyst coexists with the reactants in the same phase (Figure 1.1). Catalysts are essentially unchanged during the catalytic reactions, but realistically lost by degeneration, physical scattering, and so forth. Hence, it is of great importance to improve reusability of catalysts. Heterogeneous catalysts can be immobilized on a solid surface to facilitate recovery and reuse, which is a distinctive advantage from homogeneous catalysts. Because of such an advantage, many researchers are intensively studying to put functionalities of known homogeneous catalysts into heterogeneous systems by immobilization.[1-4] Heterogeneous catalysts, however, have also a disadvantage: The chance of interaction between a catalyst and a reactant molecule is limited compared to homogeneous catalysts, which lowers the total catalytic efficiency. It is required to achieve high efficiency and reusability simultaneously. A heterogeneous catalyst, especially in a solid state, works in a solid/liquid or solid/gas interface, which has been investigated as surface sciences.

1.2. Automotive three-way catalyst

One of the most important applications of a heterogeneous catalyst is for purification of harmful automotive exhaust gases. Automobiles are indispensable for the modern life, but also have problems: They emit pollutants into the atmosphere. Most of motorcars burn petroleum for power, where ideally carbon dioxide, nitrogen, and water are emitted. Indeed, undesired formation of by-products, such as carbon monoxide, nitrogen oxides, and small hydrocarbons, are inevitable, and they actually pollute the atmosphere. One strategy of reducing those harmful by-products is optimization of the burning conditions, e.g. the air-fuel

ratio, to prevent side reactions. The burning conditions are, however, determined not only by the amount of pollutant but also by performance and economy. For example, typical diesel engines operate under "lean-burn" conditions, where excess air is introduced for burning fuel compared to stoichiometry. The lean-burn conditions are adopted because of its high efficiency, but known to generate nitrogen oxides in a higher extent.[5] As stated, reducing pollutants at the source is limited as long as keeping performance is demanded. Accordingly, removing harmful by-products after generation is a realistic solution.

The main pollutants to be removed are CO, NO_x, and hydrocarbons. If they were thermodynamically stable, additional energy consumption would be needed for dealing them. Fortunately, each NO_x species has a positive enthalpy of formation, making the purification reactions to be exothermic, e.g.,[6]

$$CO + N_2O \rightarrow CO_2 + N_2 \qquad \Delta H^\circ = -3.78 \text{ eV} \qquad (1.1)$$

$$CO + NO \rightarrow CO_2 + 1/2\ N_2 \qquad \Delta H^\circ = -3.87 \text{ eV} \qquad (1.2)$$

$$CO + 1/2\ NO_2 \rightarrow CO_2 + 1/4\ N_2 \qquad \Delta H^\circ = -3.10 \text{ eV} \qquad (1.3)$$

$$CH_4 + 2\ NO_2 \rightarrow CO_2 + N_2 + 2\ H_2O \qquad \Delta H^\circ = -9.00 \text{ eV} \qquad (1.4)$$

which means that these species are just kinetically formed. Therefore, the purification reactions can work catalytically, without additional energy, in terms of the energetic balance. Catalysts which convert CO, NO_x, and hydrocarbons to CO_2, N_2, and H_2O are called a "three-way catalyst" (TWC). TWCs currently use precious metals, e.g. platinum, rhodium, and palladium, as an active center for redox reactions combined with oxygen storage materials, e.g. cerium-zirconium oxide.[5, 7-9] The amount of precious metals in the catalysts is desired to be reduced without deteriorating their functionalities.

The TWC is a heterogeneous redox catalyst, which is a general understanding in chemistry and industry. There are some requirements specific to automobiles. Generally, the condition in which a catalyst works in the best performance is limited. Nevertheless, automotive engines work in a cycle, and hence, the catalytic condition varies periodically. When the air-fuel ratio changes, a richer reactant occupies the catalyst's surface and rejects the other reactants, impeding further reactions. The TWCs are required to keep their efficiency even in the changing environment. Atmospheric pollution is not particular in automobiles but a common problem with power stations, chemical plants, etc. The information of the exhaust-gas purification system can be shared with such applications. Automobiles are, however, difficult to be managed strictly compared to these plants because

they are used by inexpert citizens at any time and place. For instance, vanadium is known to have high catalytic ability but is volatile at high temperature, thus a monitoring and controlling system is needed. Hence, this is undesired for motorcars. In addition, probability of improper disposal is higher for automobiles than for plants. Accordingly, the automotive TWCs are especially required to be made of highly safe and harmless materials.

1.3. Nanosized materials

The simplest strategy for improving ability of a heterogeneous catalyst is enlarging surface area of the catalyst by reducing the particle size because the catalytic reactions occur at the interface. The specific surface area increases with a decrease in the size. It is known that not only the extent of surface area but also its physical and chemical properties are changed in nanosized materials. The structure and energetics of the surface are generally different from the inner structure. The surface effect becomes ruling the particle's property when the ratio of atoms on the surface is much larger than that of a bulk phase. Let me estimate the atomic ratio of the surface roughly: Assuming a sphere particle with the radius of R which is made of atoms with the radii of r (see Figure 1.2), the whole volume (V_{tot}) and non-surface volume ($V_{\mathrm{tot}} - V_{\mathrm{sur}}$) of the particle are given approximately by

$$V_{\mathrm{tot}} = \frac{4}{3}\pi R^3 \tag{1.5}$$

$$V_{\mathrm{tot}} - V_{\mathrm{sur}} = \frac{4}{3}\pi (R-2r)^3 \tag{1.6}$$

Given that the atomic density of the surface layer is the same as that of the whole particle, the ratio of surface atoms can be calculated as

$$\frac{V_{\mathrm{sur}}}{V_{\mathrm{tot}}} = 6\left(\frac{r}{R}\right) - 12\left(\frac{r}{R}\right)^2 + 8\left(\frac{r}{R}\right)^3 \tag{1.7}$$

For example, a gold atom has a 144 pm metallic radius.[10] The surface-atomic ratio of a gold nanoparticle is estimated as shown in Figure 1.3. Especially below the diameter of 1 nm, over 90% of atoms are on the surface, which means no longer the inner atoms are dominant. That is why nanoparticles have a specific behavior.

Even in a ubiquitous material, novel functionalities have been found by the nanotechnology. Such nanosize effects have been intensively investigated on physical properties, e.g., an unusual phase of iron sesquioxide, ε-Fe_2O_3, has been found in

nanoparticles, showing an extremely high magnetic coercivity.[11] The specific properties are considered to originate from the crystal structure of nanoparticles, which can be different from that of the bulk. In the field of catalysis, one of the most important discoveries of nanosize specific properties is a high catalytic ability of nanosized gold. Although ordinary bulk-phase gold is almost inert, gold nanoparticles catalyze oxidation of CO at a temperature far below 0 °C.[12, 13] Consequently, to consider the catalytic ability of nanoparticles, the size-specific features as well as the large specific surface area are of importance.

1.4. Clusters

Decreasing the size of nanoparticles below the order of nanometers, they are considered to be a kind of clusters. Clusters are aggregates of atoms, the number of which is below several tens or hundreds. They are mainly measured by mass spectrometry. Because clusters are close to a molecule or an atom in size, they are adequate for investigations in an atomic or molecular level.

Clusters can be classified into some types based on their bonding: covalent, ionic, metallic, hydrogen, ion-induced dipole, or van der Waals bonding. The most famous cluster is probably C_{60}, known also as a unique name, buckminsterfullerene, reported in 1985.[14] C_{60} is a representative instance of carbon clusters called fullerenes. Carbon atoms in fullerenes are bound by covalent bonds. C_{60} was first found in the gas phase,[14] but later elucidated capable to exist as a solid phase.[15] Fullerenes are considered to be a category of allotropes of carbon distinct from conventional ones, i.e. graphite, diamond, and amorphous carbon.

Other types of cluster are built up with intermolecular forces, e.g. van der Waals bonding, ion-induced dipole force, and hydrogen bonding, which are weaker than covalent bond. For instance, rare gas clusters such as helium clusters are formed by van der Waals force. A bond in a helium cluster is extremely weak and long: In helium dimer (He_2), the binding energy is 9×10^{-8} eV, and the bond length is 52 Å.[16] Due to such a weak binding, helium clusters can exist only at a cryogenic temperature, and they have a flexibility in their structure, where helium atoms can move around easily. Such structurally flex clusters can be treated as a small liquid droplet. Indeed, larger helium clusters are also called helium nanodroplets and investigated in relation to cryogenic sciences. A cluster with mightier bond is water clusters, in which water molecules are bound with each other by hydrogen bonding. They can be treated as a model system of a hydrogen-bonding network of water. Basic

intermolecular interactions of water have been investigated, e.g. an energy transfer from one water molecule to the other have been reported in a water dimer.[17] Water clusters combined with another molecule is also investigated. Biomolecule–water clusters are used as a clue to the functionalities of biomolecules in cells.[18]

Clusters corresponding to an extension of nanoparticles are formed by stronger bond than intermolecular bonds, such as ionic bond and metallic bond. Alkali halide clusters, such as sodium fluoride (NaF) clusters, are made of alkali metal cations and halide anions like an ionic crystal. Properties, reactions, and structures of alkali halide clusters have been investigated in relation with the reaction mechanism and solvation process of bulk crystals.[19-26] Metal clusters have also been intensively investigated. For instance, the melting point of a sodium (Na) cluster varies with the cluster's size.[27, 28] Since small clusters containing just a few atoms no longer hold the properties of bulk, it is controversial whether such small metal cluster is metallic or not. In the aspect of the physical properties, they are not metallic because the small cluster lacks a continuous conducting band, which is the most important feature of metal. In contrast, the binding force of atoms in the metal clusters can be regarded as metallic bond or its analogue. Generally, they are called metal clusters just based on the fact that they are composed of metallic elements. Clusters of transition metals and their oxides have been studied in relation to catalysis. As mentioned above, clusters are used as models of various chemical systems. Gas-phase clusters are considered to be model systems of heterogeneous catalysts.[29] Elementary reactions on the catalyst surface are examined on the clusters, providing molecular-level information of catalytic reactions.

1.5. Cerium oxide

Cerium ($_{58}$Ce) is a rare earth element and the second element of lanthanides. Cerium has four valence electrons (4f 5d $6s^2$). Although general lanthanides prefer an oxidation state of +3, Ce takes a +4 state as well as +3. The most famous cerium oxide is CeO_2 (ceria), in which Ce atoms hold the +4 oxidation state. CeO_2 has a fluorite type structure, in which a Ce atom is cubically coordinated by eight O atoms, and an O atom is tetrahedrally coordinated by four Ce atoms (Figure 1.4).[30] CeO_2 is widely used as an active component and/or a supporting material of catalysts of industrially important reactions, such as water–gas shift, steam reforming, and various redox reactions.[31] One of the most important application of CeO_2 is automotive three-way catalyst.[5, 32] Cerium oxide has oxygen storage capacity (OSC), i.e., it

can adsorb and release oxygen depending on the surrounding conditions. The OSC of cerium oxide originates from its two oxidation states, +3 and +4. Thanks to that ability, cerium oxide mediates redox reactions. In relation to the catalytic activity, cerium oxide clusters have been investigated both experimentally and theoretically by several groups.[33-44]

1.6. This thesis

The purpose of this thesis is to obtain novel insights of redox reactions on cerium oxide clusters for further understanding of cerium oxide based catalysts. My investigations have been performed with a newly developed experimental apparatus and methodology. In this thesis, I present my experimental investigations on the stability and redox reactivity of gas-phase cerium oxide clusters. Target clusters are near-stoichiometric cerium oxide clusters (O/Ce ≈ 2) in Chapters 2 and 4, and oxygen deficient clusters (O/Ce < 2) in Chapter 3. All the experiments were carried out in a vacuum chamber. A schematic diagram of the experimental setup used in this thesis is shown in Chapter 2. The clusters were generated by a laser ablation technique and detected by a time-of-flight mass spectrometer (TOF-MS). Before detection, the clusters were exposed to reactant gas molecules to be examined on their reactivity at room temperature, and then they were heated up to a certain temperature for investigations of their thermal stability and decomposition processes. From the viewpoint of each cluster, the heating treatment is following the room-temperature reactions, which is called post-heating.[45] By varying the temperature of the post-heating, releasing processes of small molecules from the clusters were observed. Such a temperature scanning measurement can be thought as an analogue in gas-phase clusters of temperature-programmed desorption (TPD), which is used in surface sciences. From the results of temperature dependence, energetics, in particular, activation energies, of the thermal processes were estimated based on the Arrhenius equation. The group which I belong to has recently reported several investigations including activation energy estimation by the gas-phase TPD method.[46-50] The results presented in Chapter 2 are the first report of such a methodology.

In Chapter 2, I investigated the stable stoichiometry of cerium oxide cluster cations, $Ce_nO_{2n+x}^+$ (n = 2–9, x = −1 to +2). Heating experiments revealed the stable compositions of cerium oxide clusters. Processes of oxygen release from oxygen-rich species were observed by gas-phase TPD measurements, and the activation energies of those processes were estimated. Reactivity of cerium oxide clusters with CO was also examined to know stable

stoichiometry by reducing the clusters.

In Chapter 3, I focused on the reactivity of oxygen-deficient cerium oxide clusters, $Ce_nO_m^+$ (n = 2–10, $m \leq 2n$), with small gaseous molecules, CO, CO_2, NO, N_2O, and O_2. While the oxygen losing process was investigated in the preceding chapter, oxygen gaining process was observed in experiments of Chapter 3: The oxygen-deficient species extracted oxygen atoms from the gaseous molecules. The oxygen transfer reactions were explained in terms of an energy balance. In addition, generating oxygen-deficient cerium oxide clusters was examined by heating stoichiometric cerium oxide clusters.

In Chapter 4, I focused on a detailed reaction mechanism on cerium oxide clusters. The oxidation reaction of NO by stoichiometric cerium oxide cluster cations, $Ce_nO_{2n}^+$ (n = 2–9) was investigated by the gas-phase TPD measurement. The NO oxidation progressed via two separate processes, reactant NO adsorption on and product NO_2 desorption from the clusters. An energy diagram of the NO oxidation reaction was suggested based on the experimental data. I also estimated the activation energy of the NO_2 release process. To the best of my knowledge, this is the first result of isolation and energetic analysis of intermediates of a redox reaction on cerium oxide clusters.

In Chapter 5, finally, a brief summary and perspectives of this thesis are presented.

1.7. References

(1) Hattori, H. Heterogeneous Basic Catalysis. *Chem. Rev.* **1995**, *95*, 537-558.

(2) Corma, A.; García, H. Lewis Acids: From Conventional Homogeneous to Green Homogeneous and Heterogeneous Catalysis. *Chem. Rev.* **2003**, *103*, 4307-4366.

(3) Wilson, K.; Clark, J. H. Solid Acids and their use as Environmentally Friendly Catalysts in Organic Synthesis. *Pure Appl. Chem.* **2000**, *72*, 1313-1319.

(4) Bailey, D. C.; Langer, S. H. Immobilized Transition-Metal Carbonyls and Related Catalysts. *Chem. Rev.* **1981**, *81*, 109-148.

(5) Fritz, A.; Pitchon, V. The Current State of Research on Automotive Lean NO_x Catalysis. *Appl. Catal. B-Environ.* **1997**, *13*, 1-25.

(6) Linstrom, P.; Mallard, W., Eds.; In *NIST Chemistry WebBook, NIST Standard Reference Database Number 69;* National Institute of Standards and Technology: Gaithersburg, U.S.A., http://webbook.nist.gov, retrieved August 2, 2015.

(7) Matsumoto, S. Recent Advances in Automobile Exhaust Catalysts. *Catal. Today* **2004**, *90*,

183-190.

(8) Takahashi, N.; Shinjoh, H.; Iijima, T.; Suzuki, T.; Yamazaki, K.; Yokota, K.; Suzuki, H.; Miyoshi, N.; Matsumoto, S.; Tanizawa, T.; Tanaka, T.; Tateishi, S.; Kasahara, K. The New Concept 3-Way Catalyst for Automotive Lean-Burn Engine: NO_x Storage and Reduction Catalyst. *Catal. Today* **1996**, *27*, 63-69.

(9) Rankovic, N.; Nicolle, A.; Da Costa, P. Detailed Kinetic Modeling Study of NOx Oxidation and Storage and their Interactions Over Pt/Ba/Al_2O_3 Monolith Catalysts. *J. Phys. Chem. C* **2010**, *114*, 7102-7111.

(10) Swanson, H. E.; Tatge, E., Eds.; In *Standard x-ray diffraction powder patterns: National Bureau of Standards circular, 539;* U.S. Dept. of Commerce, National Bureau of Standards: Washington, DC, 1953; Vol. 1.

(11) Jin, J.; Ohkoshi, S.; Hashimoto, K. Giant Coercive Field of Nanometer-Sized Iron Oxide. *Adv. Mater.* **2004**, *16*, 48-51.

(12) Haruta, M.; Kobayashi, T.; Sano, H.; Yamada, N. Novel Gold Catalysts for the Oxidation of Carbon Monoxide at a Temperature Far Below 0 °C. *Chem. Lett.* **1987**, *16*, 405-408.

(13) Haruta, M. Size- and Support-Dependency in the Catalysis of Gold. *Catal. Today* **1997**, *36*, 153-166.

(14) Kroto, H. W.; Heath, J. R.; O'Brien, S. C.; Curl, R. F.; Smalley, R. E. C_{60}: Buckminsterfullerene. *Nature* **1985**, *318*, 162-163.

(15) Krätschmer, W.; Lamb, L. D.; Fostiropoulos, K.; Huffman, D. R. Solid C_{60}: A New Form of Carbon. *Nature* **1990**, *347*, 354-358.

(16) Grisenti, R. E.; Schöllkopf, W.; Toennies, J. P.; Hegerfeldt, G. C.; Köhler, T.; Stoll, M. Determination of the Bond Length and Binding Energy of the Helium Dimer by Diffraction from a Transmission Grating. *Phys. Rev. Lett.* **2000**, *85*, 2284-2287.

(17) Jahnke, T., et al Ultrafast Energy Transfer between Water Molecules. *Nat. Phys.* **2010**, *6*, 139-142.

(18) Nagornova, N. S.; Rizzo, T. R.; Boyarkin, O. V. Interplay of Intra- and Intermolecular H-Bonding in a Progressively Solvated Macrocyclic Peptide. *Science* **2012**, *336*, 320-323.

(19) Barlak, T. M.; Campana, J. E.; Wyatt, J. R.; Dunlap, B. I.; Colton, R. J. Secondary Ion Mass Spectrometry of Metal Salts: Polyatomic Ion Emission. *Int. J. Mass Spectrom. Ion Process.* **1983**, *46*, 523-526.

(20) Taylor, J. A.; Rabalais, J. W. Molecular Rearrangement and Cluster Formation in the Secondary Ion Mass Spectra (SIMS) of Fluoride Salts. *Surf. Sci.* **1978**, *74*, 229-236.

(21) Ince, M. P.; Perera, B. A.; Van Stipdonk, M. J. Production, Dissociation, and Gas Phase Stability of Sodium Fluoride Cluster Ions Studied using Electrospray Ionization Ion Trap Mass Spectrometry. *Int. J. Mass Spectrom.* **2001**, *207*, 41-55.

(22) Honea, E. C.; Homer, M. L.; Whetten, R. L. Electron Binding and Stability of Excess-Electron Alkali Halide Clusters: Localization and Surface States. *Phys. Rev. B* **1993**, *47*, 7480-7493.

(23) Beck, R. D.; John, P. S.; Homer, M. L.; Whetten, R. L. Impact-Induced Cleaving and Melting of Alkali-Halide Nanocrystals. *Science* **1991**, *253*, 879-883.

(24) Honea, E. C.; Homer, M. L.; Whetten, R. L. Excess-Electron and Excess-Hole States of Charged Alkali Halide Clusters. *Int. J. Mass Spectrom. Ion Process.* **1990**, *102*, 213-226.

(25) Homer, M. L.; Livingston, F. E.; Whetten, R. L. Molecular Adsorption-Desorption Reactions of Ammonia on Alkali Halide Clusters and Nanocrystals. *J. Phys. Chem.* **1995**, *99*, 7604-7612.

(26) Ohshimo, K.; Takahashi, T.; Moriyama, R.; Misaizu, F. Compact Non-Rock-Salt Structures in Sodium Fluoride Cluster Ions at Specific Sizes Revealed by Ion Mobility Mass Spectrometry. *J. Phys. Chem. A* **2014**, *118*, 9970-9975.

(27) Martin, T. P.; Näher, U.; Schaber, H.; Zimmermann, U. Evidence for a size‐dependent Melting of Sodium Clusters. *J. Chem. Phys.* **1994**, *100*, 2322-2324.

(28) Schmidt, M.; Kusche, R.; von Issendorff, B.; Haberland, H. Irregular Variations in the Melting Point of Size-Selected Atomic Clusters. *Nature* **1998**, *393*, 238-240.

(29) Lang, S. M.; Bernhardt, T. M. Gas Phase Metal Cluster Model Systems for Heterogeneous Catalysis. *Phys. Chem. Chem. Phys.* **2012**, *14*, 9255-9269.

(30) Whitfield, H.; Roman, D.; Palmer, A. X-Ray Study of the System ThO_2-CeO_2-Ce_2O_3. *J. Inorg. Nucl. Chem.* **1966**, *28*, 2817-2825.

(31) Trovarelli, A. Catalytic Properties of Ceria and CeO_2-Containing Materials. *Catal. Rev.* **1996**, *38*, 439-520.

(32) Yao, H.; Yao, Y. Ceria in Automotive Exhaust Catalysts: I. Oxygen Storage. *J. Catal.* **1984**, *86*, 254-265.

(33) Mele, A.; Consalvo, D.; Stranges, D.; Giardini-Guidoni, A.; Teghil, R. Chemical

Reactivity of Ionic Clusters Formed by Laser Ablation of Solid Oxides Utilized in Superconducting Materials. *Int. J. Mass Spectrom. Ion Process.* **1990**, *95*, 359-373.

(34) Chen, C.; Chen, H.; Weng, M.; Ju, S.; Chang, J.; Chang, C. Structural Properties of $(CeO_2)_n$ (n = 1–5) Nanoparticle: Molecular Mechanics and First Principle Studies. *Chin. J. Catal.* **2008**, *29*, 1117-1121.

(35) Aubriet, F.; Gaumet, J.; De Jong, W. A.; Groenewold, G. S.; Gianotto, A. K.; McIlwain, M. E.; Van Stipdonk, M. J.; Leavitt, C. M. Cerium Oxyhydroxide Clusters: Formation, Structure, and Reactivity. *J. Phys. Chem. A* **2009**, *113*, 6239-6252.

(36) Wu, X.; Zhao, Y.; Xue, W.; Wang, Z.; He, S.; Ding, X. Active Sites of Stoichiometric Cerium Oxide Cations ($Ce_mO_{2m}^+$) Probed by Reactions with Carbon Monoxide and Small Hydrocarbon Molecules. *Phys. Chem. Chem. Phys.* **2010**, *12*, 3984-3997.

(37) Wu, X.; Ding, X.; Bai, S.; Xu, B.; He, S.; Shi, Q. Experimental and Theoretical Study of the Reactions between Cerium Oxide Cluster Anions and Carbon Monoxide: Size-Dependent Reactivity of $Ce_nO_{2n+1}^-$ (n = 1–21). *J. Phys. Chem. C* **2011**, *115*, 13329-13337.

(38) Ding, X.; Wu, X.; Zhao, Y.; Ma, J.; He, S. Double-Oxygen-Atom Transfer in Reactions of $Ce_mO_{2m}^+$ (m = 2–6) with C_2H_2. *ChemPhysChem* **2011**, *12*, 2110-2117.

(39) Burow, A. M.; Wende, T.; Sierka, M.; Włodarczyk, R.; Sauer, J.; Claes, P.; Jiang, L.; Meijer, G.; Lievens, P.; Asmis, K. R. Structures and Vibrational Spectroscopy of Partially Reduced Gas-Phase Cerium Oxide Clusters. *Phys. Chem. Chem. Phys.* **2011**, *13*, 19393-19400.

(40) Vayssilov, G. N.; Migani, A.; Neyman, K. Density Functional Modeling of the Interactions of Platinum Clusters with CeO_2 Nanoparticles of Different Size. *J. Phys. Chem. C* **2011**, *115*, 16081-16086.

(41) Zhang, J.; Fu, Z.; Yang, Z.; Li, S. The Highly Active Ce_4O_8 Nanoparticle for CO Oxidation. *Phys. Lett. A* **2012**, *376*, 3235-3240.

(42) Hirabayashi, S.; Ichihashi, M. Oxidation of Composition-Selected Cerium Oxide Cluster Cations by O_2. *Chem. Phys. Lett.* **2013**, *564*, 16-20.

(43) Hirabayashi, S.; Ichihashi, M. Oxidation of CO and NO on Composition-Selected Cerium Oxide Cluster Cations. *J. Phys. Chem. A* **2013**, *117*, 9005-9010.

(44) Meng, J.; He, S. Thermal Dihydrogen Activation by a Closed-Shell $AuCeO_2^+$ Cluster. *J. Phys. Chem. Lett.* **2014**, *5*, 3890-3894.

(45) Sakuma, K.; Miyajima, K.; Mafuné, F. Oxidation of CO by Nickel Oxide Clusters Revealed by Post Heating. *J. Phys. Chem. A* **2013**, *117*, 3260-3265.

(46) Koyama, K.; Kudoh, S.; Miyajima, K.; Mafuné, F. Dissociation Energy for O_2 Release from Gas-Phase Iron Oxide Clusters Measured by Temperature-Programmed Desorption Experiments. *Chem. Phys. Lett.* **2015**, *625*, 104-109.

(47) Takenouchi, M.; Kudoh, S.; Miyajima, K.; Mafuné, F. Adsorption and Desorption of Hydrogen by Gas-Phase Palladium Clusters Revealed by in Situ Thermal Desorption Spectroscopy. *J. Phys. Chem. A* **2015**, *119*, 6766-6772.

(48) Miyajima, K.; Mafuné, F. Release of Oxygen from Palladium Oxide Cluster Ions by Heat. *J. Phys. Chem. A* **2015**, *119*, 8055-8061.

(49) Tawaraya, Y.; Kudoh, S.; Miyajima, K.; Mafuné, F. Thermal Desorption and Reaction of NO Adsorbed on Rhodium Cluster Ions Studied by Thermal Desorption Spectroscopy. *J. Phys. Chem. A* **2015**, *119*, 8461-8468.

(50) Koyama, K.; Kudoh, S.; Miyajima, K.; Mafuné, F. Stable Stoichiometry of Gas-Phase Manganese Oxide Cluster Ions Revealed by Temperature-Programmed Desorption. *J. Phys. Chem. A* **2015**, *119*, 8433-8442.

(51) Momma, K.; Izumi, F. *VESTA 3* for Three-Dimensional Visualization of Crystal, Volumetric and Morphology Data. *J. Appl. Cryst.* **2011**, *44*, 1272-1276.

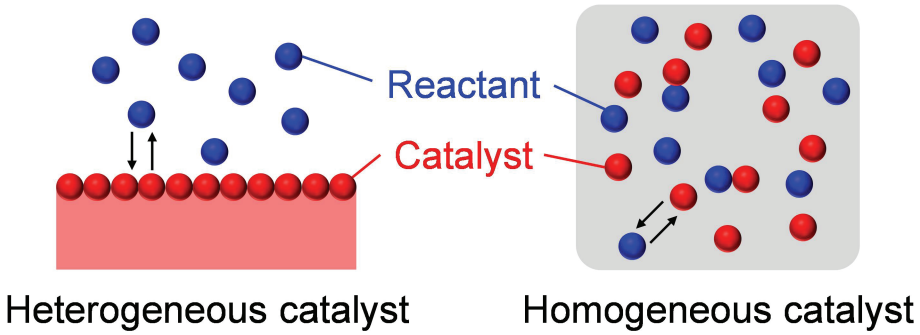

Figure 1.1. Concept illustration of heterogeneous and homogeneous catalysts.

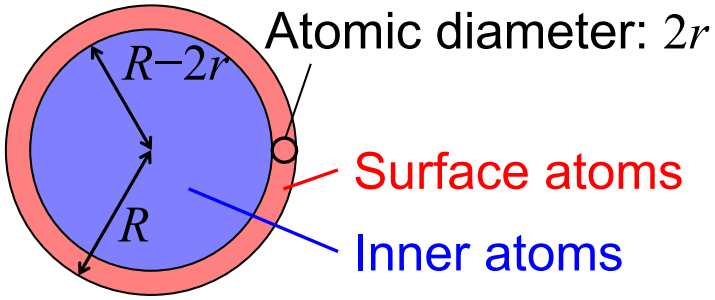

Figure 1.2. Simple estimation model for the surface-atomic ratio in a particle.

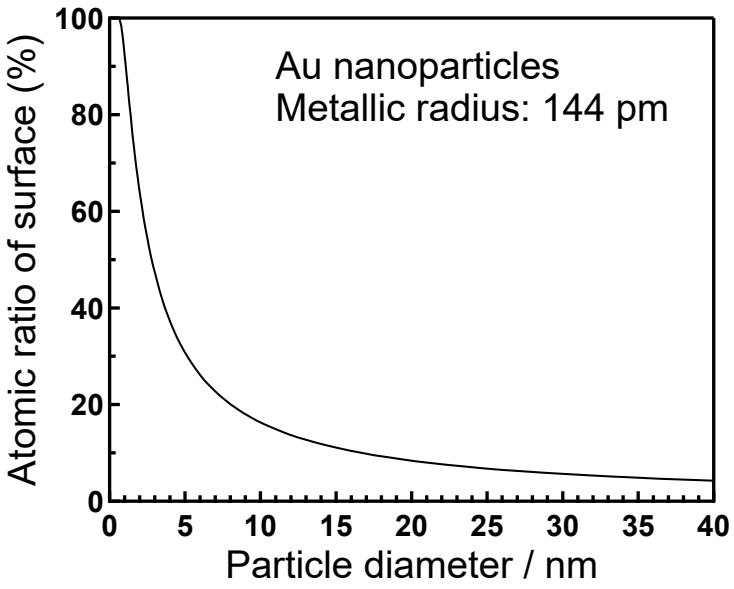

Figure 1.3. Approximate atomic ratio of a surface in a gold nanoparticle.

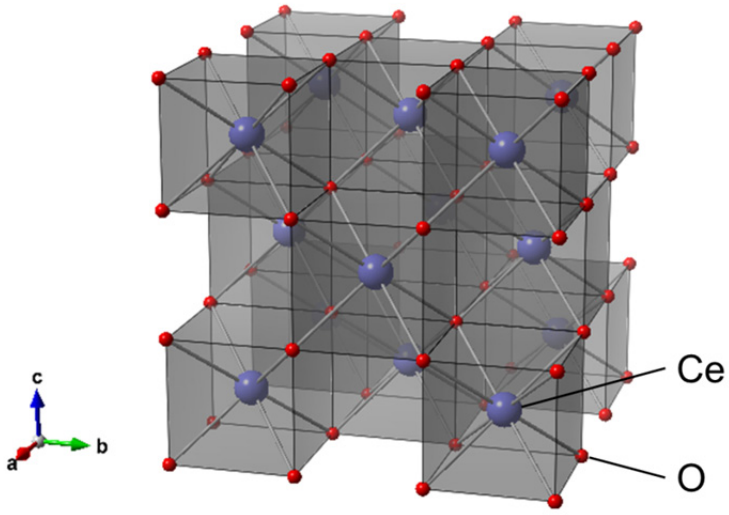

Figure 1.4. Crystal structure of CeO_2.[30] The cubic coordination around Ce atoms is emphasized. This graphic was produced by the VESTA program.[51]

Chapter 2

Stable Stoichiometry of Gas-Phase Cerium Oxide Cluster Ions and Their Reactions with CO

Cerium oxide cluster ions, $Ce_nO_{2n+x}^+$ (n = 2–9, x = −1 to +2), were prepared in the gas phase by laser ablation of a cerium oxide rod in the presence of oxygen diluted in He as the carrier gas. The stable stoichiometry of the cluster ions was investigated using a mass spectrometer in combination with a newly developed post-heating device. The oxygen-rich clusters, $Ce_nO_{2n+x}^+$ (x = 1, 2), were found to release oxygen molecules, and $Ce_nO_{2n+x}^+$ (x = −1, 0) were exclusively formed by post-heating treatment at 573 K. The $Ce_nO_{2n-1}^+$ and $Ce_nO_{2n}^+$ clusters were found to be thermally stable and the oxygen-rich clusters consisted of robust $Ce_nO_{2n-1}^+$ and $Ce_nO_{2n}^+$ and weakly bound oxygen atoms. Evaluation of the reactivity of $Ce_nO_{2n+x}^+$ with CO molecules demonstrated that $Ce_nO_{2n}^+$ oxidized CO to form $Ce_nO_{2n-1}^+$ and CO_2, and the rate constants of the reaction were in the range of 10^{-12}–10^{-16} cm^3 s^{-1}. The CO oxidation reaction was distinct for n = 5, which occurred in parallel with the CO attachment reaction.

(Reproduced with permission from T. Nagata et al., *J. Phys. Chem. A* **2015**, *119*, 1813–1819.

2.1. Introduction

Cerium oxide (CeO_2, ceria) is a major component of automotive three-way catalysts that are used to convert harmful exhaust gases including NO_x, CO, and small hydrocarbons into N_2, CO_2, and H_2O.[1] In this process, cerium oxide releases and absorbs oxygen depending on whether reductive or oxidative atmospheric conditions are employed. The absorption and release of oxygen by cerium oxide is termed its oxygen storage capacity (OSC).[2, 3] Owing to this ability, cerium oxide may act as an oxygen buffer to promote redox reactions. The OSC of ceria originates from two different oxidation states of the cerium atom, Ce^{3+} and Ce^{4+}. It is known that a CO molecule can extract a lattice O atom of CeO_2, thereby forming an oxygen vacancy and reducing Ce^{4+} into Ce^{3+}.[4, 5] Elucidating the specific features of each oxidation state of cerium oxide and the processes governing transitions between these oxidation states on the atomic and molecular levels is of extreme importance for understanding the mechanism underlying the OSC and for designing high-performance catalysts using cerium oxide.

In view of this, isolated cerium oxide clusters have recently been investigated in the gas phase by certain groups. Wu and coworkers experimentally and computationally evaluated the structures, active sites, and reactivities with CO molecules of cationic ($Ce_mO_{2m}^+$, m = 2–16) and anionic ($Ce_nO_{2n+1}^-$, n = 1–21) cerium oxide clusters.[6, 7] In the cationic cerium oxide clusters, an active radical site, which plays a central role in redox reactions, was found to be delocalized over the CeO_2 moiety, resulting in lower reactivity than that in anionic clusters where the radical site is localized on a single terminal oxygen atom. Hirabayashi and Ichihashi reported the redox reactions of cerium oxide cationic clusters of certain compositions with O_2, CO, and NO molecules based on single collision experiments.[8, 9] They classified the oxidation states of cerium atoms in the cerium oxide clusters in terms of the average oxidation number (AON), and concluded that clusters with lower AON (~3) absorb O_2 molecules strongly, whereas those with higher AON (~4) can transfer oxygen atoms to CO and NO molecules.

In this chapter, I focused my attention on the stability of cerium oxide cationic clusters and their reactivity with CO molecules. Considering that less stable clusters tend to dissociate into the more stable counterparts, the thermally stable compositions were investigated by using a newly developed post-heating method.[10-12] The temperature dependence of the signal intensities of the clusters facilitated elucidation of the mechanism of thermal dissociation and the activation energies of these processes. In addition, the reactions of the clusters with CO

were quantitatively evaluated; this reaction also modifies the oxidation state in an alternative mechanism to heating. I estimated the rate constants of the reactions and revealed the dependence of reactivity on the cluster size.

2.2. Experimental section

The stability and reactivity of cerium oxide clusters were investigated using a reflectron-equipped time-of-flight mass spectrometer (see Figure 2.1).[11, 12] The clusters were prepared by laser ablation in a cluster source. A ceria rod (Rare Metallic Co., Ltd., 99.9%) was vaporized using the focused second harmonic (532 nm) of a Nd:YAG laser at a typical pulse energy of 10 mJ in the presence of oxygen (0.02–1%; Japan Fine Products Co., Ltd., >99.9% purity) diluted in helium (0.8–1.1 MPa; Japan Fine Products Co., Ltd., >99.99995%). The clusters were formed in the gas flow from a pulsed valve and then passed through a reaction gas cell (2 mm inner diameter, 60 mm long), where the reactant CO gas (0–12.5%; Japan Fine Products Co., Ltd., >99.95% purity) diluted with helium (0.1 MPa) was injected using another pulsed valve. The typical gas density inside the reaction gas cell was estimated to be 10^{17}–10^{18} molecules cm^{-3}. The residence time of the cluster ions in the reaction gas cell was estimated to be ~70 μs. After passing through the reaction gas cell, the cluster ions were introduced into an extension tube (4 mm inner diameter, 120 mm long) before expansion into a vacuum chamber. The temperature of the extension tube was varied in the range of 298–600 K using a resistive heater and monitored using a thermocouple (type K). The residence time of the cluster ions and the density of the He gas in the extension tube were estimated to be ~100 μs and ~10^{17} molecules cm^{-3}, respectively. Hence, thermal equilibrium of the clusters was achieved through collisions with the He carrier gas well before expansion into the vacuum. In my experimental setup, the reaction of the clusters with CO occurred in the reaction gas cell, which was maintained at room temperature, after which the clusters were heated in the extension tube.[10-12]

The cluster ions gained kinetic energy of 3.5 keV in the acceleration region for the mass analysis. The ions were steered and focused by a set of vertical and horizontal deflectors and an einzel lens. After traveling in a 1 m field-free region, the ions were reversed by the reflectron and detected using a Hamamatsu double-microchannel plate detector. Signals from the detector were amplified with a 350 MHz preamplifier (Stanford SR445A) and digitized

using an oscilloscope (LeCroy LT344L). Averaged TOF spectra (typically 1000 sweeps) were analyzed on a computer. Mass spectrometer was calibrated using known mass spectrometric patterns of some metal clusters (e.g. Nb_n^+, Au_n^+), detailed in Appendix. The mass resolution $m/\Delta m$ was ~1000, which was sufficient for estimating the ion intensity of each cluster.

2.3. Results

Figure 2.2a displays a mass spectrum of the cationic cerium oxide clusters that were produced by the laser ablation of a ceria rod in the presence of 0.05% oxygen gas in He (0.8 MPa). Ions assignable to $Ce_nO_{2n+x}^+$ ($2 \le n \le 9$, $-1 \le x \le +2$) are seen in the spectrum. Each observed $Ce_nO_{2n+x}^+$ ion, which has an odd number of electrons, is thought to be a radical cation, $Ce_nO_{2n+x}^{\bullet+}$. The unpaired electron can be located in an oxygen atom forming a radical state or can occupy a 4f orbital of a cerium atom. However, as I am not able to identify the radical state explicitly, the radical notation has been unspecified for each chemical formula throughout this thesis, which will be referred later. When the partial pressure of oxygen in the He gas was reduced by 1–2 orders of magnitude, oxygen-poor clusters ($x = -2$) appeared in the mass spectrum. On the other hand, when the partial pressure of oxygen in the He gas was set to >0.5%, the intensity of the peaks of the oxygen-rich clusters ($x = +1$ and $+2$) increased and a trace amount of $x = +3$ and $+4$ clusters appeared in the mass spectrum.[13, 14] The oxygen-rich clusters are likely to consist of a robust cerium oxide moiety and weakly bound oxygen atoms. To identify the weakly bound oxygen atoms in the clusters, the prepared cluster ions were introduced into an extension tube, where the cluster ions in the flowing gas were heated by using the resistive heater. Figure 2.2b shows the mass spectrum of $Ce_nO_{2n+x}^+$ after heating at 573 K. The oxygen-rich clusters ($x \ge +1$) disappeared completely, with a concomitant increase in the peak intensity of the stoichiometric $Ce_nO_{2n}^+$ and one oxygen deficient $Ce_nO_{2n-1}^+$ clusters. The intensity changes indicate that oxygen was released from the oxygen-rich $Ce_nO_{2n+x}^+$ clusters by the post-heating treatment. Note that some peaks assignable to clusters containing hydrogen atoms ($Ce_nO_{2n+x}H_i^+$) were also observed, which overlapped with the isotopic satellite peaks of $Ce_nO_{2n+x}^+$ (see Figure 2.3). The ion intensity of $Ce_nO_{2n+x}^+$ was obtained based on the intensity of the $^{140}Ce_nO_{2n+x}^+$ peak, which was free from contributions from other ions.

Figure 2.4a shows the relative intensities of the $Ce_4O_{7,8,9,10}^+$ peaks as a function of the temperature at the extension tube. The intensities of the $Ce_4O_9^+$ and $Ce_4O_{10}^+$ peaks decrease,

and the intensities of the $Ce_4O_7^+$ and $Ce_4O_8^+$ peaks increase with increasing temperature. Close examination of the intensity changes shows that the peak intensity of $Ce_4O_9^+$ begins to decrease and that of $Ce_4O_7^+$ begins to increase at ~350 K, and the extent of the decrease in the intensity of the $Ce_4O_9^+$ peak is equivalent to the increase in the intensity of the $Ce_4O_7^+$ peak. In addition, a similar concomitant respective decrease and increase of $Ce_4O_{10}^+$ and $Ce_4O_8^+$ peaks occurs around 330–450 K. Similar intensity changes were observed for all the observed cluster ions, indicating that oxygen molecules were released from $Ce_nO_{2n+2}^+$ and $Ce_nO_{2n+1}^+$ as:

$$Ce_nO_{2n+2}^+ \rightarrow Ce_nO_{2n}^+ + O_2 \quad (2.1)$$

$$Ce_nO_{2n+1}^+ \rightarrow Ce_nO_{2n-1}^+ + O_2 \quad (2.2)$$

For quantitative analysis of the temperature dependence of the intensity changes, let me propose a kinetic model: First, in the present experiment, not only the forward but also the following backward reactions could occur to a certain extent, because oxygen molecules in the carrier gas are present in the extension tube:

$$XO_2^+ \rightarrow X^+ + O_2 \quad \text{forward reaction} \quad (2.3)$$

$$X^+ + O_2 \rightarrow XO_2^+ \quad \text{backward reaction} \quad (2.4)$$

where X stands for $Ce_nO_{2n-1}^+$ or $Ce_nO_{2n}^+$. The rate of the backward reaction depends linearly on the number density of oxygen species in the extension tube. When the partial pressure of oxygen in the carrier gas is sufficiently low, the backward reaction may be disregarded. As is evidenced by the intensity changes in different oxygen concentrations (see Figure 2.4), the temperature dependence remains almost unchanged in the range between 0.02–0.1%, although oxygen-rich clusters ($Ce_nO_{2n+x}^+$; x = +1 and +2) form at high partial pressures of oxygen. Hence, the backward reactions (2.4) are deduced to be negligible in this treatment. Hence, the rate equation is given by:

$$[XO_2^+] = [XO_2^+]_0 \exp(-kt) \quad (2.5)$$

where the rate constant of the unimolecular O_2 release reaction is defined as k, and the initial number density of XO_2^+ and the number density of XO_2^+ after the reaction are defined as $[XO_2^+]_0$ and $[XO_2^+]$, respectively, and t is the reaction time in the extension tube.

Secondly, as an oxygen molecule is released from the oxygen-rich cluster at a sufficiently high temperature, the reaction is considered to occur when the energy of the cluster ion overcomes the activation barrier. According to the Arrhenius equation, the rate constant, k is given by:

$$k = A \exp\left(-\frac{E_a}{k_B T} \right) \tag{2.6}$$

where A, E_a, k_B, and T are the pre-exponential factor of the Arrhenius equation, the activation energy, the Boltzmann constant, and the temperature, respectively. By combining Equations (2.5) and (2.6), I obtain the following equation:

$$[XO_2^+] = [XO_2^+]_0 \exp\left(-At \exp\left(-\frac{E_a}{k_B T} \right) \right) \tag{2.7}$$

The fitting curves in Figure 2.4 were obtained by using Equation (2.7), which adequately reproduce the experimental results. The data for $Ce_3O_{5-8}^+$, $Ce_5O_{9-12}^+$, and $Ce_6O_{11-14}^+$ are also presented in Figure 2.5. The activation energies for oxygen release were estimated by fitting the data and are summarized in Table 2.1.

Knowing the thermal stability of the clusters, the reactivity of $Ce_nO_{2n+x}^+$ with CO was also investigated. In addition to the He gas, introduction of CO gas into the reaction gas cell induced a decrease in the intensities of the peaks of the $Ce_nO_{2n}^+$ and $Ce_nO_{2n+2}^+$ species, with a concomitant increase in the peak intensities of the $Ce_nO_{2n-1}^+$ and $Ce_nO_{2n+1}^+$ species in the mass spectrum (see Figure 2.6). The corresponding increase and decrease in ion intensities suggest that $Ce_nO_{2n}^+$ and $Ce_nO_{2n+2}^+$ lost one oxygen atom by collision with CO. The characteristic spectral changes undoubtedly indicate that a CO molecule extracts an oxygen atom from $Ce_nO_{2n}^+$ and $Ce_nO_{2n+2}^+$ to generate CO_2 in the He buffer gas, and they are not caused by an oxygen atom release by collision-induced dissociation, because (i) such oxygen loss was not observed when the reaction gas cell was filled by He gas only (see Figure 2.6), and (ii) the reaction occurs at room temperature without any energetic treatment (e.g. heating or ion acceleration), though releasing the atomic oxygen radical requires much energy.[8] Hence, the only likely pathway is CO_2 formation. The reactions with CO can be described as:

$$Ce_nO_{2n}^+ + CO \rightarrow Ce_nO_{2n-1}^+ + CO_2, \tag{2.8}$$

$$Ce_nO_{2n+2}^+ + CO \rightarrow Ce_nO_{2n+1}^+ + CO_2. \tag{2.9}$$

The oxidation reaction of CO given by Equation (2.8) has been observed by Wu et al.[6] In this chapter, pseudo-first order rate constants were estimated for the reaction of the cerium oxide clusters with CO by changing the number density of CO in the reaction gas cell as a function of the cluster size. In my experimental setup, the number of $Ce_nO_{2n+x}^+$ species in the reaction gas cell is significantly smaller than that of CO. Hence, the number density of CO is

considered to remain unchanged throughout the reactions. The number density of CO was actually estimated by the reaction of Ni^+ with CO, whose rate constant is known to be 5.6×10^{-13} cm^3 s^{-1},[15] conducted under the identical experimental conditions as a reference.

Figure 2.7 show the intensity of the $Ce_nO_{2n}^+$ (n = 4–6) peaks as a function of the number density of CO in the reaction gas cell. The intensity of the $Ce_5O_{10}^+$ peak decreases and the intensity of the $Ce_5O_9^+$ peak increases, as the number density of CO increases. To estimate the pseudo-first order rate constant, I set the rate constant as k_{CO} and the intensity of the $Ce_nO_{2n}^+$ peak after the reaction as $[Ce_nO_{2n}^+]$, and the intensity of the peak of pristine $Ce_nO_{2n}^+$ as $[Ce_nO_{2n}^+]_0$. Here, the relative intensity is given by:

$$\frac{[Ce_nO_{2n}^+]}{[Ce_nO_{2n}^+]_0} = \exp(-k_{CO}Nt) \qquad (2.10)$$

where N and t are the number density of CO and the reaction time, respectively. As shown in Figure 2.7, the plots are reproduced reasonably well by this fitting in the lower CO density region. As the gas density of CO increases, the experimental data are not fully reproduced by the fitting (see Figure 2.8). It is likely that there are non-reactive inert isomers of $Ce_5O_{10}^+$ or CO-appended clusters with short lifetimes that can release CO molecules before detection by the TOF spectrometer. The rate constants of the reaction with CO (see Figure 2.9) were obtained from the slope given in Figure 2.7. The rate constants ranged from 10^{-12}–10^{-16} cm^3 s^{-1}, and the rate constants were higher for n = 5 and 10. Taking the possible non-reactive isomers of $Ce_5O_{10}^+$ into consideration, the rate constant for the reactive isomer of $Ce_5O_{10}^+$ would be 1.9×10^{-12} cm^3 s^{-1}.

CO oxidation by $Ce_nO_{2n+2}^+$, designated by Equation (2.9), was also observed. Figure 2.10 shows the intensity of the $Ce_nO_{2n+2}^+$ (n = 4–6) peaks as a function of the number density of CO in the reaction gas cell. The rate constants of CO oxidation were estimated to be k = 2.7×10^{-13} cm^3 s^{-1} for $Ce_5O_{12}^+$ and k = 4.8×10^{-14} cm^3 s^{-1} for $Ce_6O_{14}^+$. By contrast, CO oxidation reaction by $Ce_nO_{2n+2}^+$ (n = 3, 4, 7–10) was not observed beyond the noise level. The size dependence of the CO oxidation reactivity of $Ce_nO_{2n+2}^+$ resembles that of $Ce_nO_{2n}^+$, suggesting that excess oxygen atoms are involved in $Ce_nO_{2n+2}^+$ in such a manner that they do not change the reactivity of $Ce_nO_{2n}^+$ drastically. In the presence of a high density of CO gas ($>10^{16}$ molecules cm^{-3}), peaks assignable to the CO-appended clusters ($Ce_nO_{2n+x}(CO)^+$) appeared in the mass spectrum (see Figure 2.6c and d), decreasing the intensities of the

$Ce_nO_{2n}^+$ and $Ce_nO_{2n+2}^+$ peaks by CO oxidation and CO attachment as well. In the estimation of the rate constants for CO oxidation, the intensities of the CO-appended clusters ($Ce_nO_{2n+x}(CO)^+$) were included in the intensities of the corresponding $Ce_nO_{2n+x}^+$ clusters in Figure 2.7, 2.8, and 2.10.

2.4. Discussion

2.4.1. Stable cerium oxide clusters

Cerium oxide clusters, $Ce_nO_{2n+x}^+$, were formed by laser ablation of a ceria rod in the presence of oxygen diluted in He. They are radical cations, $Ce_nO_{2n+x}^{\bullet+}$, because they have at least one unpaired electron due to their odd number of electrons. The radicals can play a definitive role in the reactions of clusters, which will be discussed later. $Ce_nO_{2n}^+$ species are considered to hold an oxygen-centered radical,[6, 16, 17] whereas $Ce_nO_{2n-1}^+$ have one unpaired electron located in Ce 4f orbitals.[18] For $Ce_nO_{2n+1}^+$ and $Ce_nO_{2n+2}^+$, the spin distribution remains unidentified as far as I know, and thus some possibilities are considerable; e.g. $Ce_nO_{2n+1}^+$ is likely to hold an equivalent of a superoxide expressed as $[(Ce^{4+})_n(O^{2-})_{2n-1}(O_2^{\bullet-})]$, or may hold one Ce^{3+} and one dioxygen moiety close to molecular oxygen designated as $[(Ce^{4+})_{n-1}(Ce^{3+})(O^{2-})_{2n-1}(O_2)]$. The number of oxygen atoms involved in the cerium oxide clusters changed sensitively with the partial pressure of oxygen. In particular, oxygen-rich clusters (x = +1–+4) tended to be generated when the partial pressure was sufficiently high (>1%). The oxygen-rich clusters are thought to consist of robust cerium oxide clusters with adjunct oxygen molecules weakly bound to them, because stoichiometric and oxygen deficient $Ce_nO_{2n+x}^+$ (x = 0 and −1) species were formed selectively and dominantly after rupturing the weaker bonds in the clusters by post-heating treatment (see Figure 2.2), and the temperature dependence study evidently demonstrated that oxygen atoms were released as molecular oxygen during those processes (see Figure 2.4). In a related phenomenon, Aubriet and coworkers reported the structure of an oxygen-rich ceria cluster anion CeO_4^-; according to their calculations, CeO_4^- contains excess oxygen atoms that are present as an O_2 moiety side-on bound with the Ce center in the most stable structure.[19] Thus, the number ratio of cerium atoms and oxygen atoms in a stable cluster is 1:2, indicating that the cerium atom and the oxygen atom adopt the +4 and −2 charge states, respectively.

Some clusters containing hydrogen atoms, $Ce_nO_{2n+x}H_i^+$, were also observed in the present experiments. Aubriet and coworkers reported that anionic cerium oxyhydroxide

clusters, $[Ce_xO_y(OH)_z]^-$, were formed by laser ablation of CeO_2 in a trace amount of H_2O vapor. DFT calculations showed that those clusters have terminal hydroxide moieties and do not have molecular water.[19] The hydrogen-containing clusters obtained in the present study can have hydroxide moieties, although the structures of those clusters have not been determined, yet. For the reference, the hydrogen-containing clusters were found to remain unchanged even after post-heating at 573K (see Figure 2.3), which is out of scope in this chapter.

It must be emphasized that $Ce_nO_{2n+x}^+$ ($x = -2$) was not formed by post-heating at 573 K, although these oxygen deficient clusters ($x = -2$) were actually generated when the partial pressure of O_2 was sufficiently low (<0.02 %). To elucidate the specificity of the formation of $Ce_nO_{2n+x}^+$ ($x = -1$ and 0), I prepared oxygen deficient clusters, $Ce_nO_{2n+x}^+$ ($x \leq -2$), by laser ablation of a CeO_2 rod in the absence of oxygen (see Figure 2.11a and d). It is known that laser ablation of a metal oxide target generates oxygen deficient clusters, probably because oxygen atoms released in the gas phase upon laser ablation diffuse out of the aggregation region during cluster formation.[20-22] After preparation of the oxygen deficient cluster ions, they were subjected to collisions with O_2 molecules in the reaction gas cell downstream of the cluster source. Here, O_2 gas (12.5%) diluted in He gas (0.1 MPa) was introduced into the reaction gas cell through the pulse valve. Figure 2.11b and e show the mass spectrum and intensity distribution of $Ce_nO_{2n+x}^+$ after collision with O_2 molecules. The disappearance of oxygen deficient clusters ($x \leq -2$) and the appearance of stoichiometric and oxygen-rich clusters ($x = -1$ to +4) indicate that oxygen molecules attach to the oxygen deficient clusters to form stoichiometric and oxygen-rich $Ce_nO_{2n+x}^+$ ($x = -1$ to +4). However, post-heating of the clusters at 573 K changed the mass distribution again: $Ce_nO_{2n+x}^+$ ($x = -1$ and 0) were formed dominantly, and no $Ce_nO_{2n-2}^+$ species were formed (see Figure 2.11c and f). These findings evidently indicate that the high reactivity of the oxygen deficient clusters $Ce_nO_{2n+x}^+$ ($x \leq -2$) with O_2 causes to uptake oxygen atoms until $Ce_nO_{2n+x}^+$ ($x = -1$ and 0) species are formed. In addition, excess oxygen molecules can attach to stable $Ce_nO_{2n+x}^+$ ($x = -1$ and 0) when sufficient oxygen molecules are present in the reaction gas cell. However, the oxygen atoms are so weakly bound to the clusters that they dissociate readily upon post-heating. In fact, as shown in Table 2.1, the activation energy for oxygen release is of the order of several tenth eV. No drastic variations in the activation energy for different sized clusters were observed, consistent with the relatively weak interaction between excess oxygen atoms and a

cluster. In contrast, oxygen atoms in a stoichiometric cluster are strongly bound. According to my preliminary study, oxygen release from the stoichiometric clusters occurs only after heating up to 700–1000 K, depending on the cluster size.

It is known that the cerium atom can adopt +3 and +4 charge states in many compounds. For $Ce_nO_{2n+x}^+$, the stability is mostly explained by the model that the cerium atom and the oxygen atom respectively adopt +4 and −2 charge states. More precisely, formation of $Ce_nO_{2n-1}^+$ and $Ce_nO_{2n}^+$ indicates that the cluster ions are respectively stable when one of the cerium atoms adopts the +3 charge state or when all the cerium atoms adopts +4 charge state and the one electron is depleted in the cluster.

The question of whether the cerium oxide clusters in which the cerium atoms dominantly adopt the +3 charge state are stable remained to be explored. As shown in Figure 2.11a and d, $Ce_4O_5^+$ and $Ce_4O_6^+$ were indeed formed by laser ablation of the ceria rod. However, these species are so highly reactive with O_2 that they uptake oxygen atoms. Once the cerium oxide clusters in which the cerium atoms adopt the +4 charge state are formed, oxygen will not be released from the cluster even upon heating to 573 K. In addition, no evidence of the CO oxidation reaction of $Ce_nO_{2n+x}^+$ ($x = -1$) was observed; if the reaction occurs, it should be evidenced by the appearance of the $x = -2$ peak in the mass spectrum. As there is no $x = -2$ peak in the mass spectrum after the reaction with CO, it is highly likely that an insurmountable barrier exists preventing the transformation of $Ce_nO_{2n-1}^+$ to $Ce_nO_{2n-2}^+$.

In the bulk crystal, CeO_2 has the fluorite type structure in which one cerium atom is cubically coordinated by eight oxygen atoms, whereas one oxygen atom is tetrahedrally coordinated by four cerium atoms. Here, two cerium atoms are bridged by two oxygen atoms.[23] In the case of gas phase clusters, the bridge structure is considered to comprise the framework of the cerium oxide cluster; however, atoms in the gas phase cluster are generally not fully coordinated by the other atoms. In fact, DFT calculations suggested that the remaining oxygen atoms are bonded to the cerium atoms as terminal atoms: There are two terminal oxygen atoms in $Ce_4O_8^+$.[6] In addition, it was elucidated that the bond length of one of the terminal oxygen atoms (Ce-O) is elongated and the unpaired electron is located over the O-Ce-O moiety including this terminal oxygen assuming that $Ce_4O_8^+$ takes a compact structure. Note that despite tremendous efforts, the most stable structure of $Ce_4O_8^+$ has not been determined to date, because several isomeric structures exist within a low-lying energy range, based on the calculations reported by Wu and coworkers.[6] Computational

investigations are required for further understanding of the thermal behavior of each $Ce_nO_{2n+x}^+$ cluster.

2.4.2. Reaction of clusters with CO

When CO gas diluted in He was introduced into the reaction gas cell, the intensity of the $Ce_5O_{10}^+$ peak decreased and the intensity of the $Ce_5O_9^+$ peak increased. This spectral change evidently indicates that CO is oxidized by the collision with $Ce_5O_{10}^+$, denoted as Reaction (2.8). If this reaction proceeds by the Langmuir-Hinshelwood mechanism, the oxidation reaction (2.8) could be broken down into some elementary steps consisting of CO adsorption on $Ce_5O_{10}^+$, Reaction (2.11), followed by CO_2 release from $Ce_5O_{10}(CO)^+$, Reaction (2.12).

$$Ce_5O_{10}^+ + CO \rightarrow Ce_5O_{10}(CO)^+. \quad (2.11)$$

$$Ce_5O_{10}(CO)^+ \rightarrow Ce_5O_9^+ + CO_2. \quad (2.12)$$

However, no signals suggesting formation of the reaction intermediate, $Ce_5O_{10}(CO)^+$, were detected above the noise level (see Figure 2.6b). Hence, Reaction (2.12) is considered to proceed much faster than Reaction (2.11), if Reactions (2.11) and (2.12) occurred sequentially. In this case, Reaction (2.11) is regarded as the rate-determining step.

In contrast, when $Ce_5O_{10}^+$ was exposed to dense CO gas (>2×10^{16} molecules cm^{-3}), the adduct, $Ce_5O_{10}(CO)^+$, was detected in the mass spectrum with sufficient intensity (see Figure 2.6d); formation of the CO adducts is slower than Reaction (2.8). Hence, it is deduced that some mechanism other than the Langmuir-Hinshelwood mechanism operates for the CO oxidation. It is highly likely that CO in the gas phase directly attacks and extracts the oxygen atom from $Ce_5O_{10}^+$, as explained by the Rideal-Eley mechanism. In fact, there is a terminal oxygen atom with an unpaired electron in $Ce_5O_{10}^+$ based on DFT calculation, which behaves as an active site.[6] The rate constants for the CO oxidation are lower on the whole, relative to those of other clusters such as those containing Rh.[24] This low reactivity of $Ce_nO_{2n}^+$ with CO gas is consistent with the previously reported experimental results and the suggested electron distributions in which the radical center, considered to play a central role in the oxidation reaction, is delocalized over the CeO_2 moiety.[6] Single collision experiments and DFT calculations show that the CO oxidation by $Ce_nO_{2n}^+$ (n = 3, 4) has a certain barrier in its reaction pathway and that is overcome by a higher collision energy.[9] By contrast, $Ce_5O_{10}^+$ has a notably higher reactivity for CO oxidation than the other $Ce_nO_{2n}^+$ species have (see Figure

2.9). The difference in the CO oxidation reactivity of $Ce_nO_{2n}^+$ between n = 3, 4 and n = 5 has not been elucidated by reported DFT calculations, but they suggested that $Ce_nO_{2n}^+$ (n = 2–5) species have a common feature in the geometric and electronic structure of the active site for CO oxidation.[6] Note that in such previous investigations,[6, 9] the nature of $Ce_5O_{10}^+$ is less examined than that of smaller species, due to their experimental or computational limitations. It is highly likely that the CO oxidation by $Ce_5O_{10}^+$ has a relatively low barrier in its reaction pathway, and $Ce_5O_{10}^+$ may possibly hold a highly localized radical site unlike $Ce_nO_{2n}^+$ (n = 2–4). Revealing detailed mechanism of $Ce_5O_{10}^+$ + CO reaction is unachieved despite its importance and further investigations are required.

2.4.3. Attachment of CO to cerium oxide clusters

When the number density of CO gas in the reaction gas cell was increased to several 10^{16} molecules cm^{-3}, CO-appended clusters, $Ce_nO_{2n+x}(CO)^+$, appeared in the mass spectrum above the noise level (see Figure 2.6c and d). $Ce_nO_{2n+x}(CO)_2^+$, containing two CO units, were also observed under higher density of CO, ~10^{18} molecules cm^{-3} (not shown in the figure). Thus CO is considered to attach to the clusters in succession as:

$$Ce_nO_{2n+x}^+ \xrightarrow{+CO} Ce_nO_{2n+x}(CO)^+ \xrightarrow{+CO} Ce_nO_{2n+x}(CO)_2^+ \quad (2.13)$$

To determine the nature of the bonding of CO to $Ce_nO_{2n+x}^+$, the $Ce_nO_{2n+x}(CO)^+$ species that were prepared by the reaction with CO in the reaction gas cell were heated in the extension tube. It was found that CO can be released from $Ce_nO_{2n+x}(CO)^+$ to generate $Ce_nO_{2n+x}^+$ below room temperature as:

$$Ce_nO_{2n+x}(CO)^+ \rightarrow Ce_nO_{2n+x}^+ + CO. \quad (2.14)$$

This finding indicates that CO is so weakly adsorbed on $Ce_nO_{2n+x}^+$ that it dissociates from the cluster during post-heating. In summary, CO oxidation (2.8) and CO attachment (2.11) occur concurrently in the reaction gas cell. Both reactions could be observed separately, because the reaction rates differ by several orders of magnitude.

2.5. Conclusion

The stable stoichiometry and the reactivity of gas-phase cerium oxide cluster ions, $Ce_nO_{2n+x}^+$, were examined based on mass spectrometry in combination with a newly developed post-heating method. It was found that $Ce_nO_{2n-1}^+$ and $Ce_nO_{2n}^+$, in which the cerium

atom and oxygen atom respectively adopt the +4 and −2 charge states, are thermally stable. The very high reactivity of the oxygen-poor $Ce_nO_{2n+x}^+$ ($x \leq -2$) species with oxygen results in uptake of oxygen atoms in the presence of oxygen molecules until $Ce_nO_{2n+x}^+$ ($x = -1$ and 0) species are formed. The oxygen-rich $Ce_nO_{2n+x}^+$ ($x \geq +1$) species are comprised of robust $Ce_nO_{2n-1}^+$ and $Ce_nO_{2n}^+$ and weakly associated oxygen molecules; the oxygen molecules are so weakly bound to the clusters that they dissociate readily upon post-heating treatment.

Evaluation of the reactivity of $Ce_nO_{2n+x}^+$ with CO molecules demonstrated that $Ce_nO_{2n}^+$ can oxidize CO to form $Ce_nO_{2n-1}^+$ and CO_2. The rate constants of the CO oxidation reactions are in the range of 10^{-12}–10^{-16} cm^3 s^{-1}, which is lower than those of Rh clusters by several orders of magnitude. This is consistent with the fact that cerium oxide is a promoter of catalysts and does not exhibit high reactivity by itself.

2.6. Appendix

2.6.1. Ion assignment and calibration method of time-of-flight mass spectrometer

A mass number, *m*/*z*, of each cluster ion was obtained from the flight time in the time-of-flight mass spectrometer (see Figure 2.1). The conversion into the mass number from the directly measured time of flight has been confirmed by measurements for atomic ions having several isotopes with intensities proportional to their natural abundances and cluster ions, Nb_n^+ and Ta_n^+, prepared in the same apparatus under the same conditions. Fine calibrations were performed using Nb_n^+ ions just before or after the main measurements. In addition, I observed ceria clusters and gold clusters coexisting in the same mass spectrum in order to address concerns over inaccuracy of mass assignment for $Ce_nO_{2n+x}^+$ ions. In reality, a ceria rod and a gold rod were ablated simultaneously by using two separate pulse lasers and the clusters thus formed were detected by the mass spectrometer. Figure 2.12 shows a mass spectrum of ceria clusters ($Ce_nO_{2n+x}^+$), gold clusters (Au_n^+), and their mixtures ($Au_mCe_nO_{2n+x}^+$). Assignment of $^{197}Au_n^+$ clusters is accurate because Au is a monoisotopic element, unlike Ce. This result supports that the main products from laser ablation of CeO_2 in this study are surely $Ce_nO_{2n+x}^+$ ions.

2.7. References

(1) Trovarelli, A. Catalytic Properties of Ceria and CeO_2-Containing Materials. *Catal. Rev.* **1996**, *38*, 439-520.

(2) Skorodumova, N.; Simak, S.; Lundqvist, B. I.; Abrikosov, I.; Johansson, B. Quantum Origin of the Oxygen Storage Capability of Ceria. *Phys. Rev. Lett.* **2002**, *89*, 166601.

(3) Jiang, Y.; Adams, J. B.; van Schilfgaarde, M.; Sharma, R.; Crozier, P. A. Theoretical Study of Environmental Dependence of Oxygen Vacancy Formation in CeO_2. *Appl. Phys. Lett.* **2005**, *87*, 141917.

(4) Carrettin, S.; Concepción, P.; Corma, A.; Lopez Nieto, J. M.; Puntes, V. F. Nanocrystalline CeO_2 Increases the Activity of Au for CO Oxidation by Two Orders of Magnitude. *Angew. Chem. Int. Ed.* **2004**, *43*, 2538-2540.

(5) Camellone, M. F.; Fabris, S. Reaction Mechanisms for the CO Oxidation on Au/CeO_2 Catalysts: Activity of Substitutional Au^{3+}/Au^{+} Cations and Deactivation of Supported Au^{+} Adatoms. *J. Am. Chem. Soc.* **2009**, *131*, 10473-10483.

(6) Wu, X.; Zhao, Y.; Xue, W.; Wang, Z.; He, S.; Ding, X. Active Sites of Stoichiometric Cerium Oxide Cations ($Ce_mO_{2m}^{+}$) Probed by Reactions with Carbon Monoxide and Small Hydrocarbon Molecules. *Phys. Chem. Chem. Phys.* **2010**, *12*, 3984-3997.

(7) Wu, X.; Ding, X.; Bai, S.; Xu, B.; He, S.; Shi, Q. Experimental and Theoretical Study of the Reactions between Cerium Oxide Cluster Anions and Carbon Monoxide: Size-Dependent Reactivity of $Ce_nO_{2n+1}^{-}$ (n = 1–21). *J. Phys. Chem. C* **2011**, *115*, 13329-13337.

(8) Hirabayashi, S.; Ichihashi, M. Oxidation of Composition-Selected Cerium Oxide Cluster Cations by O_2. *Chem. Phys. Lett.* **2013**, *564*, 16-20.

(9) Hirabayashi, S.; Ichihashi, M. Oxidation of CO and NO on Composition-Selected Cerium Oxide Cluster Cations. *J. Phys. Chem. A* **2013**, *117*, 9005-9010.

(10) Miyajima, K.; Himeno, H.; Yamada, A.; Yamamoto, H.; Mafuné, F. Nanoalloy Formation of Ta-Containing Trimetallic Small Clusters. *J. Phys. Chem. A* **2011**, *115*, 1516-1520.

(11) Sakuma, K.; Miyajima, K.; Mafuné, F. Oxidation of CO by Nickel Oxide Clusters Revealed by Post Heating. *J. Phys. Chem. A* **2013**, *117*, 3260-3265.

(12) Morita, K.; Sakuma, K.; Miyajima, K.; Mafuné, F. Thermally and Chemically Stable Mixed Valence Copper Oxide Cluster Ions Revealed by Post Heating. *J. Phys. Chem. A* **2013**, *117*, 10145-10150.

(13) Foltin, M.; Stueber, G.; Bernstein, E. On the Growth Dynamics of Neutral Vanadium Oxide and Titanium Oxide Clusters. *J. Chem. Phys.* **1999**, *111*, 9577-9586.

(14) Yin, S.; Xue, W.; Ding, X.; Wang, W.; He, S.; Ge, M. Formation, Distribution, and Structures of Oxygen-Rich Iron and Cobalt Oxide Clusters. *Int. J. Mass Spectrom.* **2009**, *281*, 72-78.

(15) Jarvis, M. J. Y.; Pisterzi, L. F.; Blagojevic, V.; Koyanagi, G. K.; Bohme, D. K. Gas-Phase Kinetic Measurements and Quantum Chemical Calculations of the Ligation of Ni^+, Cu^+, $Ni^+(Pyrrole)_{1,2}$ and $Cu^+(Pyrrole)_{1,2}$ with O_2 and CO. *Int. J. Mass Spectrom.* **2003**, *227*, 161-173.

(16) Zhao, Y.; Ding, X.; Ma, Y.; Wang, Z.; He, S. Transition Metal Oxide Clusters with Character of Oxygen-Centered Radical: A DFT Study. *Theor. Chem. Acc.* **2010**, *127*, 449-465.

(17) Zhao, Y.; Wu, X.; Ma, J.; He, S.; Ding, X. Characterization and Reactivity of Oxygen-Centred Radicals over Transition Metal Oxide Clusters. *Phys. Chem. Chem. Phys.* **2011**, *13*, 1925-1938.

(18) Burow, A. M.; Wende, T.; Sierka, M.; Włodarczyk, R.; Sauer, J.; Claes, P.; Jiang, L.; Meijer, G.; Lievens, P.; Asmis, K. R. Structures and Vibrational Spectroscopy of Partially Reduced Gas-Phase Cerium Oxide Clusters. *Phys. Chem. Chem. Phys.* **2011**, *13*, 19393-19400.

(19) Aubriet, F.; Gaumet, J.; De Jong, W. A.; Groenewold, G. S.; Gianotto, A. K.; McIlwain, M. E.; Van Stipdonk, M. J.; Leavitt, C. M. Cerium Oxyhydroxide Clusters: Formation, Structure, and Reactivity. *J. Phys. Chem. A* **2009**, *113*, 6239-6252.

(20) Gord, J.; Bemish, R.; Freiser, B. Collision-Induced Dissociation of Positive and Negative Copper Oxide Cluster Ions Generated by Direct Laser Desorption/Ionization of Copper Oxide. *Int. J. Mass Spectrom. Ion Process.* **1990**, *102*, 115-132.

(21) Aubriet, F.; Poleunis, C.; Bertrand, P. Capabilities of Static TOF-SIMS in the Differentiation of First-Row Transition Metal Oxides. *J. Mass Spectrom.* **2001**, *36*, 641-651.

(22) Aubriet, F.; Muller, J. About the Atypical Behavior of CrO_3, MoO_3, and WO_3 during their UV Laser Ablation/Ionization. *J. Phys. Chem. A* **2002**, *106*, 6053-6059.

(23) Whitfield, H.; Roman, D.; Palmer, A. X-Ray Study of the System ThO_2-CeO_2-Ce_2O_3. *J. Inorg. Nucl. Chem.* **1966**, *28*, 2817-2825.

(24) Yamada, A.; Miyajima, K.; Mafuné, F. Catalytic Reactions on Neutral Rh Oxide Clusters More Efficient than on Neutral Rh Clusters. *Phys. Chem. Chem. Phys.* **2012**, *14*, 4188-4195.

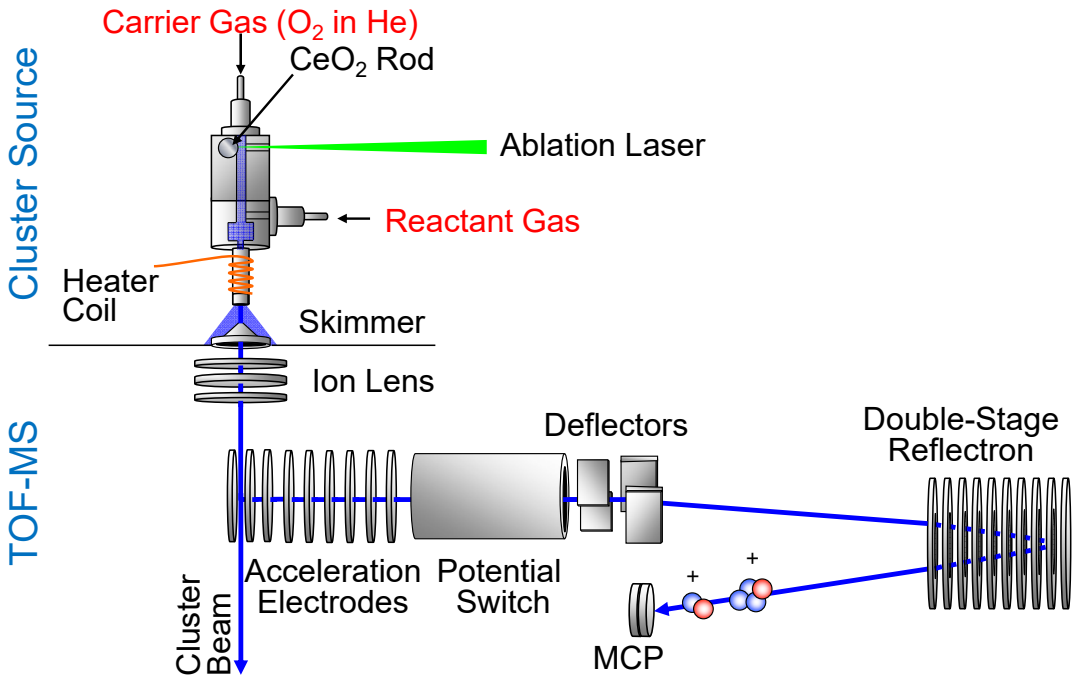

Figure 2.1. Schematic diagram of the experimental setup used in this thesis.

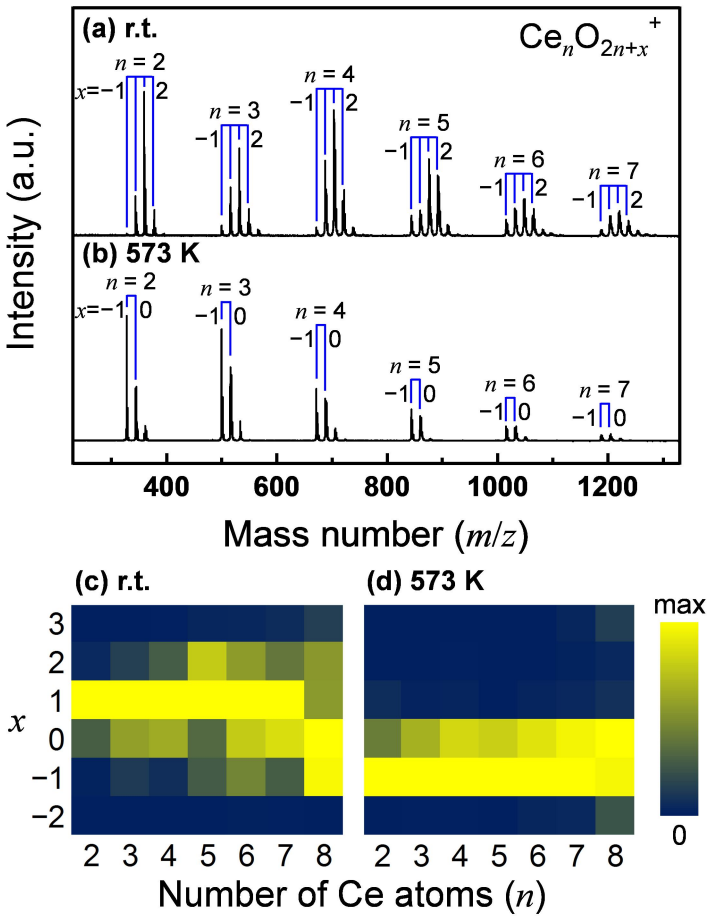

Figure 2.2. (a) Mass spectrum of $Ce_nO_{2n+x}^+$ clusters produced by laser ablation of a CeO_2 rod in the presence of O_2 gas (0.05%) diluted in He (0.8 MPa). (b) Mass spectrum of $Ce_nO_{2n+x}^+$ after heating in the extension tube set at 573 K. (c), (d) Intensities of $Ce_nO_{2n+x}^+$ illustrated as a color map for different n and x at room temperature and 573 K, respectively.

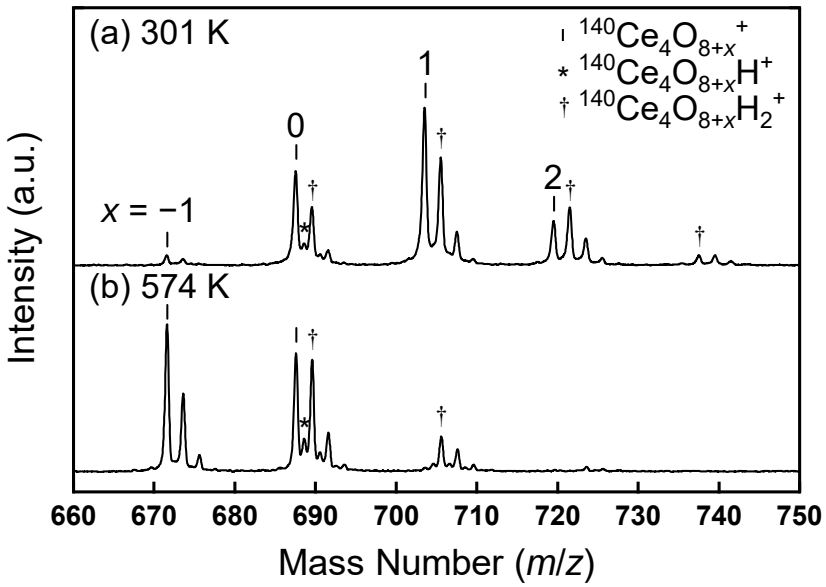

Figure 2.3. Expanded mass spectra of $Ce_4O_{8+x}^+$ (x = −1 to 2) clusters produced by laser ablation of a CeO_2 rod in the presence of O_2 gas (0.05%) diluted in He (0.8 MPa) at room temperature (a) and after heating in the extension tube set at 574 K (b). Each mass peak has satellite peaks originating from cerium isotopes (^{140}Ce:$^{142}Ce \approx 1:0.13$). Some peaks assignable to clusters containing one or two hydrogen atoms, considered to originate from residual water in the vacuum chamber, are also observed as shown in the figure. Because $^{140}Ce_nO_{2n+x}H_2^+$ peaks overlap with $^{142}Ce_nO_{2n+x}^+$ peaks, the ion intensities of $Ce_nO_{2n+x}^+$ were obtained based on the intensities of $^{140}Ce_nO_{2n+x}^+$ peaks, which are free from contributions from other ions.

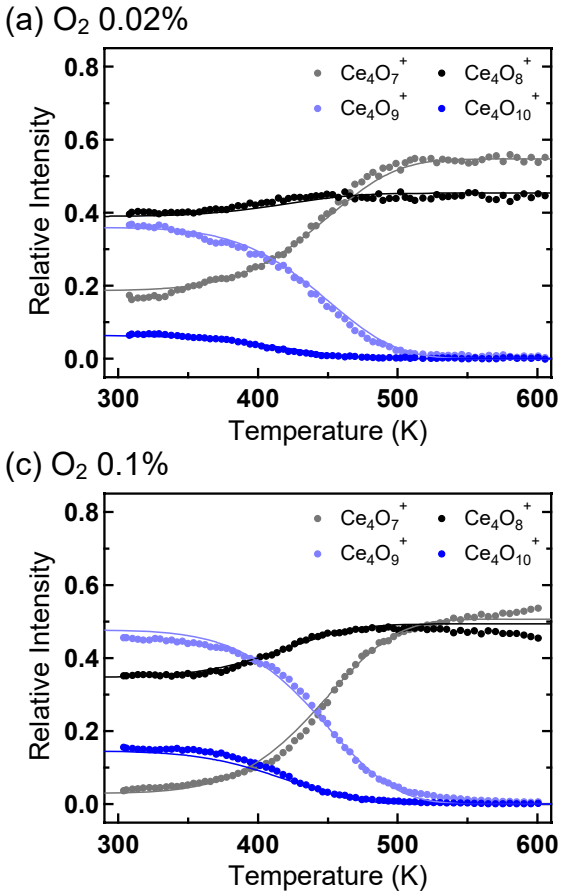

(d) T_{50}

Parent clusters	T_{50}		
	(a)	(b)	(c)
$Ce_4O_9^+$	440 K	442 K	446 K
$Ce_4O_{10}^+$	406 K	412 K	418 K

Figure 2.4. (a–c) Relative intensities of mass peaks of $Ce_4O_{7,8,9,10}^+$ produced by laser ablation of a CeO_2 rod in the presence of oxygen gas in He (0.8 MPa) as a function of temperature in the extension tube. The concentration of oxygen in He gas was varied as: (a) 0.02, (b) 0.05, and (c) 0.1%. The solid lines represent fittings based on Arrhenius equation. (d) Temperatures at which cluster ions decay by 50% are shown as T_{50} for comparison. The temperatures remain constant in the range of 0.02–0.1% oxygen, suggesting that the reverse reaction is negligible.

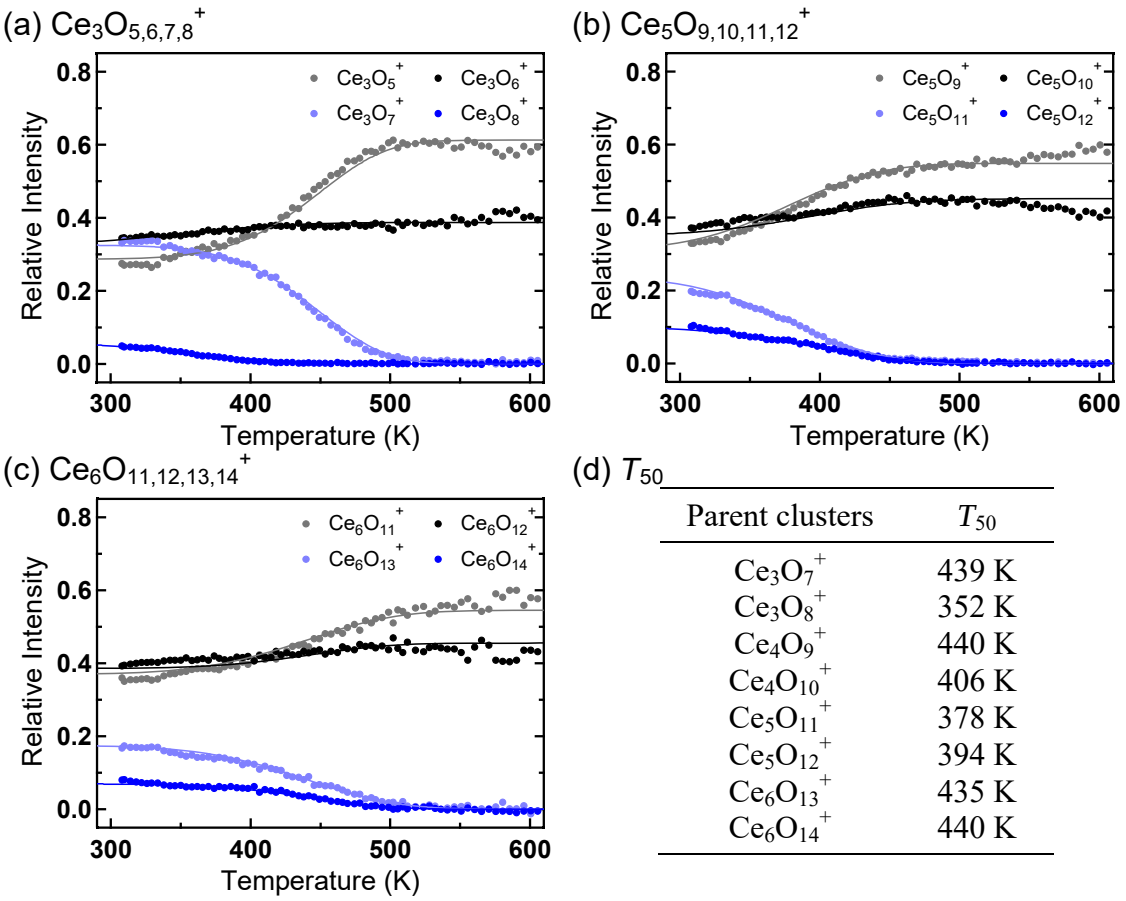

(d) T_{50}

Parent clusters	T_{50}
$Ce_3O_7^+$	439 K
$Ce_3O_8^+$	352 K
$Ce_4O_9^+$	440 K
$Ce_4O_{10}^+$	406 K
$Ce_5O_{11}^+$	378 K
$Ce_5O_{12}^+$	394 K
$Ce_6O_{13}^+$	435 K
$Ce_6O_{14}^+$	440 K

Figure 2.5. (a–c) Relative intensities of (a) $Ce_3O_{5,6,7,8}^+$, (b) $Ce_5O_{9,10,11,12}^+$, and (c) $Ce_6O_{11,12,13,14}^+$ produced by laser ablation of a CeO_2 rod in the presence of oxygen gas (0.02%) in He (0.8 MPa) as a function of temperature in the extension tube. The solid lines represent fittings based on Arrhenius equation. (d) Temperatures at which cluster ions decay by 50% are shown as T_{50}.

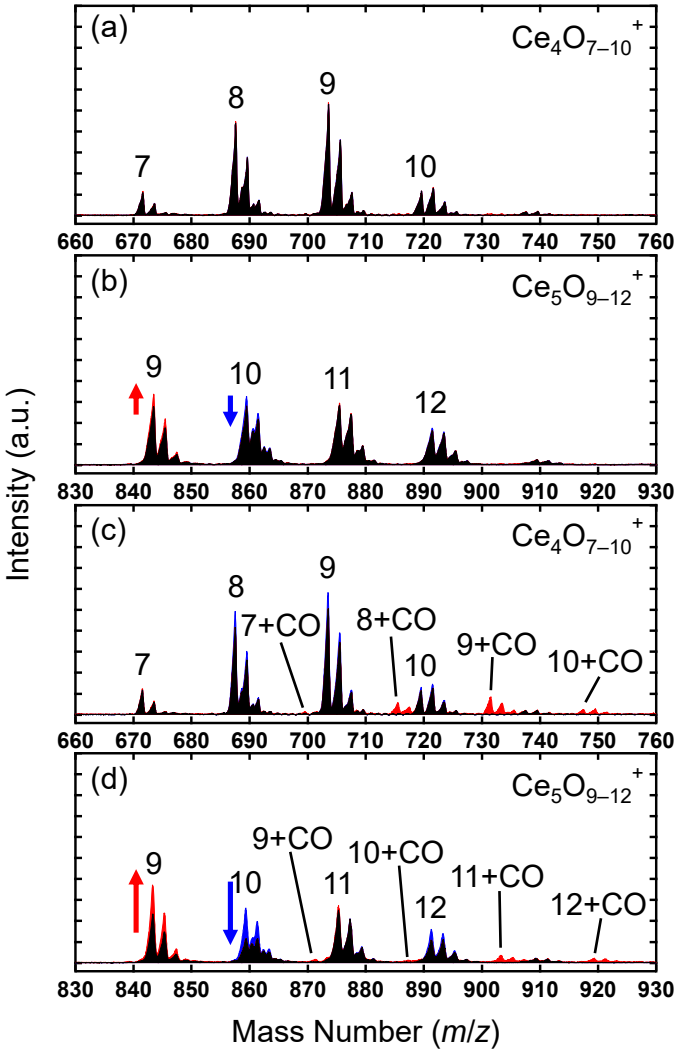

Figure 2.6. Mass spectra of (a,c) $Ce_4O_{7,8,9,10}^+$ and (b,d) $Ce_5O_{9,10,11,12}^+$ clusters after passing the reaction gas cell filled by CO diluted in He (3.5×10^{17} molecules cm^{-3}). The number density of CO in the reaction gas cell was 0 (a–d, blue), 2.6×10^{15} (a,b, red), and 4.4×10^{16} (c,d, red) molecules cm^{-3}. Overlapped areas of the ion peaks are filled with black. The signal intensities in panels (a)–(d) are not scaled and can be compared with each other directly.

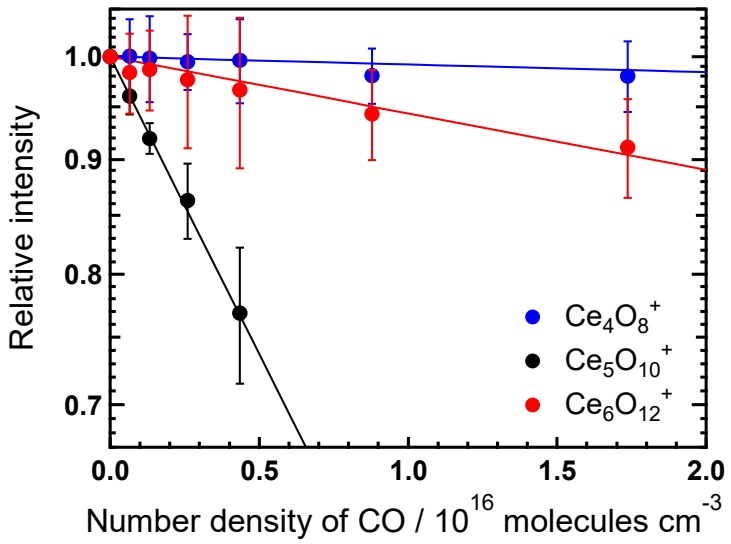

Figure 2.7. Semi-logarithmic plot of relative intensities of $Ce_nO_{2n}^+$ (n = 4, 5, 6) after reaction with CO in the reaction gas cell as a function of the number density of CO. In order to consider the CO oxidation reaction separately from the CO attachment reaction, the CO-appended clusters ($Ce_nO_{2n}(CO)^+$) are regarded as corresponding $Ce_nO_{2n}^+$ clusters in this plot. Solid lines show intensities calculated using rate constants shown in Figure 2.9.

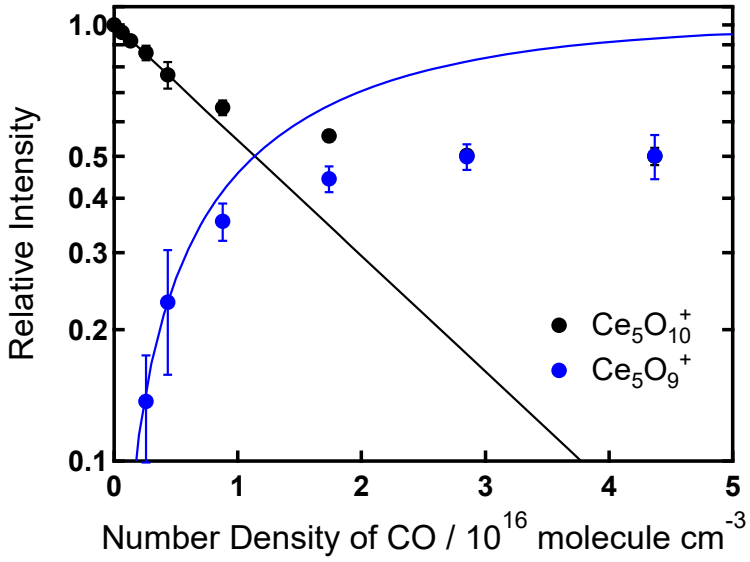

Figure 2.8. Semi-logarithmic plot of relative intensities of $Ce_5O_{10}^+$ and $Ce_5O_9^+$ after reaction with CO in the reaction gas cell as a function of the number density of CO. Here, the intensity of $Ce_5O_9^+$ was obtained by subtracting the initial intensity from the observed intensity. In order to consider the CO oxidation reaction separately from the CO attachment reaction, the CO-appended clusters ($Ce_5O_{9,10}(CO)^+$) are regarded as corresponding $Ce_5O_{9,10}^+$ clusters in this plot. Solid lines show intensities calculated using a rate constant shown in Figure 2.9 ($k = 8.7 \times 10^{-13}$ cm^3 molecules^{-1} s^{-1}).

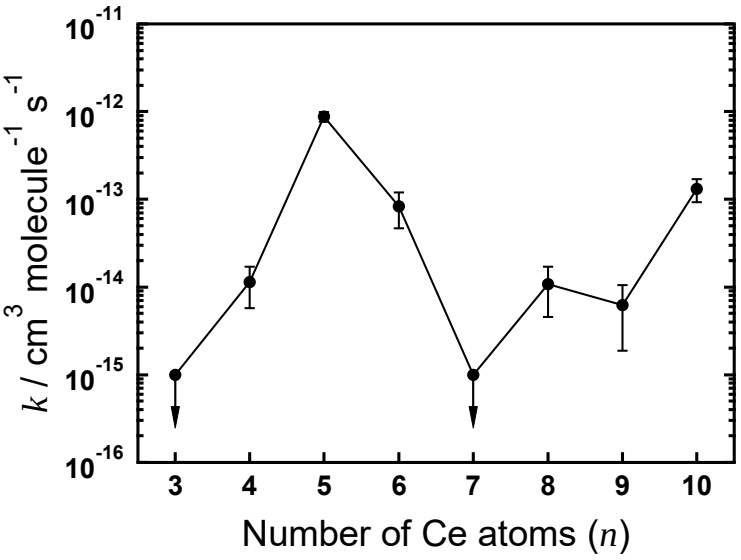

Figure 2.9. Rate constants, k, for the CO oxidation reaction, $Ce_nO_{2n}^+ + CO \rightarrow Ce_nO_{2n-1}^+ + CO_2$, as a function of the cluster size.

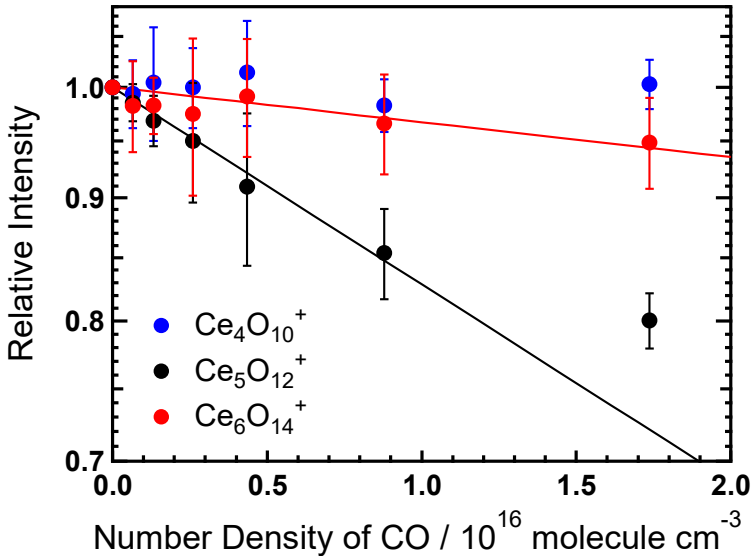

Figure 2.10. Semi-logarithmic plot of relative intensities of $Ce_nO_{2n+2}^+$ (n = 4, 5, 6) after reaction with CO in the reaction gas cell as a function of the number density of CO. In order to consider the CO oxidation reaction separately from the CO attachment reaction, the CO-appended clusters ($Ce_nO_{2n+2}(CO)^+$) are regarded as corresponding $Ce_nO_{2n+2}^+$ clusters in this plot. Solid lines show intensities calculated using rate constants $k = 2.7 \times 10^{-13}$ cm^3 molecules^{-1} s^{-1} for $Ce_5O_{12}^+$ and $k = 4.8 \times 10^{-14}$ cm^3 molecules^{-1} s^{-1} for $Ce_6O_{14}^+$. CO oxidation reaction was not observed on $Ce_4O_{10}^+$ and $Ce_nO_{2n+2}^+$ (n = 3, 7, 8, 9, 10; not shown here) beyond the noise level.

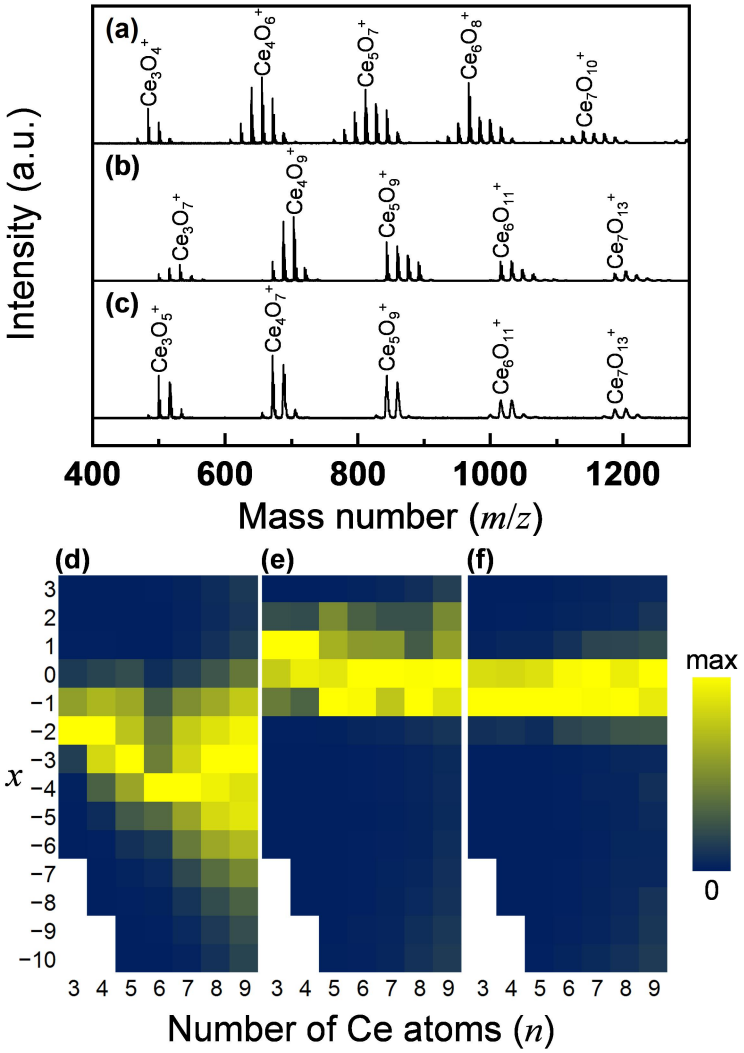

Figure 2.11. (a) Mass spectrum of $Ce_nO_{2n+x}^+$ produced by laser ablation of a cerium oxide rod in He. (b) Mass spectrum of $Ce_nO_{2n+x}^+$ after reaction with O_2 in the reaction gas cell. (c) Mass spectrum of $Ce_nO_{2n+x}^+$ after post-heating at 573 K in the extension tube. (d), (e), (f) Intensities of $Ce_nO_{2n+x}^+$ illustrated as a color map for different n and x corresponding to the mass spectra (a), (b), and (c), respectively.

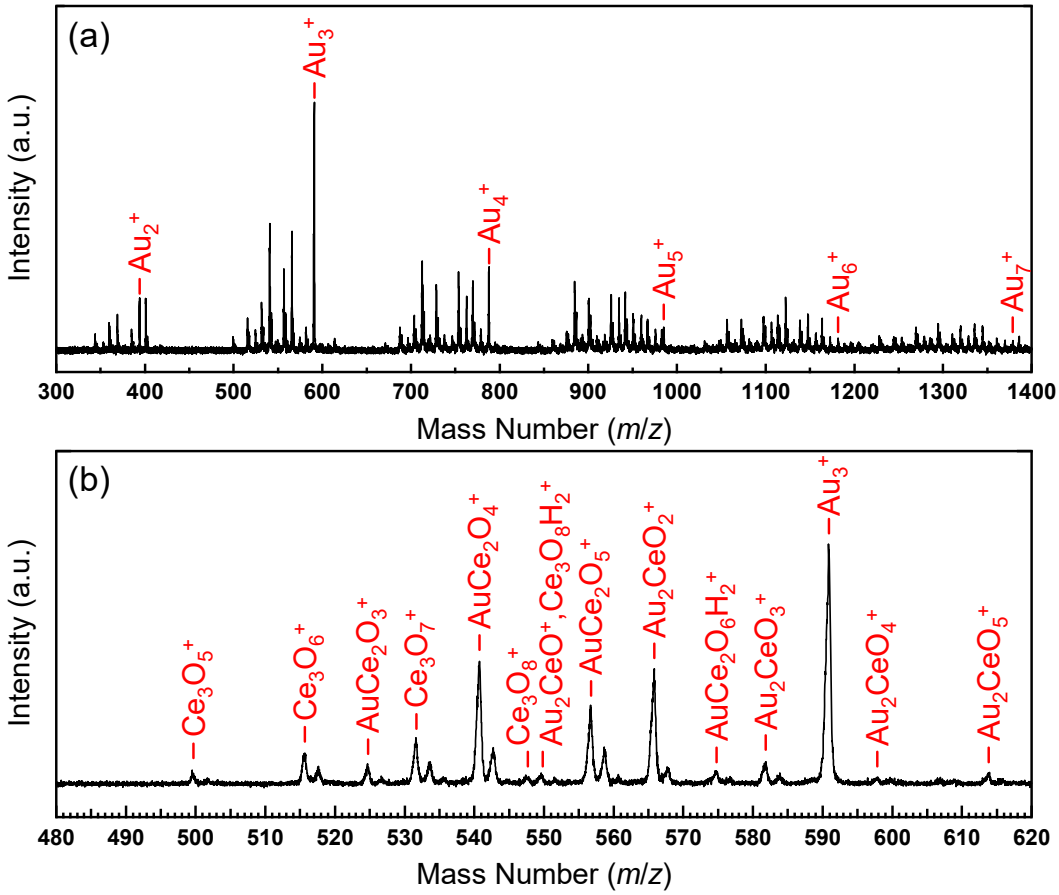

Figure 2.12. (a) Mass spectrum of ceria clusters, gold clusters, and their mixtures generated by laser ablation of CeO_2 and Au rods at the same time. (b) Expanded view of (a). Red markers show calculated positons of ions without ^{142}Ce or other minor isotopes.

Table 2.1. Activation energies for O_2 desorption from oxygen-rich cluster ions.

Clusters	E_a / eV
$Ce_3O_7^+$	0.44 ± 0.08
$Ce_3O_8^+$	0.19 ± 0.05
$Ce_4O_9^+$	0.43 ± 0.08
$Ce_4O_{10}^+$	0.38 ± 0.10
$Ce_5O_{11}^+$	0.26 ± 0.03
$Ce_5O_{12}^+$	0.25 ± 0.05
$Ce_6O_{13}^+$	0.34 ± 0.08
$Ce_6O_{14}^+$	0.4 ± 0.2

Chapter 3

Reactivity of Oxygen Deficient Cerium Oxide Clusters with Small Gaseous Molecules

Oxygen deficient cerium oxide cluster ions, $Ce_nO_m^+$ (n = 2–10, $1 \leq m \leq 2n$) were prepared in the gas phase by laser ablation of a cerium oxide rod. The reactivity of the cluster ions was investigated using mass spectrometry, finding that oxygen deficient clusters are able to extract oxygen atoms from CO, CO_2, NO, N_2O, and O_2 in the gas phase. The oxygen transfer reaction is explained in terms of the energy balance between the bond dissociation energy of an oxygen containing molecule and the oxygen affinity of the oxygen-deficient cerium oxide clusters. The reverse reaction, i.e. formation of the oxygen deficient cluster ions from the stoichiometric ones was also examined. It was found that intensive heating of the stoichiometric clusters results in formation of oxygen deficient clusters via $Ce_nO_{2n}^+ \rightarrow Ce_nO_{2n-2}^+ + O_2$ which was found to occur at different temperatures depending on cluster size, n.

(Reproduced in part with permission from T. Nagata et al., *J. Phys. Chem. A* **2015**, *119*, 5545–5552. Copyright 2015 American Chemical Society.)

3.1. Introduction

Cerium oxide (ceria) is one of the most important rare earth oxides and is widely used as an active component or supporting material in many catalytic reactions, such as water-gas shift, steam reforming, and oxidation reactions.[1] The most prevalent application of ceria is as a support in automotive three-way catalysts (TWC) due to its oxygen storage capacity (OSC), i.e. ceria can take and release oxygen during the catalytic reactions.[2-5] This ability originates from the transition between two oxidation states of cerium atoms, $Ce^{3+} \leftrightarrow Ce^{4+}$, in response to a change in the surrounding redox potential. Understanding the reaction mechanism is important to improve performance of catalysts. Many investigations on the nature of the reaction center in ceria-based catalysts have been reported,[6-13] which shows that partially reduced ceria contains an oxygen vacancy and a reduced cerium atom (Ce^{3+}) is highly reactive and plays a central role in redox reactions. Partially reduced ceria, i.e. nonstoichiometric cerium oxide (CeO_{2-x}), has also been intensively investigated.[14-18] These studies show that reduced cerium oxide is unstable; the equilibrium pressure of oxygen on CeO_2 is $\sim 10^{-40}$ atm at 573 K, indicating that the equilibrium completely shifts to the fully oxidized state under realistic conditions.[18] Even so, the reduced state is likely to exist on a surface of ceria or in an interface between ceria and supported material, where Ce^{3+} is considered to be stabilized.[8, 9, 19-24] The stability and abundance of Ce^{3+} in ceria-based material can be modified by the size and preparation method of ceria nanoparticles and transition metal doping.[14, 15, 19, 20, 25-27] The high reactivity of reduced ceria is advantageous to industrial applications. For example, nonstoichiometric cerium oxide promotes the thermal dissociation of water and carbon dioxide, which is a key reaction of solar-driven chemical fuel production.[28] Consequently, nonstoichiometric cerium oxide is an important subject of research.

My interest lies in sub-nanometer sized particles of cerium oxide in the gas phase. Isolated ceria clusters composed of a few cerium atoms and oxygen atoms have been studied, both experimentally and computationally.[29-36] Ceria clusters with stoichiometric compositions, i.e. $Ce_nO_{2n}^+$ and $Ce_nO_{2n+1}^-$, are known to oxidize small molecules.[31-33, 35] Ionized ceria clusters have an oxygen centered radical, which works as an active site of redox reactions.[37, 38] The radical is more localized in anionic ceria clusters, which results in a higher reactivity than cationic clusters.[31, 32] Collision-energy dependence of reactivity revealed that the reaction energetics differ with reactant molecules; CO oxidation has a small barrier in its reaction

pathway, whereas NO oxidation progressed without an activation barrier.[35] Oxygen deficient clusters have also been studied; structures of the clusters, $Ce_2O_2^+$, $Ce_3O_4^+$, and $(CeO_2)_mCeO^+$ (m = 0–4), have been determined by a combination of DFT calculations and infrared vibrational spectroscopy[39] and concluded to be similar to a part of the structure of bulk ceria. Thus, such clusters can be considered as models for ceria-based catalysts. Oxidation reactions of cerium oxide cluster cations by O_2 under a single collision condition have been reported.[34] The reaction products depend on an average oxidation number (AON) of Ce atoms in the cluster, which is defined as $(2m+1)/n$ for $Ce_nO_m^+$; O_2-capturing for $3 \leq \text{AON} < 3.5$, generation of atomic oxygen radial and/or fragmentation for AON < 3, and no reaction for AON ≈ 4 (near-stoichiometric) were observed.

In Chapter 2, the stoichiometry and the reactivity of stable cerium oxide cluster cations ($Ce_nO_{2n+x}^+$) were examined by mass spectrometry using a newly developed post-heating device. $Ce_nO_{2n+x}^+$ (x = −1, 0) species are found to be thermally stable after heating up to 600 K, where the Ce and O atoms hold +4 and −2 charge states, respectively; these are considered to be of stable stoichiometry. Oxygen-rich clusters, $Ce_nO_{2n+x}^+$ ($x \geq +1$), release oxygen molecules upon heating (< 600 K), resulting in exclusive generation of $Ce_nO_{2n+x}^+$ (x = −1, 0) compositions. These oxygen-rich clusters are considered to be robust stoichiometric ceria clusters associated with weakly bound oxygen molecules. Clusters with reduced compositions, $Ce_nO_{2n+x}^+$ ($x \leq -2$), are highly reactive with oxygen; they are oxidized by O_2 to stoichiometric and oxygen-rich compositions ($x \geq -1$), and once stoichiometric clusters are formed they do not reform oxygen deficient species, $Ce_nO_{2n+x}^+$ ($x \leq -2$), even under post-heating treatment (~600 K). Behaviors of cerium oxide clusters in a reductive atmosphere have also been observed. $Ce_nO_{2n}^+$ can release one oxygen atom to form $Ce_nO_{2n-1}^+$ by the reaction with CO and then CO is oxidized to be CO_2. The reactivity with CO is size dependent; $Ce_nO_{2n}^+$ (n = 5, 6, 10) are particularly reactive compared to others. In addition, no $Ce_nO_{2n-2}^+$ formation was observed, which supports the stability of stoichiometric ceria clusters composed of atoms in Ce^{4+} and O^{2-} charge states.

In this chapter, I focus my attention on oxygen-deficient cerium oxide clusters. The reactivity of clusters with various degrees of oxygen-deficiency is examined with small gaseous molecules containing oxygen atoms. Oxygen atom extraction by the oxygen-deficient clusters is dominant and the reactivity is elucidated in terms of the oxygen affinity of each

cluster. In addition, I examine the reverse reaction, formation of the oxygen deficient clusters from the stoichiometric species by heating to 1000 K.

3.2. Experimental section

The experimental setup used in this chapter is similar to that shown in Chapter 2, therefore brief descriptions are given below. Cerium oxide clusters are prepared by laser ablation of a cerium oxide (CeO_2) rod (Rare Metallic Co., Ltd., 99.9%) using the focused second harmonic of a Nd:YAG pulse laser at a typical pulse energy of 10 mJ in the presence of oxygen (0–0.02%; Japan Fine Products Co., Ltd., >99.9% purity) diluted in helium (0.5–0.8 MPa; Japan Fine Products Co., Ltd., >99.99995%) as a carrier gas. The clusters are formed in a gas flow from a pulsed valve and then passed through a reaction gas cell (2 mm diameter, 60 mm long), where reactant gas (0–10%) diluted by He was injected using another pulsed valve. A control experiment was performed using only He as a reactant. Typical gas density inside the reaction gas cell is estimated to be ~10^{18} molecules cm^{-3}. The residence time of the cluster ions in the reaction gas cell is estimated to be ~70 μs. After the reaction gas cell, the cluster ions are introduced into an extension tube (4 mm diameter, 120 mm long) before expansion into a vacuum chamber. The temperature of the extension tube is controlled in the range of 298–1000 K by a PID programmable controller (Omron, E5CN-HT) using a resistive heater and monitored with a thermocouple (type K). The residence time of the cluster ions and the density of the He gas in the extension tube are estimated to be ~100 μs and 10^{17} molecules cm^{-3}, respectively. Hence, thermal equilibrium of the clusters is achieved by collisions with the He carrier gas well before expansion into the vacuum. In this experimental setup, the reaction of the clusters with small molecules occurs in the reaction gas cell, which is maintained at room temperature and then the clusters are heated at the extension tube (post-heating[40, 41]).

The cluster ions gain kinetic energy of ~3.5 keV in the acceleration region for the mass analysis. After traveling in a 1 m field-free region, the ions are reversed by the dual-stage reflectron and detected using a Hamamatsu double-microchannel plate detector. Signals from the detector are amplified with a 350 MHz preamplifier (Stanford Research Systems, SR445A) and digitized using an oscilloscope (LeCroy, LT344L). Averaged TOF spectra (typically 500 sweeps) were sent to a computer for analysis. The mass resolution $m/\Delta m$ was ~1000, which was sufficient to estimate the ion intensity of each cluster.

3.3. Results

Figure 3.1a displays the mass spectrum of nascent cationic cerium oxide clusters produced by laser ablation of CeO_2 in He. Ion peaks assignable to $Ce_nO_m^+$ (n = 2–10, $m \leq 2n$) are observed in the spectrum. Abundances of cerium oxide clusters are plotted as a color map in Figure 3.1b. The yellow colored region just below a n:m = 2:3 line indicates abundant cerium oxide clusters. The number of oxygen atoms, m, attached to cerium atoms, n, ranges in $m < 1.5n$, which suggests a preference for oxygen atoms to have a −2 charge and cerium atoms to have a +3 charge or less in the cluster.

In Chapter 2, I prepared cerium oxide clusters, $Ce_nO_{2n+x}^+$ (n = 2–9, x = −1 to +2) in the presence of oxygen gas diluted by He and found that $Ce_nO_{2n}^+$ and $Ce_nO_{2n-1}^+$ are thermally stable. Considering that the oxygen and cerium atoms take −2 and +4 charge states, respectively, $Ce_nO_{2n}^+$ and $Ce_nO_{2n-1}^+$ are regarded as "stoichiometric". In comparison, $Ce_nO_m^+$ (n = 2–10, $m < 2n-1$) produced in the present study are considered as "oxygen-deficient" clusters with respect to the stoichiometric clusters.

Figure 3.2a shows a mass spectrum after the reaction of cerium oxide with CO_2 (2.5%, diluted in He) in the reaction gas cell. It is seen that the oxygen deficient clusters disappear and clusters with more oxygen atoms increase in intensity. For example, at n = 3, the nascent $Ce_3O_{1-3}^+$ clusters mostly disappear, whereas $Ce_3O_4^+$ increases in intensity. A similar change was observed to occur for different n between $Ce_4O_5^+$ and $Ce_4O_6^+$, $Ce_5O_5^+$ and $Ce_5O_6^+$, $Ce_6O_7^+$ and $Ce_6O_8^+$, and between $Ce_7O_9^+$ and $Ce_7O_{10}^+$; the product clusters locate around the line of 2:3 as shown in Figure 3.2b. The disappearance of the oxygen deficient clusters can be interpreted as the clusters extracting oxygen from CO_2 to form cerium oxide clusters with more oxygen atoms.

I have also observed similar chemical reactions with other small molecules (Figure 3.3). Figure 3.4 summarizes the abundances of cerium oxide clusters before and after reactions with CO, CO_2, NO, N_2O and O_2 represented as color maps (detail is shown in Figures 3.5–3.8. It is seen that CO_2, NO, and N_2O are able to oxidize the oxygen deficient clusters until the ratio of the Ce and O atoms reaches about 2:3 (see also Figure 3.9). It is seen that O_2 is able to further oxidize the oxygen deficient clusters until the ratio becomes about 1:2. This suggests that cerium oxide clusters are oxidized by CO_2, NO, and N_2O until Ce atoms have a +3 charge state, whereas they are oxidized by O_2 until they have a +4 charge

state. For CO, oxidation of clusters was not observed distinctly, suggesting that the reactivity is less than the other reactants. In this relation, I prepared highly oxygen deficient clusters ($Ce_nO_m^+$; $m < n$) using CeO_2 and metallic Ce rods simultaneously for the laser ablation, and observed the reactions with CO. Oxygen deficient clusters were found to be oxidized by CO until the ratio of the Ce and O atoms reaches about 2:3 (Figure 3.10).

Reactions with small molecules suggest that oxygen deficient cerium oxide clusters should have such a high oxygen affinity that they are able to extract oxygen atoms. Let me focus on $Ce_3O_m^+$ series. Based on the fact that $Ce_3O_3^+$ disappeared (except the case of CO) and $Ce_3O_4^+$ remained (except the case of O_2) after reactions, highly oxygen deficient clusters (m = 0–3) are thought to have high oxygen affinity compared to $Ce_3O_m^+$ (m = 4, 5). Such a difference in the affinity between $Ce_3O_{0–3}^+$ and $Ce_3O_{4,5}^+$ is considered to originate from a charge state of cerium atoms: Formally, $Ce_3O_5^+$ has two Ce^{4+} and one Ce^{3+}, and $Ce_3O_4^+$ has three Ce^{3+}.[39] In contrast, $Ce_3O_{0–3}^+$ have highly reduced Ce^{2+} or even more reduced Ce atoms, which results in a high oxygen affinity. In Chapter 2, it was revealed that the stable valence state of Ce atoms in cerium oxide clusters is Ce^{4+}. Here, Ce^{3+} is also regarded as being stable to a certain extent, even though the stability would be less than Ce^{4+}.

As shown above, oxygen-deficient cerium oxide clusters are reactive with molecules containing an oxygen atom. Chapter 2 has shown that once stoichiometric and oxygen-rich clusters are formed, the oxygen deficient clusters are not formed even in a reducing atmosphere containing CO. This raises the question of whether oxygen-deficient cerium oxide clusters can be formed by releasing molecular oxygen when stoichiometric clusters are heated. Figure 3.11 shows the relative intensities of oxygen rich and stoichiometric cerium oxide clusters prepared in the cluster source by mixing oxygen (0.02%) in helium (0.8 MPa) as a carrier gas and then heated to various temperatures in an extension tube. Figure 3.12 shows representative mass spectra during the heating experiment. Here, the relative intensities determined by normalizing the total intensity of $Ce_3O_m^+$ (m = 4–8) clusters to one. It is clearly seen that as the temperature rises to 450 K, the intensity of $Ce_3O_7^+$ decreases and the intensity of $Ce_3O_5^+$ increases. As the temperature rises further to 850 K, oxygen deficient $Ce_3O_4^+$ starts to appear at the expense of $Ce_3O_6^+$. Clearly, oxygen deficient clusters are able to be prepared when heated to high temperature.

3.4. Discussion

3.4.1. Oxidation reactions of oxygen-deficient cerium oxide clusters

As described above, some of the oxygen deficient clusters, $Ce_nO_m^+$ ($m < 2n$), disappear in the mass spectrum and others increase following reaction with oxygen containing molecules, indicating that oxygen deficient $Ce_nO_m^+$ can be oxidized to form clusters with more oxygen atoms. An oxygen atom is considered to be extracted by $Ce_nO_m^+$ as:

$$Ce_nO_m^+ + XO \rightarrow Ce_nO_{m+1}^+ + X \quad (3.1)$$

where XO = CO, CO_2, NO, N_2O or O_2. The bond dissociation energy of CO_2 is endothermic:[42]

$$CO_2 \rightarrow CO + O \qquad \Delta E = 5.5 \text{ eV} \quad (3.2)$$

and reaction (3.1) is only allowed when the oxygen affinity of $Ce_nO_m^+$ exceeds 5.5 eV. For example, $Ce_3O_{0,1,2,3}^+$ clusters disappear and $Ce_3O_4^+$ increases in intensity (Figure 3.4c), indicating that the oxygen affinity of $Ce_3O_m^+$ is higher than 5.5 eV for $m \leq 3$, so that $Ce_3O_{0,1,2,3}^+$ reacts with CO_2 sequentially until $Ce_3O_4^+$ is finally formed.

A similar mechanism holds for NO, where the bond dissociation energy of NO is given by:[42]

$$NO \rightarrow N + O \qquad \Delta E = 6.5 \text{ eV} \quad (3.3)$$

Hence, reaction (3.1) is expected to occur as far as the oxygen affinity of $Ce_nO_m^+$ exceeds 6.5 eV and it is observed that $Ce_3O_m^+$ ($m \leq 3$) disappears and $Ce_3O_4^+$ is produced. However, formation of $Ce_3O_5^+$ is also observed and cannot be explained by the energy balance, because the bond dissociation energy of NO is higher than CO_2 (6.5 eV > 5.5 eV). It is likely that other mechanism can operate for the formation of $Ce_3O_5^+$. A possible pathway includes two NO molecules followed by N_2 release, as:

$$Ce_nO_m^+ + NO \rightleftarrows Ce_nO_m(NO)^+ \quad (3.4a)$$

$$Ce_nO_m(NO)^+ + NO \rightleftarrows Ce_nO_m(NO)_2^+ \rightarrow Ce_nO_{m+2}^+ + N_2 \quad (3.4b)$$

In fact, peaks assignable to NO attached species, $Ce_nO_m^+(NO)$, were observed after reaction with NO (see Figure 3.7). The N-N bond formation (ΔE = −9.8 eV, $^1\Sigma_g^+$) is highly exothermic.[42] If the sum of the oxygen affinities for $Ce_3O_3^+$ and $Ce_3O_4^+$ and N-N bond formation energy exceeds that of two NO bond dissociation energies (6.5 eV × 2), $Ce_3O_5^+$ production is energetically allowed via this pathway.

A similar sequential reaction scheme can be applied to CO. The bond dissociation energy of CO in the gas phase is 11.2 eV,[42] and hence, oxygen extraction from CO with an accompanying release of C atom into the gas phase i.e.:

$$Ce_nO_m^+ + CO \rightarrow Ce_nO_{m+1}^+ + C \quad (3.5)$$

requires the oxygen affinity higher than 11.2 eV. Instead, sequential reaction scheme in which two CO molecules are involved as:

$$Ce_nO_m^+ + CO \rightleftarrows Ce_nO_m(CO)^+ \quad (3.6a)$$

$$Ce_nO_m(CO)^+ + CO \rightleftarrows Ce_nO_m(CO)_2^+ \rightarrow Ce_nO_{m+2}^+ + C_2 \quad (3.6b)$$

can explain oxidation of $Ce_nO_m^+$ clusters even if they have less affinity. It is well known that C_2 is a stable species in the gas phase with a bond energy of 6.2 eV ($^1\Sigma_g^+$).[42] In this reaction scheme, the reaction can proceed when the sum of the oxygen affinities of two adjacent $Ce_nO_m^+$ and $Ce_nO_{m+1}^+$ exceed 16.1 eV, which equals to double dissociation energy (22.3 eV) minus bond energy of C_2 (6.2 eV).

The bond dissociation energy of O_2 is given by:[42]

$$O_2 \rightarrow O + O \qquad \Delta E = 5.2 \text{ eV} \quad (3.7)$$

Hence, reaction (3.1) can occur releasing atomic oxygen into the gas phase, at least until $Ce_3O_4^+$ is formed, because the bond dissociation energy of O_2 is lower than that of CO_2. In addition, two oxygen atoms are able to be incorporated specifically for an oxygen molecule. Hence, the reaction is expected to proceed when the total oxygen affinities of $Ce_nO_m^+$ and $Ce_nO_{m+1}^+$ exceeds 5.2 eV, which is why the clusters are completely oxidized to form Ce:O ≈ 1:2 species.

The bond dissociation energy of N_2O is given by:[42]

$$N_2O \rightarrow N_2 + O \qquad \Delta E = 1.7 \text{ eV} \quad (3.8)$$

According to the energy balance, each $Ce_3O_m^+$ (m = 0–5) could extract an oxygen atom from N_2O, because the reaction with O_2 produces $Ce_3O_7^+$, indicating the average oxygen affinity of $Ce_3O_5^+$ and $Ce_3O_6^+$ is higher than 2.6 eV (5.2 eV / 2), and $Ce_3O_5^+$ is likely to have the oxygen affinity higher than full-oxidized $Ce_3O_6^+$. However, the experimental result shows that $Ce_3O_m^+$ ($m \leq 3$) disappear after reaction with N_2O, whereas $Ce_3O_4^+$ remains and no further oxidation is observed (Figure 3.4e). In this case, it is likely that oxygen extraction by $Ce_3O_4^+$ is hampered by a barrier on its reaction pathway.

As discussed above, the oxygen transfer reaction can be generally explained in terms of the energy balance between the bond dissociation energy of the oxygen containing molecule and the oxygen affinity of the oxygen deficient cerium oxide clusters. In addition, the degree of oxidation of cerium oxide clusters after reaction can be controlled by choosing a molecule with a particular bond dissociation energy.

3.4.2. Formation of oxygen deficient clusters by heat

In the presence of oxygen, cerium oxide clusters are significantly oxidized and even clusters with >1:2 stoichiometry are formed (Figure 3.12). For n = 3, for instance, $Ce_3O_{5,6,7,8}^+$ appear in the mass spectrum. The excess oxygen atoms are attached rather weakly to the clusters, because an oxygen molecule can be released, as shown in Figure 3.11. These intensity changes are observed for all cluster sizes, n, although the transition temperature depends on n. The concomitant intensity changes indicate that oxygen molecules are released from $Ce_nO_{2n+2}^+$ and $Ce_nO_{2n+1}^+$ as:

$$Ce_nO_{2n+2}^+ \rightarrow Ce_nO_{2n}^+ + O_2 \quad (3.9)$$

$$Ce_nO_{2n+1}^+ \rightarrow Ce_nO_{2n-1}^+ + O_2 \quad (3.10)$$

I further highlight that Figure 3.11 shows the decrease of $Ce_3O_6^+$ and increase of $Ce_3O_4^+$ at ≥800 K, i.e. loss of O_2 from stoichiometric $Ce_3O_6^+$.

$$Ce_nO_{2n}^+ \rightarrow Ce_nO_{2n-2}^+ + O_2 \quad (3.11)$$

The formation temperature is estimated for different sized clusters (see Figure 3.13a). Here, the formation temperature, T_{50}, is defined as the temperature at which 50% of $Ce_nO_{2n}^+$ has been changed into $Ce_nO_{2n-2}^+$ and depends on the size, n. Oxygen release from $Ce_nO_{2n}^+$ (n = 6–9) occurs at a lower temperature than from $Ce_nO_{2n}^+$ (n = 2–5), and there is a gap between n = 5 and n = 6.

From the intensity change as a function of temperature, I estimated an activation energy, E_a, of reaction (3.11) for each $Ce_nO_{2n}^+$ cluster based on Arrhenius equation (3.12), as described in Chapter 2.

$$k(T) = A \exp\left(-\frac{E_a}{k_B T}\right) \quad (3.12)$$

where k, A, E_a, k_B, and T are the rate constant of unimolecular O_2 release, the pre-exponential

factor of the Arrhenius equation, the activation energy, the Boltzmann constant, and the temperature, respectively. The intensity of $Ce_nO_{2n}^+$ after oxygen release is given by:

$$\frac{I}{I_0} = \exp(-kt) \tag{3.13}$$

where I is the intensity after reaction, I_0 is the initial intensity, and t is the reaction time. Thus the temperature dependence in the intensity of $Ce_nO_{2n}^+$ is obtained by combining equations (3.12) and (3.13) as:

$$\frac{I}{I_0}(T) = \exp\left(-At\,\exp\left(-\frac{E_a}{k_B T}\right)\right) \tag{3.14}$$

In equation (3.14), t is set to be 100 μs, which is the residence time of the cluster ions in the extension tube, and A and E_a are parameters. The estimated activation energy of O_2 release from $Ce_nO_{2n}^+$ (n = 3–8) lies around 0.8–1.5 eV as shown in Figure 3.13b. The uncertainty of activation energy is ~0.1 eV for each n. The activation energy for $Ce_3O_6^+$ is 1.4 eV, which is consistent with a result of collision induced dissociation, from which the energy required for release of O_2 from $Ce_3O_6^+$ is estimated at 1.41 ± 0.19 eV.[34]

3.4.3. Uptake and release of an oxygen molecule by cerium oxide clusters

As discussed in the previous section, an oxygen deficient cerium oxide cluster reacts with an oxygen-containing molecule and can extract the oxygen atom(s) from one or two molecules. As a result, cerium oxide clusters are produced which possess more oxygen atoms than the nascent clusters. However, the clusters thus produced are not reactive anymore, because they do not have sufficient oxygen affinities that exceed the bond dissociation energy, X–O, of the molecule of interest. In order to recover this reactivity, oxygen atoms need to be removed from the cerium oxide cluster.

In the present study, I find that an oxygen deficient $Ce_nO_{2n-2}^+$ is formed by heating the stoichiometric cluster, $Ce_nO_{2n}^+$, at T > 800 K. Hence, uptake and release of oxygen atoms,

$$Ce_nO_{2n-2}^+ + O_2 \rightarrow Ce_nO_{2n}^+ \qquad \text{uptake by reaction} \tag{3.15}$$

$$Ce_nO_{2n}^+ \rightarrow Ce_nO_{2n-2}^+ + O_2 \qquad \text{release by heat} \tag{3.16}$$

occur repeatedly. As shown in Figure 3.13, the formation temperature changes depending on the cluster size. The dependence can be interpreted such that the formation temperature is higher than 900 K for $n \leq 5$ and is lower than 850 K for $n \geq 6$. I have never observed further

release of oxygen atoms by heat forming $Ce_nO_{2n-3}^+$, suggesting that its activation energy is higher than that available at 1000 K.

3.5. Conclusion

Oxygen deficient cerium oxide cluster ions, $Ce_nO_m^+$ (n = 2–10, $m \leq 2n$) were prepared in the gas phase by laser ablation of a cerium oxide rod. The reactivity of the cluster ions was investigated using mass spectrometry: The oxygen deficient clusters are able to extract oxygen atoms from CO, CO_2, NO, N_2O, and O_2 in the gas phase. The oxygen transfer reactions are explained in terms of the energy balance between the bond dissociation energy of the oxygen-containing molecule and the oxygen affinity of the oxygen-deficient cerium oxide cluster. The extent of oxidation of cerium oxide clusters after reaction can be controlled by choosing a molecule with a particular bond dissociation energy.

Formation of oxygen deficient cluster ions was also investigated by heating the stoichiometric cluster ions. It was found that intensive heating (T > 800 K) results in formation of oxygen deficient clusters as $Ce_nO_{2n}^+ \rightarrow Ce_nO_{2n-2}^+ + O_2$. The activation energy of the O_2 release was estimated from the temperature dependence to be around 0.8–1.5 eV, depending on the cluster size n. The activation energy is higher than the energy calculated from the bond dissociation energies, suggesting that the transition state has a distorted structure, which causes an activation barrier for molecular O_2 formation.

3.6. References

(1) Trovarelli, A. Catalytic Properties of Ceria and CeO_2-Containing Materials. *Catal. Rev.* **1996**, *38*, 439-520.

(2) Fritz, A.; Pitchon, V. The Current State of Research on Automotive Lean NO_x Catalysis. *Appl. Catal. B-Environ.* **1997**, *13*, 1-25.

(3) Skorodumova, N.; Simak, S.; Lundqvist, B. I.; Abrikosov, I.; Johansson, B. Quantum Origin of the Oxygen Storage Capability of Ceria. *Phys. Rev. Lett.* **2002**, *89*, 166601.

(4) Jiang, Y.; Adams, J. B.; van Schilfgaarde, M.; Sharma, R.; Crozier, P. A. Theoretical Study of Environmental Dependence of Oxygen Vacancy Formation in CeO_2. *Appl. Phys. Lett.* **2005**, *87*, 141917.

(5) Yao, H.; Yao, Y. Ceria in Automotive Exhaust Catalysts: I. Oxygen Storage. *J. Catal.* **1984**, *86*, 254-265.

(6) Breysse, M.; Guenin, M.; Claudel, B.; Latreille, H.; Véron, J. Catalysis of Carbon Monoxide Oxidation by Cerium Dioxide: I. Correlations between Catalytic Activity and Electrical Conductivity. *J. Catal.* **1972**, *27*, 275-280.

(7) Breysse, M.; Guenin, M.; Claudel, B.; Véron, J. Catalysis of Carbon Monoxide Oxidation by Cerium Dioxide: II. Microcalorimetric Investigation of Adsorption and Catalysis. *J. Catal.* **1973**, *28*, 54-62.

(8) Cargnello, M.; Doan-Nguyen, V. V. T.; Gordon, T. R.; Diaz, R. E.; Stach, E. A.; Gorte, R. J.; Fornasiero, P.; Murray, C. B. Control of Metal Nanocrystal Size Reveals Metal-Support Interface Role for Ceria Catalysts. *Science* **2013**, *341*, 771-773.

(9) Nagai, Y.; Dohmae, K.; Nishimura, Y. F.; Kato, H.; Hirata, H.; Takahashi, N. *Operando* XAFS Study of Catalytic NO Reduction Over Cu/CeO_2: The Effect of Copper-Ceria Interaction Under Periodic Operation. *Phys. Chem. Chem. Phys.* **2013**, *15*, 8461-8465.

(10) Li, C.; Sakata, Y.; Arai, T.; Domen, K.; Maruya, K.; Onishi, T. Carbon Monoxide and Carbon Dioxide Adsorption on Cerium Oxide Studied by Fourier-Transform Infrared Spectroscopy. Part 1.-Formation of Carbonate Species on Dehydroxylated CeO_2, at Room Temperature. *J. Chem. Soc., Faraday Trans. 1* **1989**, *85*, 929-943.

(11) Li, C.; Sakata, Y.; Arai, T.; Domen, K.; Maruya, K.; Onishi, T. Adsorption of Carbon Monoxide and Carbon Dioxide on Cerium Oxide Studied by Fourier-Transform Infrared Spectroscopy. Part 2.-Formation of Formate Species on Partially Reduced CeO_2 at Room Temperature. *J. Chem. Soc., Faraday Trans. 1* **1989**, *85*, 1451-1461.

(12) Overbury, S. H.; Mullins, D. R.; Huntley, D. R.; Kundakovic, L. Chemisorption and Reaction of NO and N_2O on Oxidized and Reduced Ceria Surfaces Studied by Soft X-Ray Photoemission Spectroscopy and Desorption Spectroscopy. *J. Catal.* **1999**, *186*, 296-309.

(13) Martínez-Arias, A.; Soria, J.; Conesa, J. C.; Seoane, X. L.; Arcoya, A.; Cataluña, R. NO Reaction at Surface Oxygen Vacancies Generated in Cerium Oxide. *J. Chem. Soc., Faraday Trans.* **1995**, *91*, 1679-1687.

(14) Tschöpe, A.; Liu, W.; Flytzani-Stephanopoulos, M.; Ying, J. Y. Redox Activity of Nonstoichiometric Cerium Oxide-Based Nanocrystalline Catalysts. *J. Catal.* **1995**, *157*, 42-50.

(15) Sørensen, O. T., Ed.; In *Nonstoichiometric oxides;* Materials Science Series; Academic Press: New York, U.S.A., 1981.

(16) Tuller, H.; Nowick, A. Defect Structure and Electrical Properties of Nonstoichiometric CeO_2 Single Crystals. *J. Electrochem. Soc.* **1979**, *126*, 209-217.

(17) VanHandel, G.; Blumenthal, R. The Temperature and Oxygen Pressure Dependence of the Ionic Transference Number of Nonstoichiometric CeO_{2-x}. *J. Electrochem. Soc.* **1974**, *121*, 1198-1202.

(18) Zhang, J.; Kang, Z. C.; Eyring, L. The Binary Higher Oxides of the Rare Earths. *J. Alloys Compounds* **1993**, *192*, 57-63.

(19) Le Normand, F.; Hilaire, L.; Kili, K.; Krill, G.; Maire, G. Oxidation State of Cerium in Cerium-Based Catalysts Investigated by Spectroscopic Probes. *J. Phys. Chem.* **1988**, *92*, 2561-2568.

(20) Zhang, F.; Wang, P.; Koberstein, J.; Khalid, S.; Chan, S. Cerium Oxidation State in Ceria Nanoparticles Studied with X-Ray Photoelectron Spectroscopy and Absorption Near Edge Spectroscopy. *Surf. Sci.* **2004**, *563*, 74-82.

(21) Naganuma, T.; Traversa, E. Air, Aqueous and Thermal Stabilities of Ce^{3+} Ions in Cerium Oxide Nanoparticle Layers with Substrates. *Nanoscale* **2014**, *6*, 6637-6645.

(22) Naganuma, T.; Traversa, E. Stability of the Ce^{3+} Valence State in Cerium Oxide Nanoparticle Layers. *Nanoscale* **2012**, *4*, 4950-4953.

(23) Holgado, J. P.; Munuera, G.; Espinós, J. P.; González-Elipe, A. R. XPS Study of Oxidation Processes of CeO_x Defective Layers. *Appl. Surf. Sci.* **2000**, *158*, 164-171.

(24) Esch, F.; Fabris, S.; Zhou, L.; Montini, T.; Africh, C.; Fornasiero, P.; Comelli, G.; Rosei, R. Electron Localization Determines Defect Formation on Ceria Substrates. *Science* **2005**, *309*, 752-755.

(25) Takeda, Y.; Mafuné, F. Formation of Wide Bandgap Cerium Oxide Nanoparticles by Laser Ablation in Aqueous Solution. *Chem. Phys. Lett.* **2014**, *599*, 110-115.

(26) Zhang, F.; Jin, Q.; Chan, S. Ceria Nanoparticles: Size, Size Distribution, and Shape. *J. Appl. Phys.* **2004**, *95*, 4319-4326.

(27) Zec, S.; Bošković, S.; Kaluđerović, B.; Bogdanov, Ž.; Popović, N. Chemical Reduction of Nanocrystalline CeO_2. *Ceram. Int.* **2009**, *35*, 195-198.

(28) Chueh, W. C.; Falter, C.; Abbott, M.; Scipio, D.; Furler, P.; Haile, S. M.; Steinfeld, A. High-Flux Solar-Driven Thermochemical Dissociation of CO_2 and H_2O using Nonstoichiometric Ceria. *Science* **2010**, *330*, 1797-1801.

(29) Mele, A.; Consalvo, D.; Stranges, D.; Giardini-Guidoni, A.; Teghil, R. Chemical Reactivity of Ionic Clusters Formed by Laser Ablation of Solid Oxides Utilized in Superconducting Materials. *Int. J. Mass Spectrom. Ion Process.* **1990**, *95*, 359-373.

(30) Chen, C.; Chen, H.; Weng, M.; Ju, S.; Chang, J.; Chang, C. Structural Properties of $(CeO_2)_n$ (n = 1–5) Nanoparticle: Molecular Mechanics and First Principle Studies. *Chin. J. Catal.* **2008**, *29*, 1117-1121.

(31) Wu, X.; Zhao, Y.; Xue, W.; Wang, Z.; He, S.; Ding, X. Active Sites of Stoichiometric Cerium Oxide Cations ($Ce_mO_{2m}^+$) Probed by Reactions with Carbon Monoxide and Small Hydrocarbon Molecules. *Phys. Chem. Chem. Phys.* **2010**, *12*, 3984-3997.

(32) Wu, X.; Ding, X.; Bai, S.; Xu, B.; He, S.; Shi, Q. Experimental and Theoretical Study of the Reactions between Cerium Oxide Cluster Anions and Carbon Monoxide: Size-Dependent Reactivity of $Ce_nO_{2n+1}^-$ (n = 1–21). *J. Phys. Chem. C* **2011**, *115*, 13329-13337.

(33) Ding, X.; Wu, X.; Zhao, Y.; Ma, J.; He, S. Double-Oxygen-Atom Transfer in Reactions of $Ce_mO_{2m}^+$ (m = 2–6) with C_2H_2. *ChemPhysChem* **2011**, *12*, 2110-2117.

(34) Hirabayashi, S.; Ichihashi, M. Oxidation of Composition-Selected Cerium Oxide Cluster Cations by O_2. *Chem. Phys. Lett.* **2013**, *564*, 16-20.

(35) Hirabayashi, S.; Ichihashi, M. Oxidation of CO and NO on Composition-Selected Cerium Oxide Cluster Cations. *J. Phys. Chem. A* **2013**, *117*, 9005-9010.

(36) Aubriet, F.; Gaumet, J.; De Jong, W. A.; Groenewold, G. S.; Gianotto, A. K.; McIlwain, M. E.; Van Stipdonk, M. J.; Leavitt, C. M. Cerium Oxyhydroxide Clusters: Formation, Structure, and Reactivity. *J. Phys. Chem. A* **2009**, *113*, 6239-6252.

(37) Zhao, Y.; Ding, X.; Ma, Y.; Wang, Z.; He, S. Transition Metal Oxide Clusters with Character of Oxygen-Centered Radical: A DFT Study. *Theor. Chem. Acc.* **2010**, *127*, 449-465.

(38) Zhao, Y.; Wu, X.; Ma, J.; He, S.; Ding, X. Characterization and Reactivity of Oxygen-Centred Radicals Over Transition Metal Oxide Clusters. *Phys. Chem. Chem. Phys.* **2011**, *13*, 1925-1938.

(39) Burow, A. M.; Wende, T.; Sierka, M.; Włodarczyk, R.; Sauer, J.; Claes, P.; Jiang, L.; Meijer, G.; Lievens, P.; Asmis, K. R. Structures and Vibrational Spectroscopy of Partially Reduced Gas-Phase Cerium Oxide Clusters. *Phys. Chem. Chem. Phys.* **2011**, *13*, 19393-19400.

(40) Sakuma, K.; Miyajima, K.; Mafuné, F. Oxidation of CO by Nickel Oxide Clusters Revealed by Post Heating. *J. Phys. Chem. A* **2013**, *117*, 3260-3265.

(41) Morita, K.; Sakuma, K.; Miyajima, K.; Mafuné, F. Thermally and Chemically Stable Mixed Valence Copper Oxide Cluster Ions Revealed by Post Heating. *J. Phys. Chem. A* **2013**, *117*, 10145-10150.

(42) Linstrom, P.; Mallard, W., Eds.; In *NIST Chemistry WebBook, NIST Standard Reference Database Number 69;* National Institute of Standards and Technology: Gaithersburg, U.S.A., http://webbook.nist.gov, retrieved August 2, 2015.

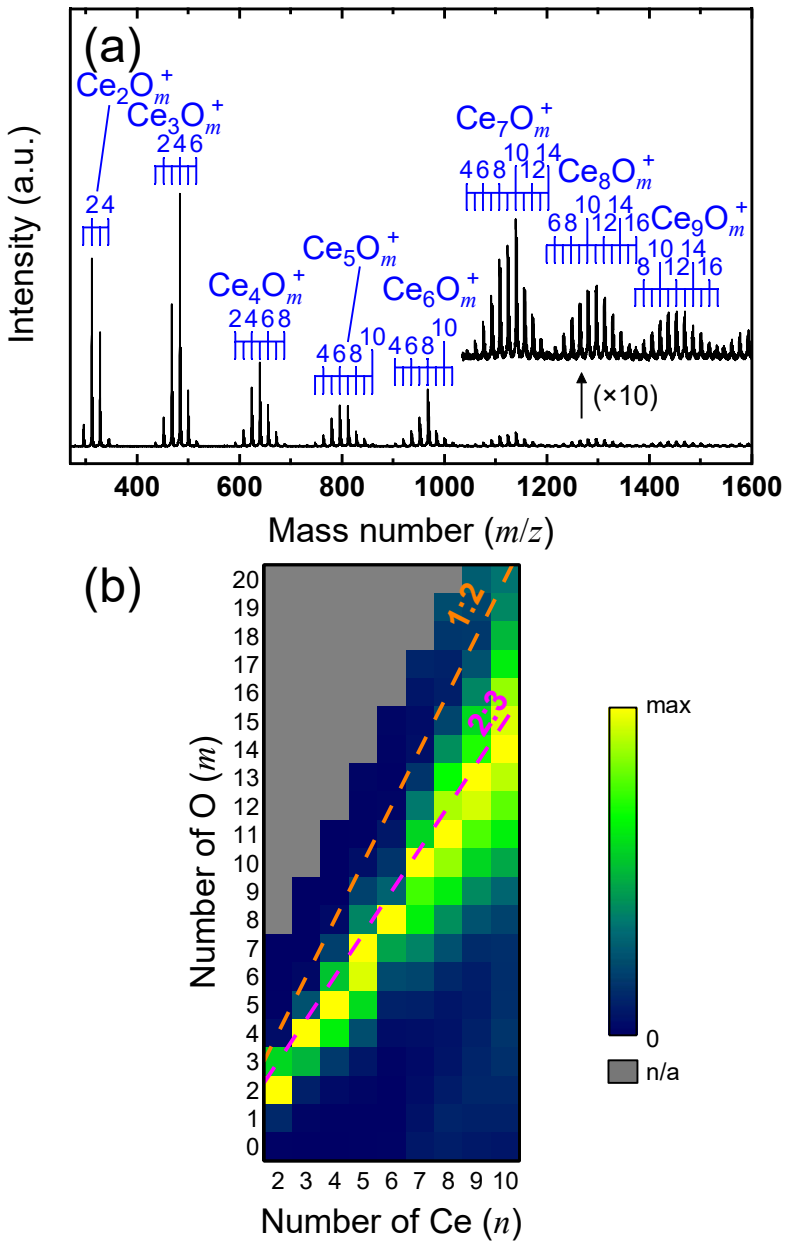

Figure 3.1. (a) Mass spectrum of cationic cerium oxide clusters produced by laser ablation of a CeO_2 rod in He carrier gas. Ion peaks assignable to $Ce_nO_m^+$ ($2 \leq n \leq 9$, $m \leq 2n$) are observed in the spectrum. (b) Color map showing abundances of $Ce_nO_m^+$ clusters.

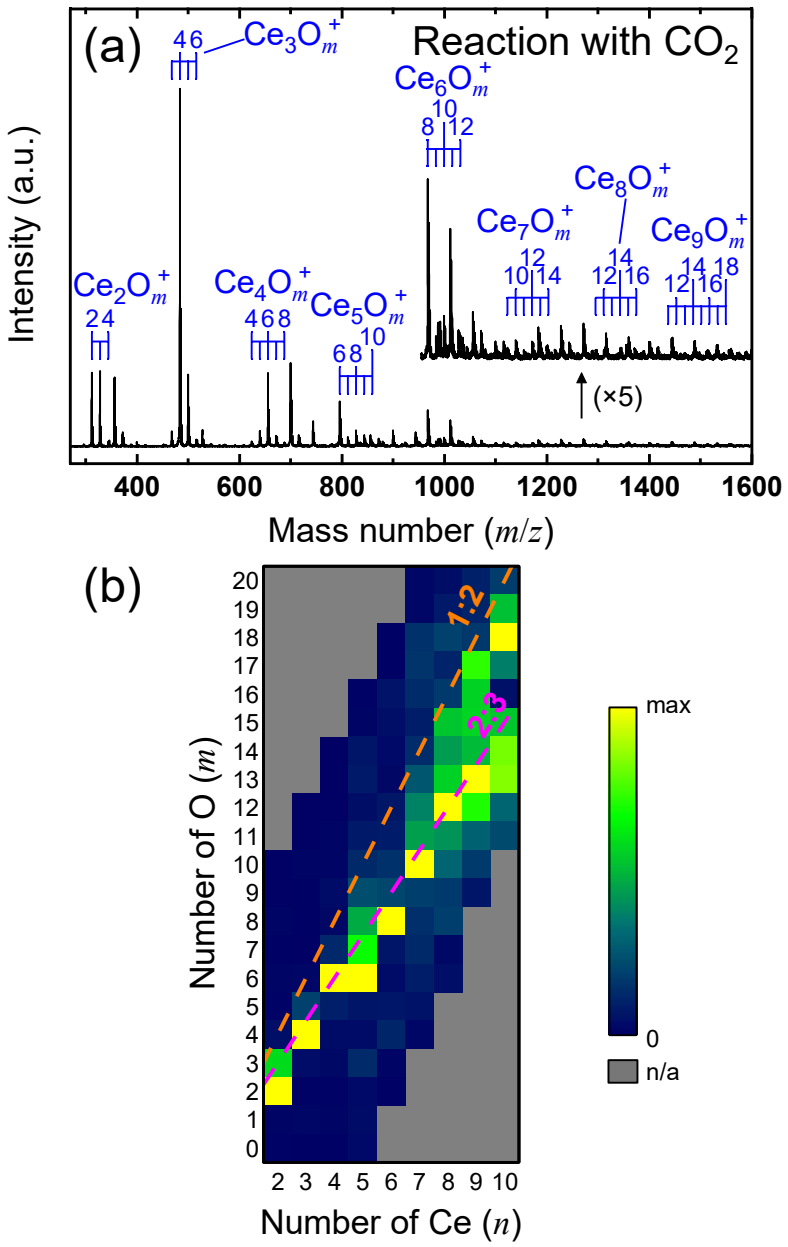

Figure 3.2. (a) Mass spectrum of cationic cerium oxide clusters after reaction with CO_2 (2.5%, diluted in He). (b) Color map showing abundances of $Ce_nO_m^+$ clusters after reaction with CO_2. CO_2-appended clusters $(Ce_nO_m(CO_2)_l^+$; l = 1, 2) are included in the corresponding $Ce_nO_m^+$ clusters in the map.

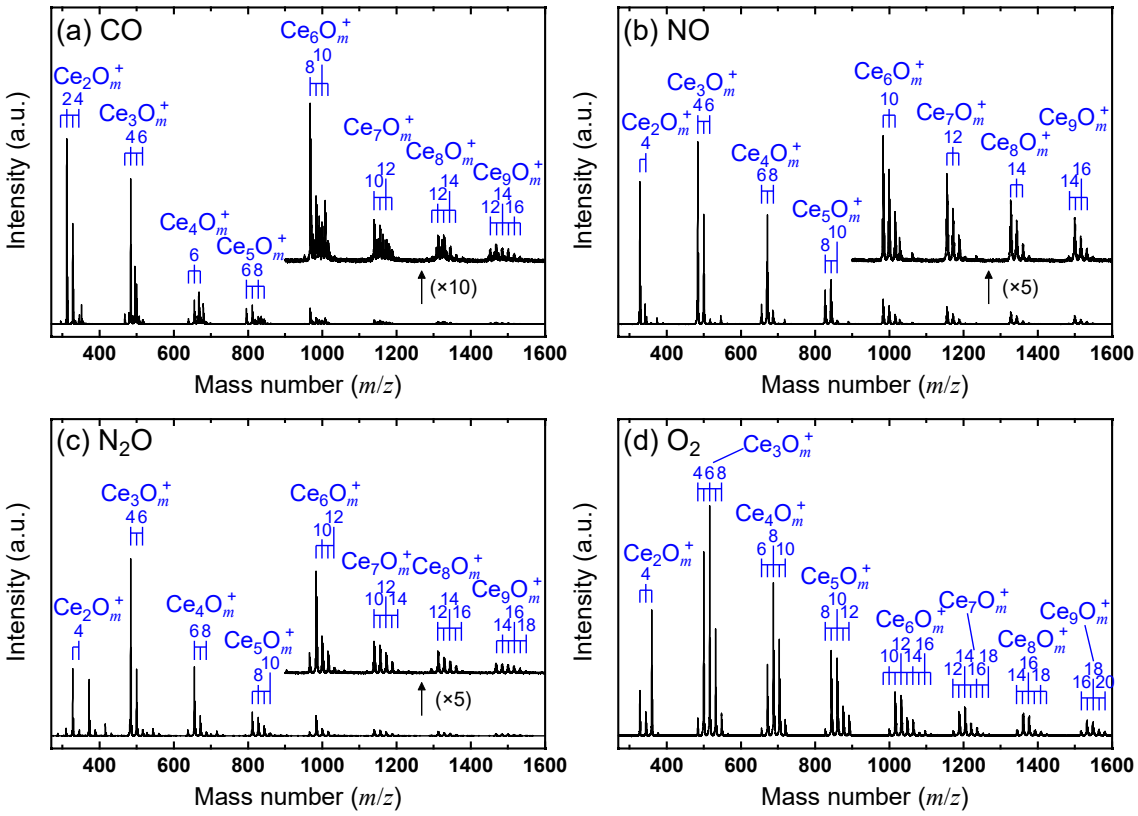

Figure 3.3. Mass spectra of cationic cerium oxide clusters after reaction with (a) CO, (b) NO, (c) N_2O, and (d) O_2. Each reactant gas is diluted in He at 10% concentration.

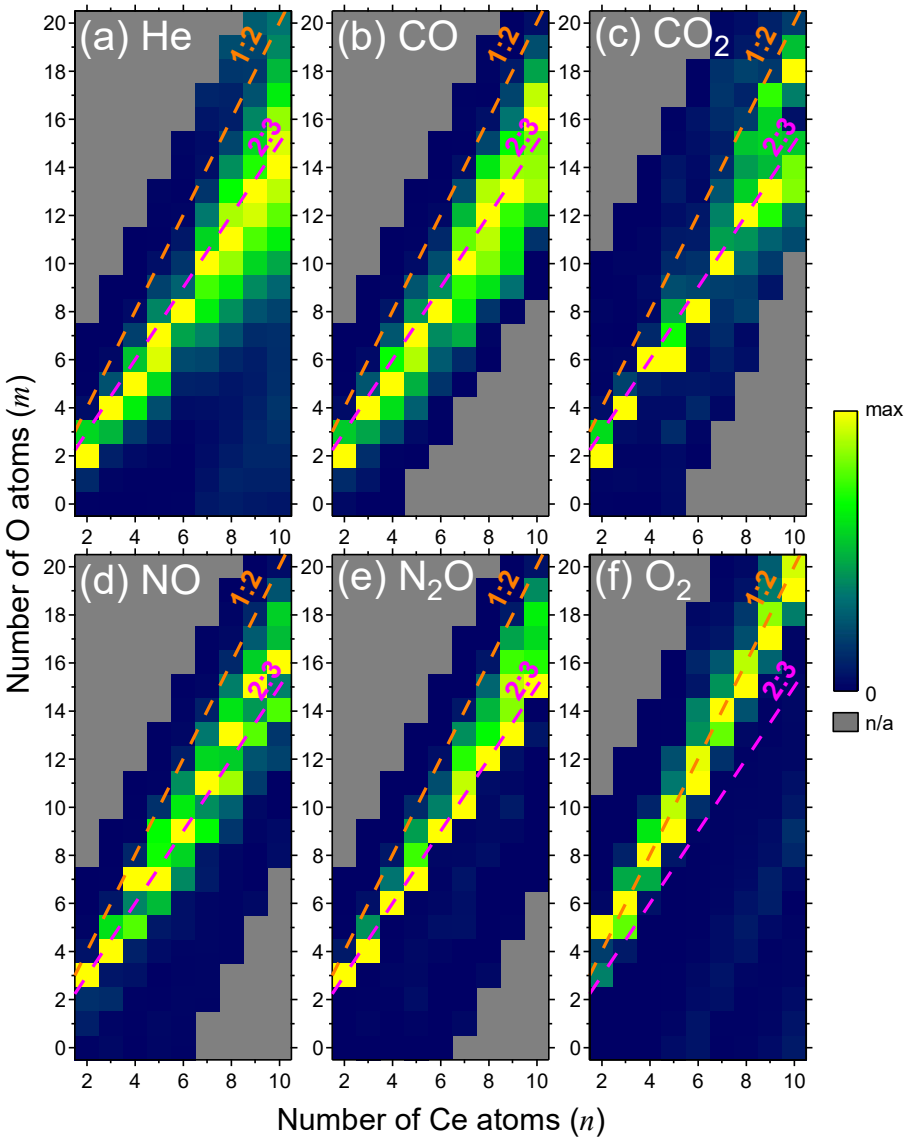

Figure 3.4. Color maps showing abundances of $Ce_nO_m^+$ clusters (a) before and after reactions with (b) CO (10%), (c) CO_2 (2.5%), (d) NO (10%), (e) N_2O (10%), and (f) O_2 (10%). Each reactant gas is diluted in He. Clusters containing attached reactant molecules ($Ce_nO_mX_l^+$; X = CO, CO_2, NO, N_2O) are included in the corresponding $Ce_nO_m^+$ clusters in the maps (abundances of each attached cluster and differences between abundances before and after reactions are given in Figure 3.5–3.9).

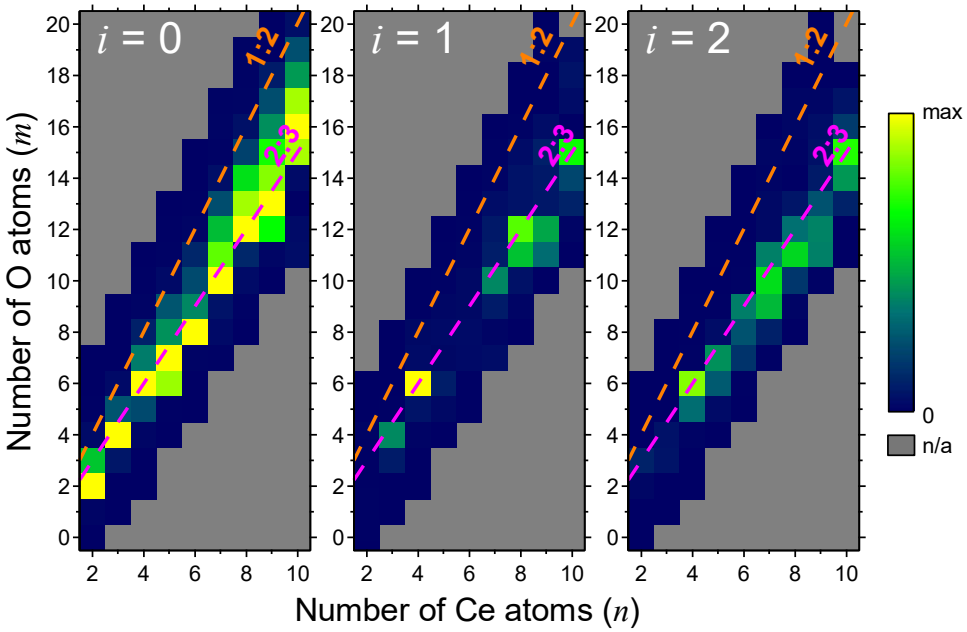

Figure 3.5. Color maps showing abundances of $Ce_nO_mC_i^+$ clusters after reaction with CO (10%, diluted in He).

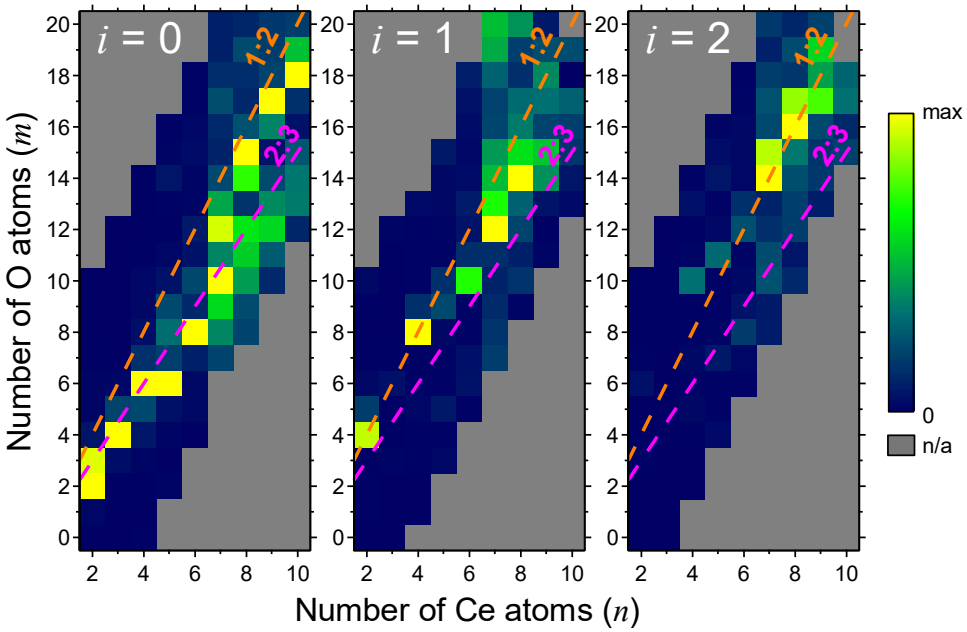

Figure 3.6. Color maps showing abundances of $Ce_nO_mC_i^+$ clusters after reaction with CO_2 (2.5%, diluted in He).

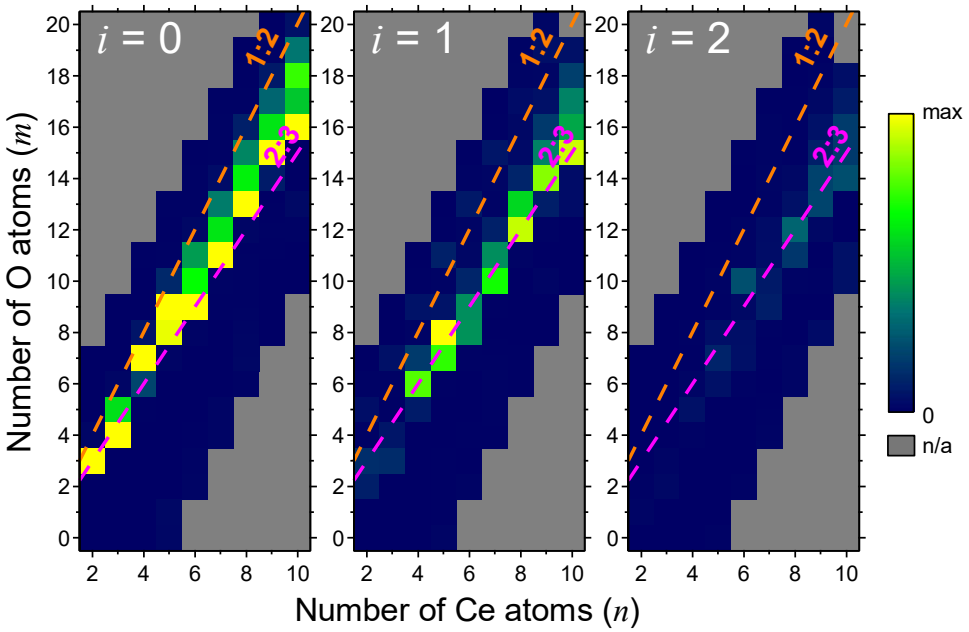

Figure 3.7. Color maps showing abundances of $Ce_nO_mN_i^+$ clusters after reaction with NO (10%, diluted in He).

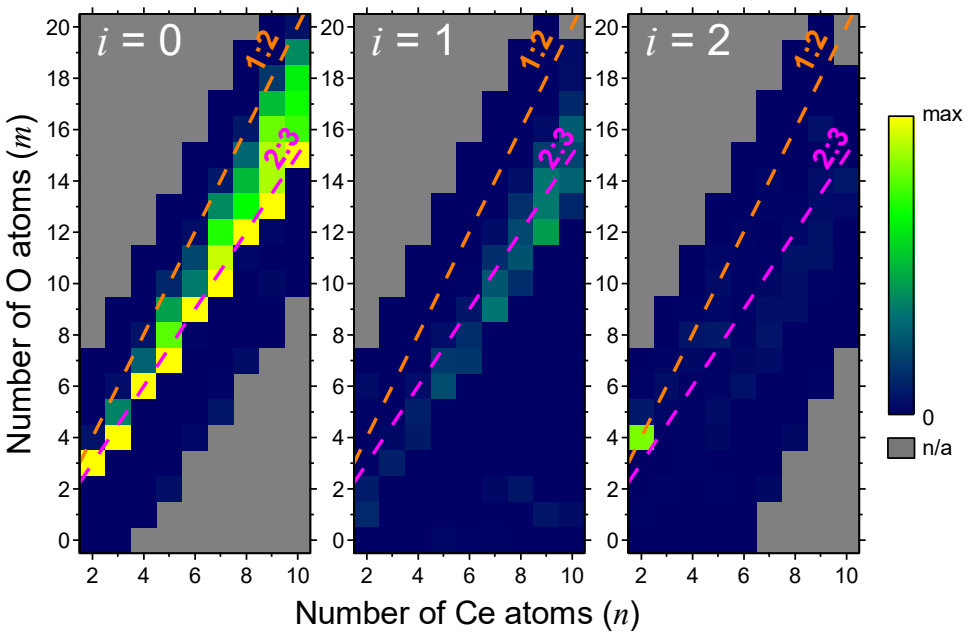

Figure 3.8. Color maps showing abundances of $Ce_nO_mN_i^+$ clusters after reaction with N_2O (10%, diluted in He).

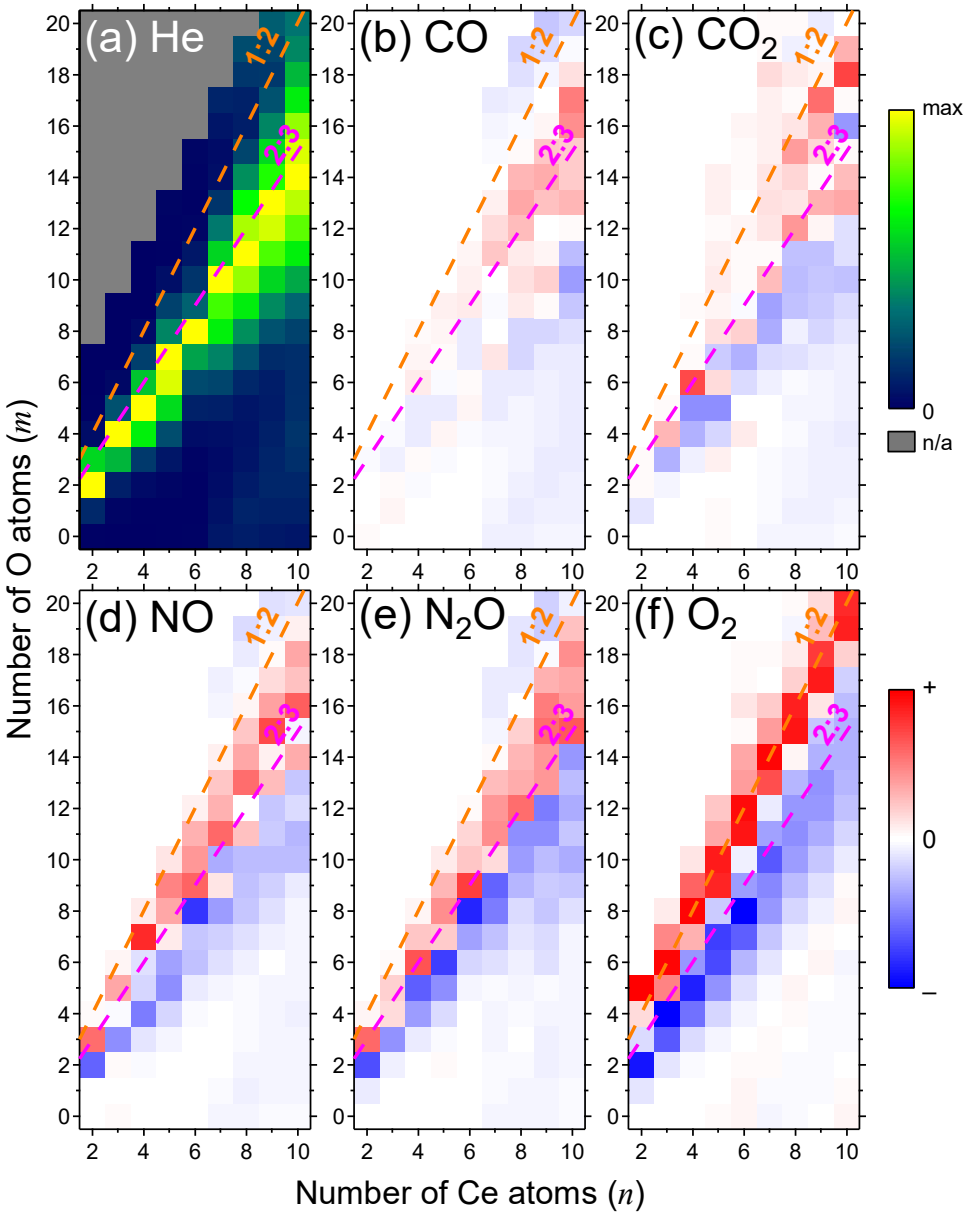

Figure 3.9. (a) Color map showing abundances of $Ce_nO_m^+$ clusters before reactions. (b–f) Color maps showing differences between abundances of $Ce_nO_m^+$ clusters before and after reactions with CO (10%; b), CO_2 (2.5%; c), NO (10%; d), N_2O (10%, e), and O_2 (10%, f). Increased and decreased species are shown as red and blue cells, respectively. Clusters containing attached reactant molecules ($Ce_nO_mX_l^+$; X = CO, CO_2, NO, N_2O) are included in the corresponding $Ce_nO_m^+$ clusters in the maps.

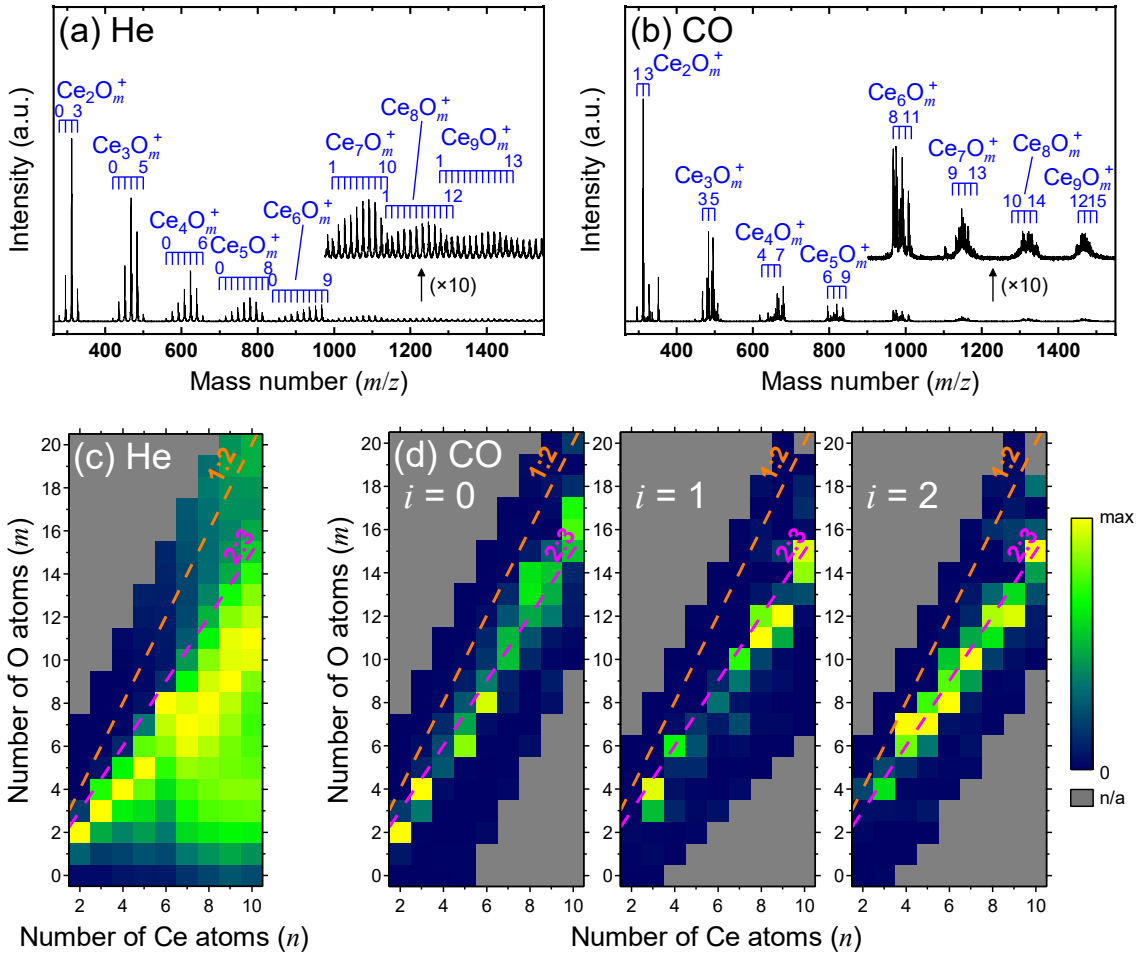

Figure 3.10. (a,b) Mass spectra of cationic cerium oxide clusters prepared by laser ablation of CeO_2 and Ce rods simultaneously (a) and after reaction with 10% CO (b). (c,d) Color maps showing abundances of $Ce_nO_m^+$ clusters prepared by laser ablation of CeO_2 and Ce rods simultaneously (c) and $Ce_nO_mC_i^+$ clusters after reaction with 10% CO (d).

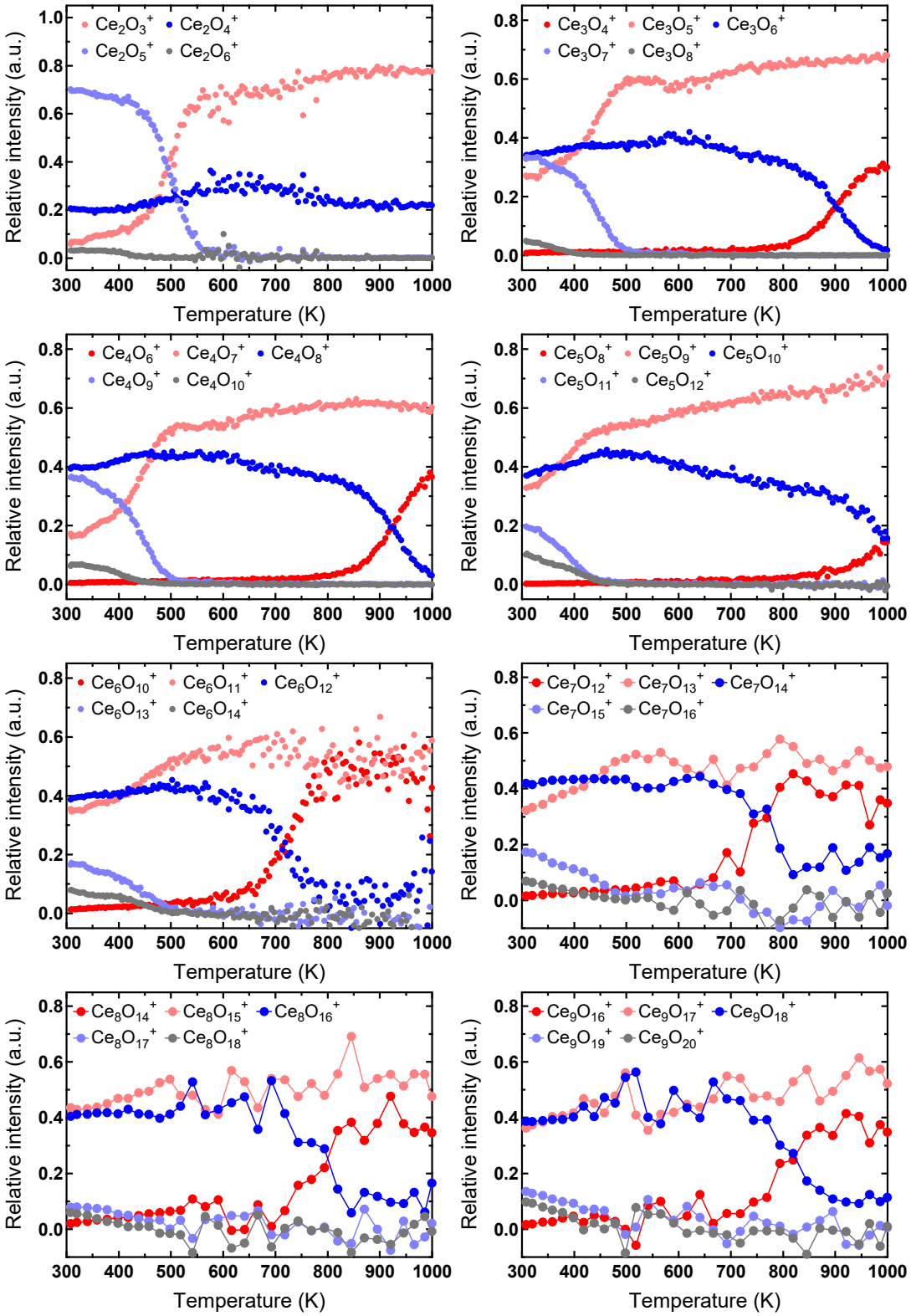

Figure 3.11. Relative intensities of $Ce_nO_m^+$ ($2 \le n \le 9$, $2n-2 \le m \le 2n+2$) produced after post-heating at the extension tube as a function of the temperature.

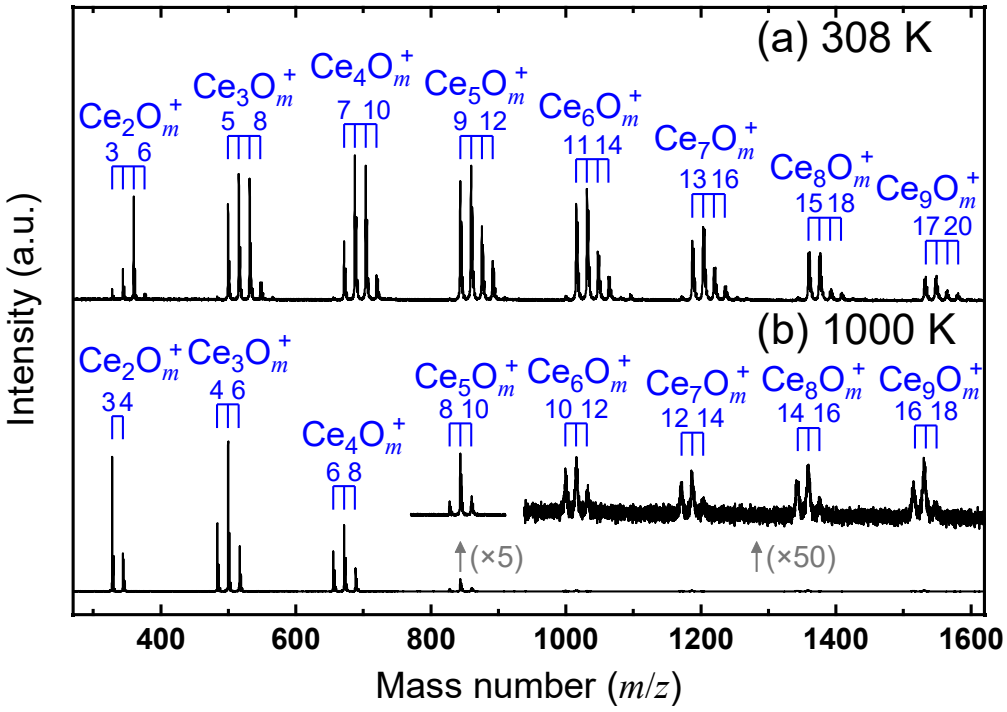

Figure 3.12. Mass spectra of cationic cerium oxide clusters prepared in the presence of oxygen (0.02%) diluted in He (0.8 MPa) as a carrier gas (a) and then heated up to 1000 K (b).

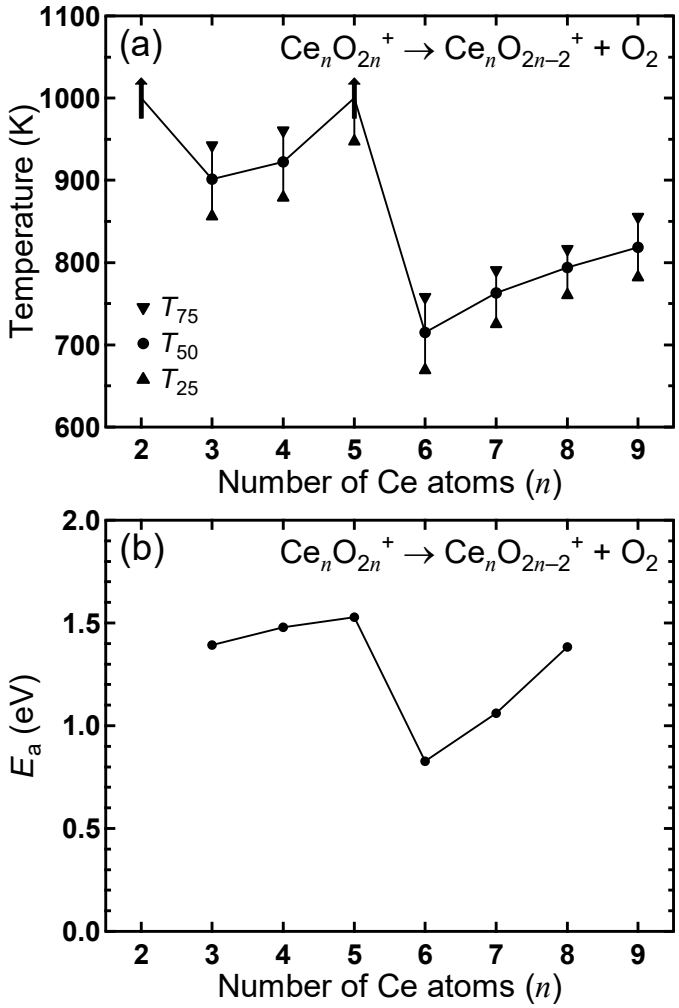

Figure 3.13. (a) Temperature and (b) activation energy for the oxygen release reaction, $Ce_nO_{2n}^+ \rightarrow Ce_nO_{2n-2}^+ + O_2$ as a function of the cluster size, n. Temperatures, T_{25}, T_{50}, and T_{75}, are defined as the temperature at which 25%, 50%, and 75% of $Ce_nO_{2n}^+$ has been changed into $Ce_nO_{2n-2}^+$, respectively.

Chapter 4

Oxidation of Nitric Oxide on Gas-Phase Cerium Oxide Clusters via Reactant Adsorption and Product Desorption Processes

The reactivity of cerium oxide cluster cations, $Ce_nO_{2n+x}^+$ (n = 2–9, x = −1 to +2), with NO was investigated using gas-phase temperature programmed desorption (TPD) combined with mass spectrometry. Target clusters were prepared in the gas phase via the laser ablation of a cerium oxide rod in the presence of oxygen, which was diluted using helium as a carrier gas. NO adsorbed onto stoichiometric and oxygen-rich clusters of $Ce_nO_{2n+x}^+$ (x = 0–2), forming $Ce_nO_{2n+x}(NO)^+$ (x = 0–2) species. Gas-phase TPD was measured for the NO-adsorbed clusters, revealing that $Ce_nO_{2n}(NO)^+$ released NO_2 at 600–900 K, forming $Ce_nO_{2n-1}^+$. Therefore, the overall reaction was the oxidation of NO by the $Ce_nO_{2n}^+$ clusters, which was explained in terms of a Langmuir–Hinshelwood type reaction. An activation barrier existed between the initial complex ($Ce_nO_{2n}(NO)^+$) and the final oxidation products ($Ce_nO_{2n-1}^+$ + NO_2). To determine the nature of the intermediates and the activation barrier, TPD was also performed on $Ce_nO_{2n-1}(NO_2)^+$, which had been prepared through the adsorption of NO_2 on $Ce_nO_{2n-1}^+$ for comparison. The activation barrier was associated with the release of NO_2 from the intermediate complex ($Ce_nO_{2n-1}^+$—NO_2 → $Ce_nO_{2n-1}^+$ + NO_2) rather than the structural rearrangement that formed NO_2 in the other intermediate complex ($Ce_nO_{2n}^+$—NO → $Ce_nO_{2n-1}^+$—NO_2).

(Reproduced with permission from T. Nagata et al., *J. Phys. Chem. A* **2015**, *119*, 10255–10263. Copyright 2015 American Chemical Society.)

4.1. Introduction

Cerium oxide (CeO_2, ceria) is an important component of automotive three-way catalysts (TWCs), which are used to remove air pollutants from exhaust gases by converting nitrogen oxides, carbon monoxide, and small hydrocarbons to less harmful gases, i.e., nitrogen, carbon dioxide, and water, by redox reactions.[1-3] The activity of CeO_2 as a redox catalyst is dependent on its oxygen storage capacity (OSC), which originates from transitions between the two oxidation states of Ce ($Ce^{3+} \leftrightarrow Ce^{4+}$).[3-9] Ceria is also widely used as a supporting material for catalysts in order to promote catalytic activity,[8, 10, 11] e.g., the ability to form oxygen vacancies in a vanadium oxide catalyst is enhanced by using ceria as a support.[12-17] An understanding of the detailed features and mechanisms of the redox activity of ceria is needed to improve its catalytic reactivity and develop novel catalysts.

Nitric oxide (NO) is a ubiquitous pollutant and is emitted in the exhaust gas of diesel engines.[2] To prevent air pollution, NO should be chemically reduced to N_2 before emission. Although seemingly paradoxical, the NO oxidation reaction is a key step in the catalytic reduction of NO in some cases. A typical NO reduction procedure uses a specific TWC called an NO_x storage and reduction (NSR) catalyst, which uses an NO oxidation process to form nitrogen dioxide (NO_2) and/or nitrate (NO_3^-) in a preliminary step. These species are temporarily stored on the catalyst in an oxidized form before being subsequently reduced.[2, 18] In these applications, catalysts containing precious metals, such as platinum, have been used to oxidize NO and then reduce the oxidized species.[2, 9, 18-21] The catalytic activity of these materials needs to be improved, while simultaneously decreasing the amount of precious metals used in the catalysts. Therefore, the oxidation and reduction of NO are important research topics for the catalytic purification of harmful exhaust pollutants.

Gas-phase clusters have been studied as a model system of practical heterogeneous catalysts.[22] Gas-phase cerium oxide clusters, consisting of a few Ce and O atoms, have been the primary focus of previous studies.[23-26] Several groups have reported the redox activities of cationic and anionic cerium oxide clusters.[27-34] As in bulk systems, cerium oxide clusters have an OSC. Oxygen-deficient species, $Ce_nO_{2n+x}^+$ ($x \leq -2$), extract oxygen atoms from small molecules, whereas stoichiometric and oxygen-rich cerium oxide clusters, $x \geq 0$, release O_2 molecules during collision-induced dissociation (CID) or thermal treatment.[30-33] The extraction or release of oxygen depends on the extent of oxygen excess or deficiency, i.e., clusters with more oxygen atoms tend to release oxygen more easily, while more oxygen

deficient clusters have a higher oxygen extraction capacity.[31-33] Stoichiometric cerium oxide cluster ions, $Ce_nO_{2n}^+$ and $Ce_nO_{2n+1}^-$, can oxidize small molecules.[27-29, 32, 34] These ionized species have an oxygen-centered radical, which is an active site for oxidation reactions.[35, 36] Indeed, clusters with a localized oxygen-centered radical are believed to have higher reactivities than radical-delocalized systems.[27]

For the investigation of chemical reactions involving gas-phase cluster ions, two different experimental strategies have been used to study either single collisions of isolated clusters in vacuum or multiple collisions of thermalized clusters in a gas flow. Under single-collision conditions, the target cluster collides once with a reactant molecule in the reaction field, where the gas density is sufficiently low, preventing secondary collisions. Conversely, under multiple-collision conditions, inert molecules (typically noble gases) are present in the reaction field at a relatively high density, allowing the target cluster ions to frequently collide with them during the reaction.

When a reaction complex is formed by collision between a cluster ion and a reactant molecule, it becomes thermally excited by gaining an amount of energy equivalent to the summation of the collision and binding energies. The relaxation rate of the thermally excited species is different between the single- and multiple-collision conditions.[37] In the single-collision condition, the complex relaxes via radiative cooling, but this process is extremely slow for the isolated clusters,[38-40] allowing excess energy to drive a subsequent reaction. In the multiple-collision condition, the excited complex is rapidly thermalized by collisions with the surroundings. From an alternative point-of-view, the single- and multiple-collision conditions are also different in terms of thermodynamics. The isolated system conserves the total energy in a manner that corresponds to an adiabatic process, while the thermalized system conserves temperature during the reaction and acts as an isothermal process.

The oxidation of NO by composition-selected $Ce_nO_{2n}^+$ clusters was previously observed upon CID under single-collision conditions, and no intermediate was experimentally identified.[34] In the present work, the oxidation of NO by cationic cerium oxide clusters was examined under the multiple-collision condition to determine detailed kinetic information. Interestingly, the reaction progressed differently than in the previous CID study. Instead, the reaction complex was trapped by thermalization, and additional excitation by heating was required to complete the oxidation process. NO adsorption and NO_2 desorption steps were found to proceed separately. Rate constants for NO adsorption were measured as a function of

cluster size. The thermal response of the reaction complex was also investigated to obtain information on the energetics of the reaction. Activation energies of NO_2 desorption were estimated from the thermal responses of different sized clusters. These results provide useful insights into the oxidation of NO by cerium oxide clusters, which are a model system for ceria-based catalysts.

4.2. Experimental section

The reactivity of cerium oxide clusters was investigated with a reflectron-equipped time-of-flight mass spectrometer (TOF-MS) coupled to a temperature-programmed desorption (TPD) device for gas-phase clusters. The experimental setup was similar to that described in Chapter 2, and, therefore, only a brief description is given in the following. The cluster ions, $Ce_nO_{2n+x}^+$ (n = 2–9, x = −1 to 2), were prepared in the gas phase by laser ablation of rod-shaped ceria (CeO_2; Rare Metallic Co., Ltd., 99.9%) with a focused second harmonic beam from a Nd:YAG pulse laser (532 nm, ~10 mJ pulse^{-1}) in oxygen-doped helium (0.02–0.1%; total pressure of 0.8 MPa at the stagnation point; Japan Fine Products Co., Ltd.; purities of O_2 and He were >99.9% and >99.99995%, respectively), which was supplied as a carrier gas via a first pulsed valve. The generated clusters were transferred via flowing carrier gas to a reaction gas cell (2 mm diameter, 60 mm long), where they were exposed to nitric oxide (0–10%; Japan Fine Products Co., Ltd., >99% purity) diluted in helium, which was introduced by a second pulsed valve (total pressure of 0.1 MPa at the stagnation point and ~10^3 Pa in the reaction gas cell). A control experiment was performed using pure helium without nitric oxide. The residence time of the clusters in the reaction gas cell was estimated to be ~70 μs. After passing through the reaction gas cell, the cluster ions were introduced into a gas-phase TPD device, which was a copper extension tube (4 mm diameter, 120 mm length). The temperature of the extension tube was monitored with a K-type thermocouple and was elevated in the range of 300–1000 K using a resistive heater, which was tuned by a programmable proportional-integral-derivative (PID) controller (Omron, E5CN-HT). The residence time of the clusters and the density of helium carrier gas in the extension tube were estimated to be ~100 μs and ~10^{18} molecules cm^{-3}, respectively. The clusters were thermalized by collision with the helium carrier gas, which mediated heat transfer between the extension tube and the clusters. The temperature of the extension tube was typically scanned at 7 K min^{-1}. In contrast to a conventional TPD measurement of a solid surface, pristine clusters were introduced to the

extension tube at each temperature in this study. Therefore, both the warming and cooling temperature scans should give essentially the same results as was experimentally confirmed.

After passing through the TPD device, the cluster ions were introduced into the vacuum and their kinetic energy was increased by 3.5 keV in the acceleration region for TOF-MS analysis. After the ions travelled through a 1 m field-free region, they were reflected by a dual-stage reflectron and detected with a Hamamatsu double-microchannel plate detector. Signals from the detector were amplified with a 350 MHz preamplifier (Stanford Research Systems, SR445A) and digitized with an oscilloscope (LeCroy, LT344L). Averaged TOF spectra (≥500 sweeps) were sent to a computer for analysis. The mass resolution, $m/\Delta m$, exceeded 1000, which was sufficient for the estimation of each cluster ion's intensity.

4.3. Results

4.3.1. Adsorption of NO on $Ce_nO_{2n+x}^+$ clusters

Figure 4.1a shows a typical mass spectrum of the pristine cerium oxide cluster cations produced by the laser ablation of CeO_2 in 0.05% O_2-doped He carrier gas. Ion peaks that were attributable to $Ce_nO_{2n+x}^+$ (n = 2–9, x = −1 to 2) were observed in the spectrum. After exposure to 5.14% NO diluted by He in the reaction gas cell, the peaks associated with the stoichiometric and oxygen-rich cerium oxide clusters, $Ce_nO_{2n+x}^+$ (x = 0–2), decreased in intensity, while the peaks of NO-added species, $Ce_nO_{2n+x}(NO)^+$ (x = 0–2), appeared (see Figure 4.1b). These spectral changes indicated NO adsorbed onto the $Ce_nO_{2n+x}^+$ (x = 0–2) clusters as

$$Ce_nO_{2n+x}^+ + NO \rightarrow Ce_nO_{2n+x}(NO)^+ \quad (x = 0\text{–}2) \tag{4.1}$$

In contrast, the partially-oxygen-deficient clusters, x = −1, remained unchanged after treatment with NO, suggesting that $Ce_nO_{2n-1}^+$ clusters did not react with NO. Figure 4.2a shows the relative intensities of $Ce_3O_{5-8}^+$ cluster ions after reaction with NO as a function of the number density of NO in the reaction gas cell. The gas density was estimated by measuring the oxidation of CO by $Ce_5O_{10}^+$ ions, namely $Ce_5O_{10}^+ + CO \rightarrow Ce_5O_9^+ + CO_2$, as a reference. The rate constant of this reaction is known to be 8.7×10^{-13} cm^3 s^{-1}.[32] The plot confirms that the oxygen deficient $Ce_3O_5^+$ was less reactive with NO. The intensity of each $Ce_nO_{2n+x}^+$ peak after reaction 4.1 can be described as

$$\frac{I}{I_0} = \exp\left(-k[\mathrm{NO}]t\right) \tag{4.2}$$

where I_0 and I are ion intensities of $Ce_nO_{2n+x}^+$ before and after the reaction, respectively, k is the pseudo-first-order rate constant of reaction 4.1, [NO] is the number density of NO in the reaction gas cell, and t is the reaction time (~70 μs). Eq. 4.2 was fit to the experimental data with good agreement as shown in Figure 4.2a. The rate constants for NO adsorption (reaction 4.1) were obtained from this fit, and they are plotted in Figure 4.2b. The rate constants for NO adsorption were on the order of 10^{-12} cm^3 s^{-1} for each $Ce_nO_{2n+x}^+$ (n = 2–9, x = 0–2) and had a slight, although not significant, size dependence.

4.3.2. Temperature-programmed desorption for NO-adsorbed clusters

To determine the features of NO binding on cerium oxide clusters, gas-phase TPD[32, 33, 41-43] of the NO-adsorbed clusters was measured. Figure 4.1c shows a mass spectrum of cerium oxide clusters after being exposed to NO and heated to 824 K. The NO-adsorbed clusters, $Ce_nO_{2n+x}(NO)^+$, nearly disappeared, and only $Ce_nO_{2n-1}^+$ species mainly remained at each cluster size, n. Figure 4.3a shows a gas-phase TPD plot, i.e., the relative intensity of each $Ce_3O_{5-8}(NO)_{0,1}^+$ ion as a function of the extension tube's temperature, for the n = 3 series. Intensity changes were observed with increasing temperature. To facilitate interpretation of the TPD results, the relative intensity of each cluster ion was numerically differentiated *vs*. temperature (see Figure 4.3b). In Figure 4.3b, positive values indicate an increase in ions during heating, while negative values indicate a decrease in ions during heating. The release of a small gas-phase molecule is expressed as a pair of negative and positive peaks corresponding to the parent and daughter ions, respectively, in the differential form of the TPD plot. The oxygen-rich NO adducts, $Ce_3O_7(NO)^+$ and $Ce_3O_8(NO)^+$, released NO and O_2 (or possibly NO_3) below 550 K to form $Ce_3O_5^+$ and $Ce_3O_6^+$, respectively. The stoichiometric NO adduct, $Ce_3O_6(NO)^+$, was unchanged until ~620 K and it released NO_2 to form $Ce_3O_5^+$ at about 700 K. Similar behaviors were observed for other cluster sizes, n, according to

$$Ce_nO_{2n+2}(NO)^+ \rightarrow Ce_nO_{2n}^+ + O_2 + NO \text{ (or } Ce_nO_{2n}^+ + NO_3) \quad (4.3)$$

$$Ce_nO_{2n+1}(NO)^+ \rightarrow Ce_nO_{2n-1}^+ + O_2 + NO \text{ (or } Ce_nO_{2n-1}^+ + NO_3) \quad (4.4)$$

$$Ce_nO_{2n}(NO)^+ \rightarrow Ce_nO_{2n-1}^+ + NO_2 \quad (4.5)$$

The NO adsorbed on $Ce_nO_{2n+x}^+$ (x = 1, 2) desorbed via reactions 4.3 and 4.4, while NO extracted an O atom from $Ce_nO_{2n}^+$ to produce NO_2 and $Ce_nO_{2n-1}^+$ via reaction 4.5. Combining reactions 4.1 and 5, the overall reaction was the oxidation of NO by $Ce_nO_{2n}^+$

$$Ce_nO_{2n}^{+} + NO \xrightarrow{rt} Ce_nO_{2n}(NO)^{+} \xrightarrow{\Delta} Ce_nO_{2n-1}^{+} + NO_2 \quad (4.6)$$

The temperature of NO_2 release is shown in Figure 4.4a for each size of $Ce_nO_{2n}(NO)^+$, where T_{25}, T_{50}, and T_{75} are defined as the temperatures at which 25%, 50%, and 75%, respectively, of the $Ce_nO_{2n}(NO)^+$ was converted to $Ce_nO_{2n-1}^+$. T_{50} was between 600 K and 800 K and exhibited a small size dependence. Moreover, the activation energy of NO_2 release (reaction 4.5) was estimated from the gas-phase TPD plots.[32, 33, 42] The rate constant of unimolecular dissociation can be described as a function of temperature, $k(T)$, using the Arrhenius equation,

$$k(T) = A \exp\left(-\frac{E_a}{k_B T}\right) \quad (4.7)$$

where A, E_a, k_B, and T are the pre-exponential factor, activation energy, Boltzmann constant, and temperature, respectively. Using the temperature-dependent rate constant, the ion fraction that decays during heating is given by

$$\frac{I(T)}{I_0} = \exp\left(-k(T)t\right) \quad (4.8)$$

where $I(T)$ is the ion intensity of the parent clusters, $Ce_nO_{2n}(NO)^+$, after heating to T, I_0 is the initial ion intensity of the parent clusters, and t is the reaction time. Combining Eqs. 4.7 and 4.8, the relationship between ion intensity and temperature is given by

$$\frac{I(T)}{I_0} = \exp\left(-At \exp\left(-\frac{E_a}{k_B T}\right)\right) \quad (4.9)$$

Eq. 4.9 fit well with the experimental data, reproducing the experimental values when I_0 was the observed relative intensity at a sufficiently low temperature, t was the residence time of cluster ions in the extension tube (~100 μs), and A and E_a were fitting parameters. Figure 4.4b shows the obtained activation energy of NO_2 release (reaction 4.5), which is approximately 1 eV for each cluster size.

4.3.3. Reactivity with NO_2

To determine the chemistry of NO adsorption on $Ce_nO_{2n+x}^+$, NO_2 adsorption was examined on $Ce_nO_{2n+x}^+$ for comparison using NO_2 as a target gas instead of NO. NO_2 adsorbed on the stoichiometric and slightly oxygen-deficient clusters, $x = -1$ and 0, while the oxygen-rich clusters, $x = 1$ and 2, were found to be inert to NO_2 (see Figure 4.5a).

$$Ce_nO_{2n+x}^{+} + NO_2 \rightarrow Ce_nO_{2n+x}(NO_2)^{+} \quad (x = -1, 0) \qquad (4.10)$$

The rate constants for NO_2 adsorption are given in Figure 4.5b. They are on the order of 10^{-11} cm^3 s^{-1} and are nearly constant for n = 2–9. It should be noted that $Ce_nO_{2n-1}(NO_2)^{+}$ had the same atomic composition ($Ce_nO_{2n+1}N^{+}$) as $Ce_nO_{2n}(NO)^{+}$. These species were considered to be isomeric. To identify the nature of NO_2 binding, gas-phase TPD was performed for the NO_2 adducts (Figure 4.6). The results suggested that $Ce_nO_{2n+x}(NO_2)^{+}$ (x = −1, 0) lost NO_2 during heating according to

$$Ce_nO_{2n}(NO_2)^{+} \rightarrow Ce_nO_{2n}^{+} + NO_2 \qquad (4.11)$$

$$Ce_nO_{2n-1}(NO_2)^{+} \rightarrow Ce_nO_{2n-1}^{+} + NO_2 \qquad (4.12)$$

Reaction 4.12 is similar to reaction 4.5, because their reactants and products share the same atomic compositions. Figure 4.7 shows the temperatures of NO_2 release from $Ce_nO_{2n-1}(NO_2)^{+}$ (reaction 4.12). The temperatures at which NO_2 was released from $Ce_nO_{2n}(NO)^{+}$ (Figure 4.4a) and $Ce_nO_{2n-1}(NO_2)^{+}$ (Figure 4.7) were approximately equal, suggesting that the $Ce_nO_{2n}(NO)^{+}$ formed via reaction 4.1 and the $Ce_nO_{2n-1}(NO_2)^{+}$ formed via reaction 4.10 had indistinguishable thermal responses.

4.4. Discussion

4.4.1. NO oxidation by cerium oxide clusters

As described above, oxidation of NO by $Ce_nO_{2n}^{+}$ clusters (reaction 4.6) proceeded with thermal excitation. The overall oxidation process was exothermic, e.g., the energy generated by NO_2 formation from NO + O (3.18 eV[44]) exceeded the energy required to remove an O atom from $Ce_3O_6^{+}$ (2.1 eV[33]). The oxidation, however, required thermal energy to reach completion, indicating that a reaction barrier existed between the initial complex and the final products. The complex could not spontaneously dissociate into $Ce_nO_{2n-1}^{+}$ and NO_2. There were two potential barriers in the oxidation pathway including (1) the structural rearrangement to form an NO_2 moiety in the complex by transferring an O atom from $Ce_nO_{2n}^{+}$ to NO and (2) the release of the formed NO_2 from the complex. Density functional theory (DFT) calculations suggested that there were two intermediates in the reaction pathway of NO oxidation.[34] One of these intermediates could be described as an NO moiety bound to $Ce_nO_{2n}^{+}$, while the other was an NO_2 bound to $Ce_nO_{2n-1}^{+}$. The two intermediates will hereafter be denoted as $Ce_nO_{2n}^{+}$—NO and $Ce_nO_{2n-1}^{+}$—NO_2. This notation is distinct from the previous use

of $Ce_nO_{2n}(NO)^+$ and $Ce_nO_{2n-1}(NO_2)^+$, which refer to the preparation of the species ($Ce_nO_{2n}^+$ + NO and $Ce_nO_{2n-1}^+$ + NO_2, respectively) regardless of their intrinsic structures and properties.

The adsorption of NO_2 onto $Ce_nO_{2n-1}^+$ can be regarded as a halfway reverse reaction, making a determination of the dominant activation barrier in the NO oxidation process possible as will be discussed below. Figure 4.8 shows a possible diagram of reaction 4.6, in which a transition state (TS) separates the two intermediates (IM1 and IM2). In this diagram, the observed reactions are shown as transitions between states. For example, for the adsorption of NO on $Ce_nO_{2n}^+$ (reaction 4.1) transitions occurred from the reactant (R) to the intermediates (R → IM1/IM2). For NO_2 adsorption on $Ce_nO_{2n-1}^+$ (reaction 4.10), transitions occurred from the product (P) to the intermediates (P → IM1/IM2), and for NO_2 release from $Ce_nO_{2n}(NO)^+$ or $Ce_nO_{2n-1}(NO_2)^+$ (reactions 4.5 or 4.12), transitions occurred from the intermediates to the product (IM1/IM2 → P). In the forward oxidation reaction, there were two reaction barriers, structural rearrangement (IM1 → IM2) and the NO_2 release (IM2 → P). The energy level of the transition state between the intermediates determines which activation barrier controls the oxidation reaction. Considering that the energy level of the reactant (E^R) is higher than that of the product (E^P), $E^R > E^P$, three patterns of the transition-state's energy level (E^{TS}) are possible including (a) $E^{TS} < E^P$, (b) $E^R > E^{TS} > E^P$, and (c) $E^R < E^{TS}$ (see Figure 4.8). Case (c) was not possible according to the results of a previous CID study,[34] which suggested that the oxidation of NO by $Ce_nO_{2n}^+$ is an overall barrierless process (a comparison with this CID study will be discussed later). As mentioned previously, $Ce_nO_{2n}(NO)^+$ and $Ce_nO_{2n-1}(NO_2)^+$ exhibited identical thermal responses during gas-phase TPD (see Figures 4.4a and 4.7), suggesting that they have the same intermediate state for NO_2 release. Therefore, case (b) is unlikely. If $E^{TS} > E^P$, the thermal responses of $Ce_nO_{2n}(NO)^+$ and $Ce_nO_{2n-1}(NO_2)^+$ would have been different because the transition from $Ce_nO_{2n}^+$—NO to $Ce_nO_{2n-1}^+$—NO_2 should require more energy than that associated with NO_2 release. Consequently, the energy levels should follow case (a), i.e., the activation barrier between the two intermediates is sufficiently low to not affect the NO_2 release process. The main activation barrier to the NO oxidation reaction was the final step, the release of NO_2. When heated, both $Ce_nO_{2n}(NO)^+$ and $Ce_nO_{2n-1}(NO_2)^+$ were thought to reach an equilibrium between $Ce_nO_{2n}^+$—NO and $Ce_nO_{2n-1}^+$—NO_2. The experimentally obtained activation energy (Figure 4.4b) corresponds to the activation barrier between the equilibrium intermediate and the final product. The effective

energy level of the equilibrium intermediate was determined by the weighted average of the two intermediate levels by the equilibrium ratio (see Appendix).

4.4.2. Comparison with collision induced dissociation

Hirabayashi and Ichihashi performed a CID study in which a selected mass of $Ce_nO_{2n}^+$ collided with a target molecule, NO, in vacuum.[34] They observed the oxidation of NO by $Ce_nO_{2n}^+$ clusters and concluded from the collision energy dependence of reaction cross sections that the NO oxidation reaction did not have an overall activation barrier, which might be inconsistent with the present results, because the reaction required thermal excitation in the present work. The major difference between the two studies was the experimental conditions. The CID study was performed under single-collision conditions (~10^{-4} Torr,[34] namely, 10^{12}–10^{13} molecules cm^{-3}), while in this chapter's study, cluster ions collided with NO and He gases much more frequently in the reaction gas cell, which was a multiple-collision environment (10^{17}–10^{18} molecules cm^{-3}). When the cluster ion formed a complex with a reactant molecule, the cluster—reactant complex gained energy equivalent to the collision energy and binding energy. In the single-collision condition, the complex was thermalized slowly via radiative cooling and was in an energetic state during the reaction time. Therefore, the oxidation reaction could proceed without further excitation as long as no higher activation barrier was present above the initial state (cases (a) and (b) in Figure 4.8). Conversely, in the multiple-collision condition, the excited complex was rapidly cooled by collisions with the He gas, leaving the cluster—reactant complex in a thermally trapped state. The depth of the trapped state was estimated using gas-phase TPD measurements. Indeed, similar differences between single- or multiple-collision conditions have been observed previously.[37] The isolated clusters in the single-collision condition conserved the total energy, while the thermalized clusters in the multiple-collision condition conserved the temperature during reaction. These two studies provide complementary investigations of reaction kinetics. This work provides information on the reaction complex, $Ce_nO_{2n}(NO)^+$, which was not observed in the single-collision experiment.

The reaction cross sections for the oxidation of NO by $Ce_nO_{2n}^+$ (n = 3–5) were measured by CID experiments (at a collision energy of 0.2 eV) under single-collision conditions to be ~4.4 $Å^2$, ~1.6 $Å^2$, and ~1.4 $Å^2$ for $Ce_3O_6^+$, $Ce_4O_8^+$, and $Ce_5O_{10}^+$,

respectively.[34] In the study of this chapter, the reaction cross sections of NO adsorption (reaction 4.1) were calculated from rate constants (Figure 4.2b) using

$$\sigma = \frac{k}{\bar{u}} = k\sqrt{\frac{\pi\mu}{8k_{\mathrm{B}}T}} \tag{4.13}$$

where σ, k, $\bar{u}$, μ, k_{B}, and T are the reaction cross section, the rate constant, the average relative velocity of the target cluster ion and the reactant gas molecule, the reduced mass of the cluster ion and reactant, the Boltzmann constant, and the temperature, respectively. The calculated reaction cross sections were 0.9 Å^2, 0.8 Å^2, and 0.5 Å^2 for $Ce_3O_6^+$, $Ce_4O_8^+$, and $Ce_5O_{10}^+$, respectively. These cross sections were smaller by a factor of 2–5 than those of NO oxidation by CID. Despite the different experimental conditions (single or multi collisions) causing the different reactions (oxidation or adsorption of NO), the reaction cross sections obtained by CID and in the present study were comparable, suggesting that NO oxidation proceeded with a relatively high probability once a cluster—reactant complex formed with sufficient internal energy for a long enough time.

4.4.3. Comparison with the CO oxidation reaction

The redox activity of cerium oxide clusters for the oxidation of CO has been reported.[27, 28, 32, 34] $Ce_nO_{2n}^+$ and $Ce_nO_{2n+2}^+$ were observed to oxidize CO, forming CO_2 at room temperature,[32] while the oxidation of NO by $Ce_nO_{2n}^+$ required heating. The overall reactions for CO and NO oxidation were similar because reactants extract an O atom from $Ce_nO_{2n}^+$ to produce $Ce_nO_{2n-1}^+$, although the reaction mechanisms and energetics are likely different. In Chapter 2, the Rideal–Eley mechanism was proposed for the CO oxidation reaction, $Ce_nO_{2n}^+ + CO \rightarrow Ce_nO_{2n-1}^+ + CO_2$, because an intermediate, $Ce_nO_{2n}(CO)^+$, was not identified during the reaction.[32] In contrast, the Langmuir–Hinshelwood mechanism can describe the NO oxidation (reaction 4.6) in this chapter, because the intermediate complex, $Ce_nO_{2n}(NO)^+$, was observed.

A reaction pathway for CO oxidation was suggested by DFT calculations for $Ce_2O_4^+$ [27] and $Ce_3O_6^+$ [34] in which two intermediates, $Ce_nO_{2n}^+$—CO and $Ce_nO_{2n-1}^+$—CO_2, were separated by a transition state. This pathway is equivalent to that shown in Figure 4.8 with "NO" replaced with "CO" and "NO_2" replaced with "CO_2". It remains unclear why NO oxidation ceased at the intermediate complex at room temperature, while CO oxidation reached

completion without thermal excitation. This might be explained by the difference in the energy level of the product in the reaction scheme. The energy generated during NO_2 formation from NO + O was 3.18 eV, which is 2.34 eV less than that generated by CO_2 formation from CO + O (5.52 eV).[44] The larger formation energy of CO oxidation decreased the product's energy level, promoting the desorption of the product. Meanwhile, the higher product energy level of NO oxidation caused by the lower formation energy could have hindered the release of NO_2. Indeed, the highest barrier for NO oxidation was the NO_2 release step ($E^{TS} < E^{P}$, case (a) in Figure 4.8), as discussed above, while the barrier of CO_2 release is believed to be lower than that of the transition state between the two intermediates ($E^{TS} > E^{P}$, cases (b) or (c) in Figure 4.8), according to DFT calculations.[27, 34] Another possible explanation was the tendency of NO_2 and CO_2 forming bonds with the clusters. CO_2 is a closed-shell molecule with an adiabatic ionization energy (IE) of 13.8 eV and an adiabatic electron affinity (EA) of −0.6 eV. NO_2 is a radical with an IE of 9.6 eV and an EA of 2.3 eV.[44] The lower IE and higher EA of NO_2 indicate that NO_2 has the tendency forming tighter bond with other species. Actually, the binding energy of $Ce_3O_5^+$—NO_2 has been predicted by DFT calculations to be 1.79 eV, which is larger than that of $Ce_3O_5^+$—CO_2, 0.55 eV.[34] The greater binding energy deepens the trapping state of the reaction complex in the oxidation of NO.

There was also a difference in size dependence for the oxidations of CO and NO by $Ce_nO_{2n}^+$. The CO oxidation had an obvious size dependence, i.e., $Ce_5O_{10}^+$ was much more reactive than other cluster sizes by several orders of magnitude.[32] In contrast, both the rate constant of NO adsorption (Figure 4.2b) and the activation energy of NO_2 desorption (Figure 4.4b) were less size dependent. These differences were likely related to the location of the highest activation barrier in the reaction pathway, as mentioned above, which were the $Ce_nO_{2n}^+$—CO → $Ce_nO_{2n-1}^+$—CO_2 step for CO oxidation and the $Ce_nO_{2n-1}^+$—NO_2 → $Ce_nO_{2n-1}^+$ + NO_2 step for NO oxidation. The structural rearrangement in the intermediate complex, the transferring of an O atom from $Ce_nO_{2n}^+$ to a CO or NO moiety, is more size dependent than other reaction steps, possibly because the rearrangement is accompanied by a structural distortion of the cluster itself. In the oxidation of NO, the $Ce_nO_{2n}^+$—NO → $Ce_nO_{2n-1}^+$—NO_2 step may have a size dependence, but it does not determine the total reaction rate as long as $E^{TS} < E^{P}$ and the equilibrium between the two intermediates is achieved.

4.5. Conclusion

Reactions of NO and $Ce_nO_{2n+x}^+$ (n = 2–9, x = −1 to +2) clusters were investigated under multiple-collision conditions using mass spectrometry combined with gas-phase TPD. The clusters were prepared in the gas phase by the laser ablation of a CeO_2 target in the presence of O_2. NO adsorption onto $Ce_nO_{2n+x}^+$ (x = 0–2) clusters was observed by exposure of the prepared clusters to NO gas at room temperature. The NO adducts of the stoichiometric clusters, $Ce_nO_{2n}(NO)^+$, released NO_2 at 600–900 K, forming a reduced species, $Ce_nO_{2n-1}^+$. Therefore, the overall reaction was the oxidation of NO by $Ce_nO_{2n}^+$, i.e., $Ce_nO_{2n}^+ + NO \rightarrow Ce_nO_{2n-1}^+ + NO_2$. Although NO oxidation was believed to be exothermic, it required thermal excitation, indicating that there was an activation barrier between the reaction complex ($Ce_nO_{2n}(NO)^+$) and the final products ($Ce_nO_{2n-1}^+ + NO_2$). Two intermediates as the reaction complex, $Ce_nO_{2n}^+$—NO and $Ce_nO_{2n-1}^+$—NO_2, were believed to exist and were separated by a transition state. By comparing to NO_2 desorption by gas-phase TPD from $Ce_nO_{2n-1}(NO_2)^+$ which were prepared by adsorption of NO_2 onto $Ce_nO_{2n-1}^+$, the activation barrier in the NO oxidation process was related to the release of NO_2 ($Ce_nO_{2n-1}^+$—$NO_2 \rightarrow Ce_nO_{2n-1}^+ + NO_2$) rather than the transition state between the two intermediates ($Ce_nO_{2n}^+$—$NO \rightarrow Ce_nO_{2n-1}^+$—$NO_2$). The intermediate complex of NO oxidation was not observed in a previous CID study under single-collision conditions.[34] Therefore, under multiple-collision conditions, the complex was trapped in the intermediate state by rapid thermalization caused by collisions with surrounding He atoms. The NO oxidation reaction was described in terms of the Langmuir–Hinshelwood mechanism, unlike CO-oxidation reaction, i.e., $Ce_nO_{2n}^+ + CO \rightarrow Ce_nO_{2n-1}^+ + CO_2$, which was described by the Rideal–Eley mechanism (see Chapter 2).

4.6. Appendix

4.6.1. Interpretation of experimentally observed activation energies

In this work, the two intermediates, $Ce_nO_{2n}^+$—NO and $Ce_nO_{2n-1}^+$—NO_2, which were present during the reaction, were unable to be separately identified by TOF-MS. Therefore, NO_2 was released (reaction 4.5) via a combination of the elemental processes shown in Figure 4.8 as

$$\mathrm{IM1} \underset{k_{-1},\,E_{a-1}}{\overset{k_1,\,E_{a1}}{\rightleftharpoons}} \mathrm{IM2} \xrightarrow{k_2,\,E_{a2}} \mathrm{P} \qquad (4.14)$$

where k_1, k_{-1}, and k_2 are rate constants and E_{a1}, E_{a-1}, and E_{a2} are the activation energies of each process. E_{a1}, E_{a-1}, and E_{a2} correspond to energy differences in Figure 4.8 as

$$E_{a1} = E^{TS} - E^{IM1}, \quad E_{a-1} = E^{TS} - E^{IM2}, \quad E_{a2} = E^{P} - E^{IM2}. \tag{4.15}$$

Assuming a steady state, the ratio of IM2 to the total intermediates (IM1 and IM2) is

$$\frac{[IM2]}{[IM1]+[IM2]} = \frac{k_1}{k_1 + k_{-1} + k_2} \tag{4.16}$$

where [IM1] and [IM2] are the number densities of IM1 and IM2, respectively. The observed rate constant of NO_2 release, k^{obs}, can be expressed as

$$k^{obs} = \frac{[IM2]}{[IM1]+[IM2]} k_2 = \frac{k_1 k_2}{k_1 + k_{-1} + k_2} \tag{4.17}$$

Based on the Arrhenius equation (Eq. 4.7), the activation energy, E_a, is the differential of the rate constant, k, as

$$E_a = -\frac{1}{k}\frac{\partial k}{\partial \beta} \tag{4.18}$$

where β is the thermodynamic beta, $1/(k_B T)$, and k_B and T are the Boltzmann constant and the temperature, respectively. Using this formula, the observed activation energy is

$$\begin{aligned} E_a^{obs} &= -\frac{1}{k^{obs}}\frac{\partial k^{obs}}{\partial \beta} = -\frac{1}{k_1}\frac{\partial k_1}{\partial \beta} - \frac{1}{k_2}\frac{\partial k_2}{\partial \beta} + \frac{1}{k_1 + k_{-1} + k_2}\left(\frac{\partial k_1}{\partial \beta} + \frac{\partial k_{-1}}{\partial \beta} + \frac{\partial k_2}{\partial \beta}\right) \\ &= E_{a1} + E_{a2} - \frac{k_1 E_{a1} + k_{-1} E_{a-1} + k_2 E_{a2}}{k_1 + k_{-1} + k_2} = \frac{(k_1 + k_{-1})E^{P} + k_2 E^{TS}}{k_1 + k_{-1} + k_2} - \frac{k_1 E^{IM2} + (k_{-1} + k_2)E^{IM1}}{k_1 + k_{-1} + k_2} \end{aligned} \tag{4.19}$$

As discussed above, the experimental results suggested that the intermediates were in an equilibrium state between IM1 and IM2 before NO_2 desorption, suggesting that k_1 and k_{-1} are much greater than k_2. Employing this limit and using Eq. 4.16, the observed activation energy in Eq. 4.19 can be expressed approximately as

$$E_a^{obs} \approx E^{P} - \frac{[IM1]E^{IM1} + [IM2]E^{IM2}}{[IM1]+[IM2]} \tag{4.20}$$

Therefore, the observed activation energy was the activation barrier between the equilibrium intermediate and the final product, and the effective energy level of the equilibrium intermediate was given by the weighted average of the two intermediate levels based on the equilibrium ratio.

4.7. References

(1) Trovarelli, A. Catalytic Properties of Ceria and CeO_2-Containing Materials. *Catal. Rev.* **1996**, *38*, 439-520.

(2) Fritz, A.; Pitchon, V. The Current State of Research on Automotive Lean NO_x Catalysis. *Appl. Catal. B-Environ.* **1997**, *13*, 1-25.

(3) Yao, H.; Yao, Y. Ceria in Automotive Exhaust Catalysts: I. Oxygen Storage. *J. Catal.* **1984**, *86*, 254-265.

(4) Skorodumova, N.; Simak, S.; Lundqvist, B. I.; Abrikosov, I.; Johansson, B. Quantum Origin of the Oxygen Storage Capability of Ceria. *Phys. Rev. Lett.* **2002**, *89*, 166601.

(5) Jiang, Y.; Adams, J. B.; van Schilfgaarde, M.; Sharma, R.; Crozier, P. A. Theoretical Study of Environmental Dependence of Oxygen Vacancy Formation in CeO_2. *Appl. Phys. Lett.* **2005**, *87*, 141917.

(6) Breysse, M.; Guenin, M.; Claudel, B.; Latreille, H.; Véron, J. Catalysis of Carbon Monoxide Oxidation by Cerium Dioxide: I. Correlations between Catalytic Activity and Electrical Conductivity. *J. Catal.* **1972**, *27*, 275-280.

(7) Breysse, M.; Guenin, M.; Claudel, B.; Véron, J. Catalysis of Carbon Monoxide Oxidation by Cerium Dioxide: II. Microcalorimetric Investigation of Adsorption and Catalysis. *J. Catal.* **1973**, *28*, 54-62.

(8) Paier, J.; Penschke, C.; Sauer, J. Oxygen Defects and Surface Chemistry of Ceria: Quantum Chemical Studies Compared to Experiment. *Chem. Rev.* **2013**, *113*, 3949-3985.

(9) Matsumoto, S. Recent Advances in Automobile Exhaust Catalysts. *Catal. Today* **2004**, *90*, 183-190.

(10) Carrettin, S.; Concepción, P.; Corma, A.; Lopez Nieto, J. M.; Puntes, V. F. Nanocrystalline CeO_2 Increases the Activity of Au for CO Oxidation by Two Orders of Magnitude. *Angew. Chem. Int. Ed.* **2004**, *43*, 2538-2540.

(11) Camellone, M. F.; Fabris, S. Reaction Mechanisms for the CO Oxidation on Au/CeO_2 Catalysts: Activity of Substitutional Au^{3+}/Au^{+} Cations and Deactivation of Supported Au^{+} Adatoms. *J. Am. Chem. Soc.* **2009**, *131*, 10473-10483.

(12) Wachs, I. E. Recent Conceptual Advances in the Catalysis Science of Mixed Metal Oxide Catalytic Materials. *Catal. Today* **2005**, *100*, 79-94.

(13) Penschke, C.; Paier, J.; Sauer, J. Oligomeric Vanadium Oxide Species Supported on the CeO_2(111) Surface: Structure and Reactivity Studied by Density Functional Theory. *J. Phys. Chem. C* **2013**, *117*, 5274-5285.

(14) Ganduglia-Pirovano, M.; Popa, C.; Sauer, J.; Abbott, H.; Uhl, A.; Baron, M.; Stacchiola, D.; Bondarchuk, O.; Shaikhutdinov, S.; Freund, H. Role of Ceria in Oxidative Dehydrogenation on Supported Vanadia Catalysts. *J. Am. Chem. Soc.* **2010**, *132*, 2345-2349.

(15) Kropp, T.; Paier, J.; Sauer, J. Support Effect in Oxide Catalysis: Methanol Oxidation on Vanadia/Ceria. *J. Am. Chem. Soc.* **2014**, *136*, 14616-14625.

(16) Abbott, H. L.; Uhl, A.; Baron, M.; Lei, Y.; Meyer, R. J.; Stacchiola, D. J.; Bondarchuk, O.; Shaikhutdinov, S.; Freund, H. J. Relating Methanol Oxidation to the Structure of Ceria-Supported Vanadia Monolayer Catalysts. *J. Catal.* **2010**, *272*, 82-91.

(17) Paier, J.; Kropp, T.; Penschke, C.; Sauer, J. Stability and Migration Barriers of Small Vanadium Oxide Clusters on the CeO_2(111) Surface Studied by Density Functional Theory. *Faraday Discuss.* **2013**, *162*, 233-245.

(18) Takahashi, N.; Shinjoh, H.; Iijima, T.; Suzuki, T.; Yamazaki, K.; Yokota, K.; Suzuki, H.; Miyoshi, N.; Matsumoto, S.; Tanizawa, T.; Tanaka, T.; Tateishi, S.; Kasahara, K. The New Concept 3-Way Catalyst for Automotive Lean-Burn Engine: NO_x Storage and Reduction Catalyst. *Catal. Today* **1996**, *27*, 63-69.

(19) Weiss, B. M.; Iglesia, E. NO Oxidation Catalysis on Pt Clusters: Elementary Steps, Structural Requirements, and Synergistic Effects of NO_2 Adsorption Sites. *J. Phys. Chem. C* **2009**, *113*, 13331-13340.

(20) Smeltz, A. D.; Delgass, W. N.; Ribeiro, F. H. Oxidation of NO with O_2 on Pt(111) and Pt(321) Large Single Crystals. *Langmuir* **2010**, *26*, 16578-16588.

(21) Rankovic, N.; Nicolle, A.; Da Costa, P. Detailed Kinetic Modeling Study of NOx Oxidation and Storage and their Interactions Over Pt/Ba/Al_2O_3 Monolith Catalysts. *J. Phys. Chem. C* **2010**, *114*, 7102-7111.

(22) Lang, S. M.; Bernhardt, T. M. Gas Phase Metal Cluster Model Systems for Heterogeneous Catalysis. *Phys. Chem. Chem. Phys.* **2012**, *14*, 9255-9269.

(23) Mele, A.; Consalvo, D.; Stranges, D.; Giardini-Guidoni, A.; Teghil, R. Chemical Reactivity of Ionic Clusters Formed by Laser Ablation of Solid Oxides Utilized in Superconducting Materials. *Int. J. Mass Spectrom. Ion Process.* **1990**, *95*, 359-373.

(24) Chen, C.; Chen, H.; Weng, M.; Ju, S.; Chang, J.; Chang, C. Structural Properties of $(CeO_2)_n$ (n = 1–5) Nanoparticle: Molecular Mechanics and First Principle Studies. *Chin. J. Catal.* **2008**, *29*, 1117-1121.

(25) Aubriet, F.; Gaumet, J.; De Jong, W. A.; Groenewold, G. S.; Gianotto, A. K.; McIlwain, M. E.; Van Stipdonk, M. J.; Leavitt, C. M. Cerium Oxyhydroxide Clusters: Formation, Structure, and Reactivity. *J. Phys. Chem. A* **2009**, *113*, 6239-6252.

(26) Burow, A. M.; Wende, T.; Sierka, M.; Włodarczyk, R.; Sauer, J.; Claes, P.; Jiang, L.; Meijer, G.; Lievens, P.; Asmis, K. R. Structures and Vibrational Spectroscopy of Partially Reduced Gas-Phase Cerium Oxide Clusters. *Phys. Chem. Chem. Phys.* **2011**, *13*, 19393-19400.

(27) Wu, X.; Zhao, Y.; Xue, W.; Wang, Z.; He, S.; Ding, X. Active Sites of Stoichiometric Cerium Oxide Cations ($Ce_mO_{2m}^+$) Probed by Reactions with Carbon Monoxide and Small Hydrocarbon Molecules. *Phys. Chem. Chem. Phys.* **2010**, *12*, 3984-3997.

(28) Wu, X.; Ding, X.; Bai, S.; Xu, B.; He, S.; Shi, Q. Experimental and Theoretical Study of the Reactions between Cerium Oxide Cluster Anions and Carbon Monoxide: Size-Dependent Reactivity of $Ce_nO_{2n+1}^-$ (n = 1–21). *J. Phys. Chem. C* **2011**, *115*, 13329-13337.

(29) Ding, X.; Wu, X.; Zhao, Y.; Ma, J.; He, S. Double-Oxygen-Atom Transfer in Reactions of $Ce_mO_{2m}^+$ (m = 2–6) with C_2H_2. *ChemPhysChem* **2011**, *12*, 2110-2117.

(30) Felton, J. A.; Ray, M.; Waller, S. E.; Kafader, J. O.; Jarrold, C. C. $Ce_xO_y^-$ (x = 2–3) + D_2O Reactions: Stoichiometric Cluster Formation from Deuteroxide Decomposition and Anti-Arrhenius Behavior. *J. Phys. Chem. A* **2014**, *118*, 9960-9969.

(31) Hirabayashi, S.; Ichihashi, M. Oxidation of Composition-Selected Cerium Oxide Cluster Cations by O_2. *Chem. Phys. Lett.* **2013**, *564*, 16-20.

(32) Nagata, T.; Miyajima, K.; Mafuné, F. Stable Stoichiometry of Gas-Phase Cerium Oxide Cluster Ions and their Reactions with CO. *J. Phys. Chem. A* **2015**, *119*, 1813-1819.

(33) Nagata, T.; Miyajima, K.; Hardy, R. A.; Metha, G. F.; Mafuné, F. Reactivity of Oxygen Deficient Cerium Oxide Clusters with Small Gaseous Molecules. *J Phys Chem A* **2015**, *119*, 5545-5552.

(34) Hirabayashi, S.; Ichihashi, M. Oxidation of CO and NO on Composition-Selected Cerium Oxide Cluster Cations. *J. Phys. Chem. A* **2013**, *117*, 9005-9010.

(35) Zhao, Y.; Ding, X.; Ma, Y.; Wang, Z.; He, S. Transition Metal Oxide Clusters with Character of Oxygen-Centered Radical: A DFT Study. *Theor. Chem. Acc.* **2010**, *127*, 449-465.

(36) Zhao, Y.; Wu, X.; Ma, J.; He, S.; Ding, X. Characterization and Reactivity of Oxygen-Centred Radicals Over Transition Metal Oxide Clusters. *Phys. Chem. Chem. Phys.* **2011**, *13*, 1925-1938.

(37) Tawaraya, Y.; Kudoh, S.; Miyajima, K.; Mafuné, F. Thermal Desorption and Reaction of NO Adsorbed on Rhodium Cluster Ions Studied by Thermal Desorption Spectroscopy. *J. Phys. Chem. A* **2015**, *119*, 8461-8468.

(38) Walther, C.; Dietrich, G.; Dostal, W.; Hansen, K.; Krückeberg, S.; Lützenkirchen, K.; Schweikhard, L. Radiative Cooling of a Small Metal Cluster: The Case of V_{13}^{+}. *Phys. Rev. Lett.* **1999**, *83*, 3816-3819.

(39) Toker, Y.; Aviv, O.; Eritt, M.; Rappaport, M. L.; Heber, O.; Schwalm, D.; Zajfman, D. Radiative Cooling of Al_4^{-} Clusters. *Phys. Rev. A* **2007**, *76*, 053201.

(40) Lange, M.; Froese, M. W.; Menk, S.; Bing, D.; Fellenberger, F.; Grieser, M.; Laux, F.; Orlov, D. A.; Repnow, R.; Sieber, T.; Toker, Y.; von Hahn, R.; Wolf, A.; Blaum, K. Radiative Cooling of Al^{-}_4 and Al^{-}_5 in a Cryogenic Environment. *New J. Phys.* **2012**, *14*, 065007.

(41) Takenouchi, M.; Kudoh, S.; Miyajima, K.; Mafuné, F. Adsorption and Desorption of Hydrogen by Gas-Phase Palladium Clusters Revealed by in Situ Thermal Desorption Spectroscopy. *J. Phys. Chem. A* **2015**, *119*, 6766-6772.

(42) Koyama, K.; Kudoh, S.; Miyajima, K.; Mafuné, F. Dissociation Energy for O_2 Release from Gas-Phase Iron Oxide Clusters Measured by Temperature-Programmed Desorption Experiments. *Chem. Phys. Lett.* **2015**, *625*, 104-109.

(43) Mafuné, F.; Miyajima, K.; Morita, K. Release of Oxygen from Copper Oxide Cluster Ions by Heat and by Reaction with NO. *J. Phys. Chem. C* **2015**, *119*, 11106-11113.

(44) Linstrom, P.; Mallard, W., Eds.; In *NIST Chemistry WebBook, NIST Standard Reference Database Number 69;* National Institute of Standards and Technology: Gaithersburg, U.S.A., http://webbook.nist.gov, retrieved August 2, 2015.

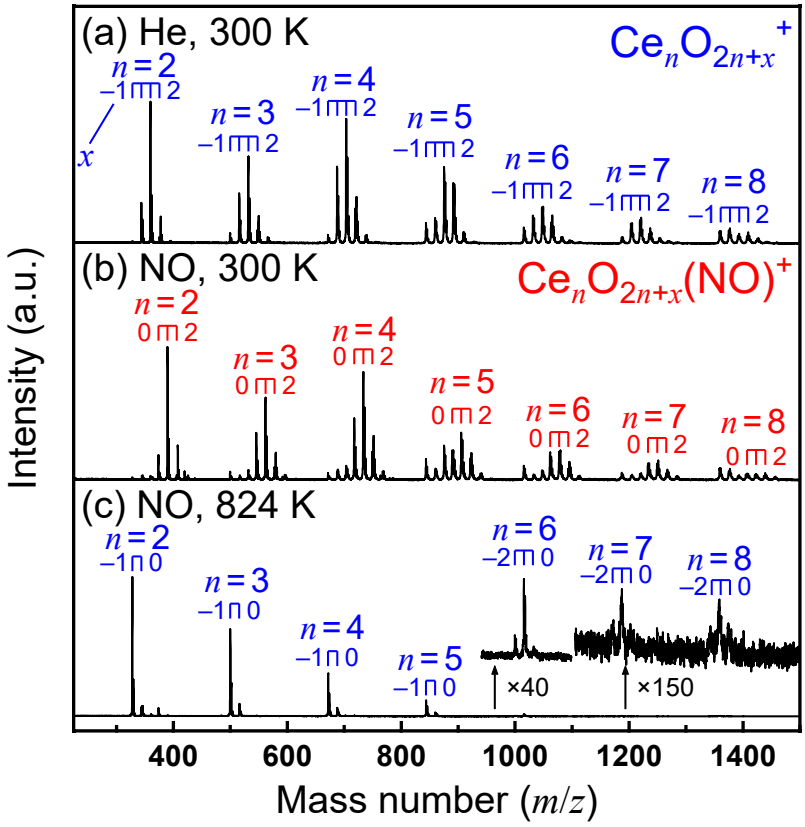

Figure 4.1. Mass spectrum of (a) $Ce_nO_{2n+x}^+$ (n = 2–8, x = −1 to +2) produced by laser ablation of a CeO_2 rod in the presence of O_2 diluted in He gas, (b) $Ce_nO_{2n+x}(NO)^+$ (n = 2–8, x = 0 to +2) after exposure to NO, and (c) $Ce_nO_{2n+x}^+$ (n = 2–8, x = −2 to 0) after exposure to NO followed by heating to 824 K. $Ce_nO_{2n+x}^+$ in panel (b) and $Ce_nO_{2n+x}(NO)^+$ in panel (c) are unlabeled.

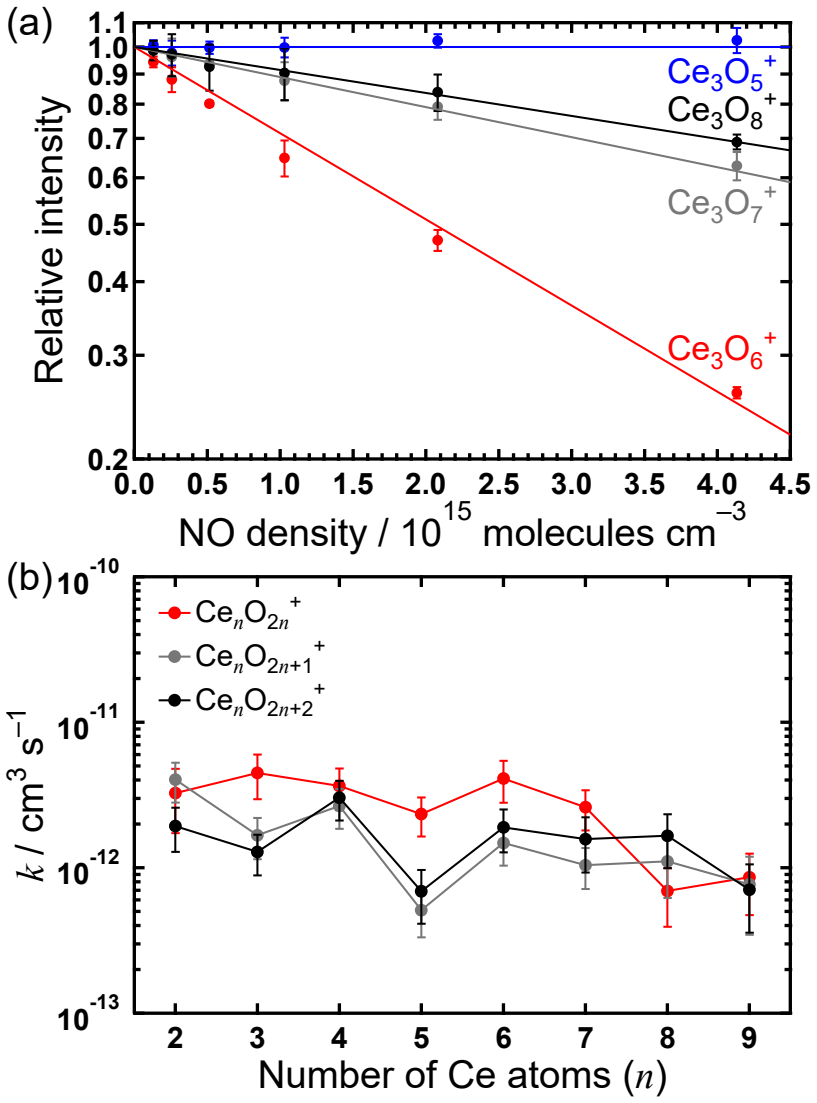

Figure 4.2. (a) Semi-logarithmic plot of relative intensities of $Ce_3O_{5-8}^+$ after exposure to NO in the reaction gas cell as a function of the concentration of NO. (b) Rate constants for NO adsorption, $Ce_nO_{2n+x}^+ + NO \rightarrow Ce_nO_{2n+x}(NO)^+$, for x = 0–2 as a function of the cluster size, n. The solid lines in panel (a) show intensities of $Ce_3O_{5-8}^+$ calculated using the rate constants shown in panel (b) for $Ce_3O_{6-8}^+$ or zero for $Ce_3O_5^+$.

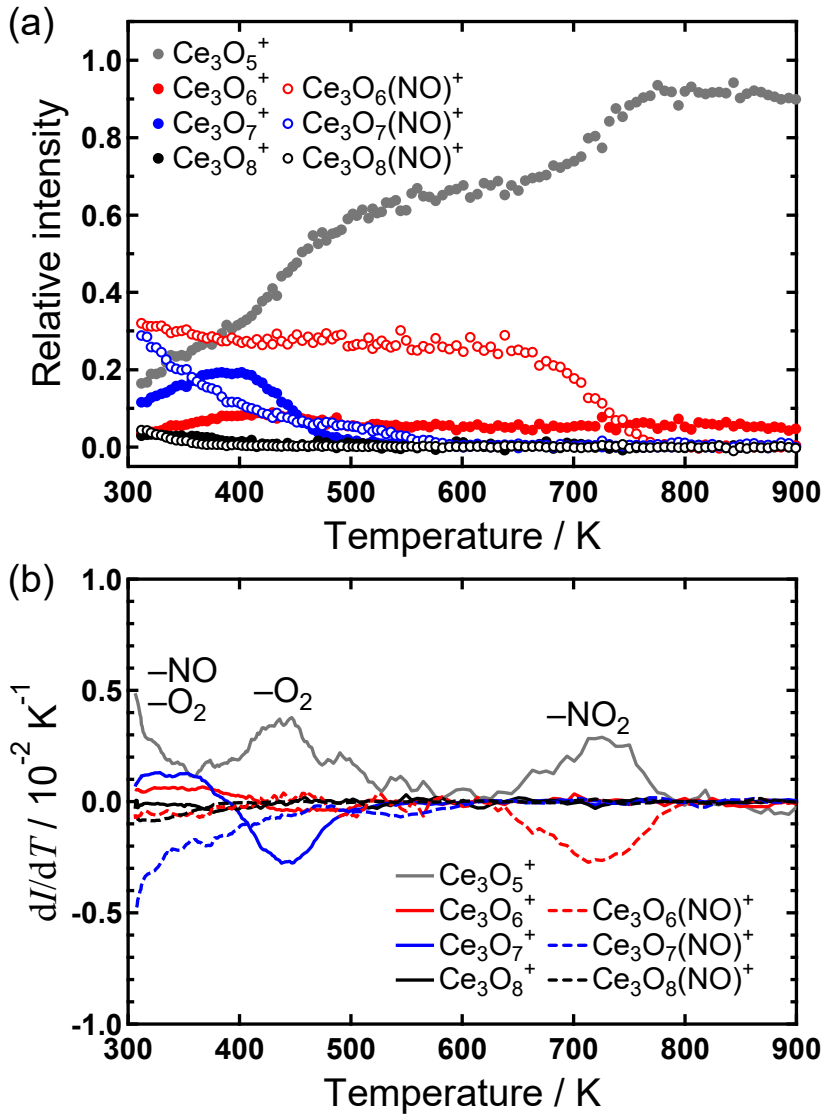

Figure 4.3. (a) Relative intensities of $Ce_3O_{5-8}(NO)_{0,1}^+$ cluster ions during TPD. (b) Differential of relative intensities of $Ce_3O_{5-8}(NO)_{0,1}^+$ cluster ions by temperature.

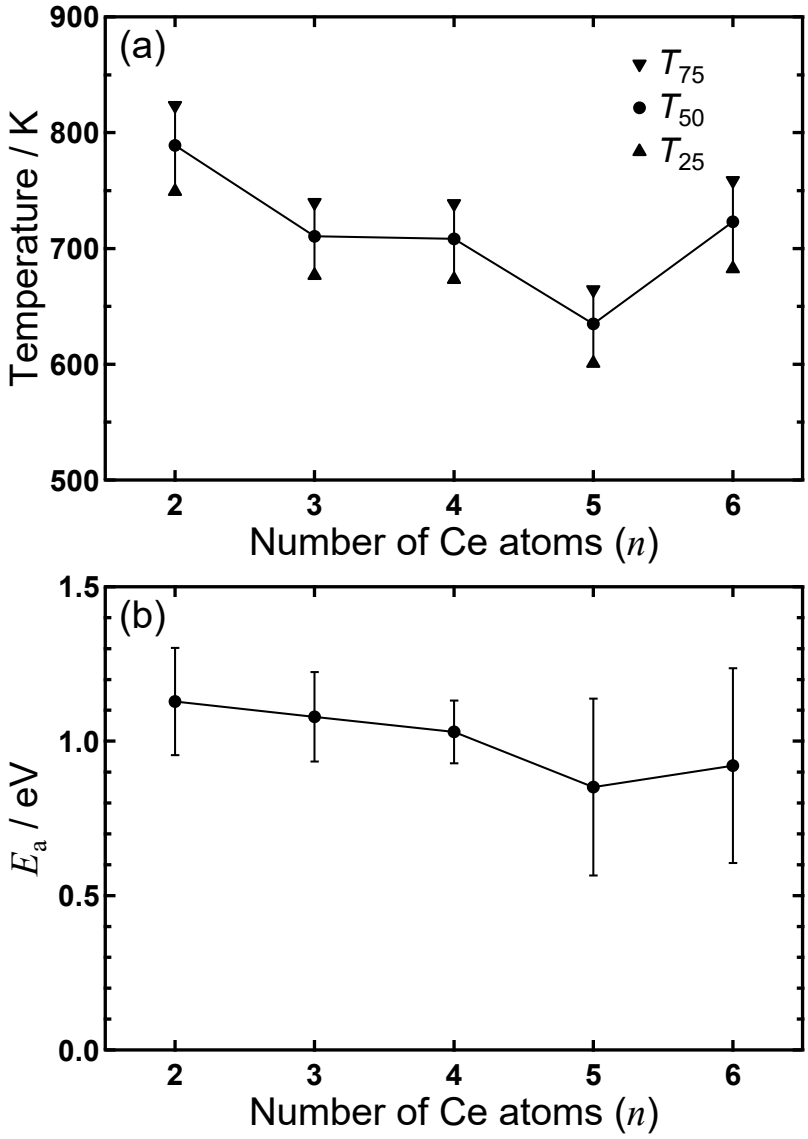

Figure 4.4. (a) Temperature and (b) activation energy for NO_2 release, $Ce_nO_{2n}(NO)^+ \rightarrow Ce_nO_{2n-1}^+ + NO_2$, as a function of cluster size, n. T_{25}, T_{50}, and T_{75} are the temperatures at which 25%, 50%, and 75% of $Ce_nO_{2n}(NO)^+$ had released NO_2, respectively.

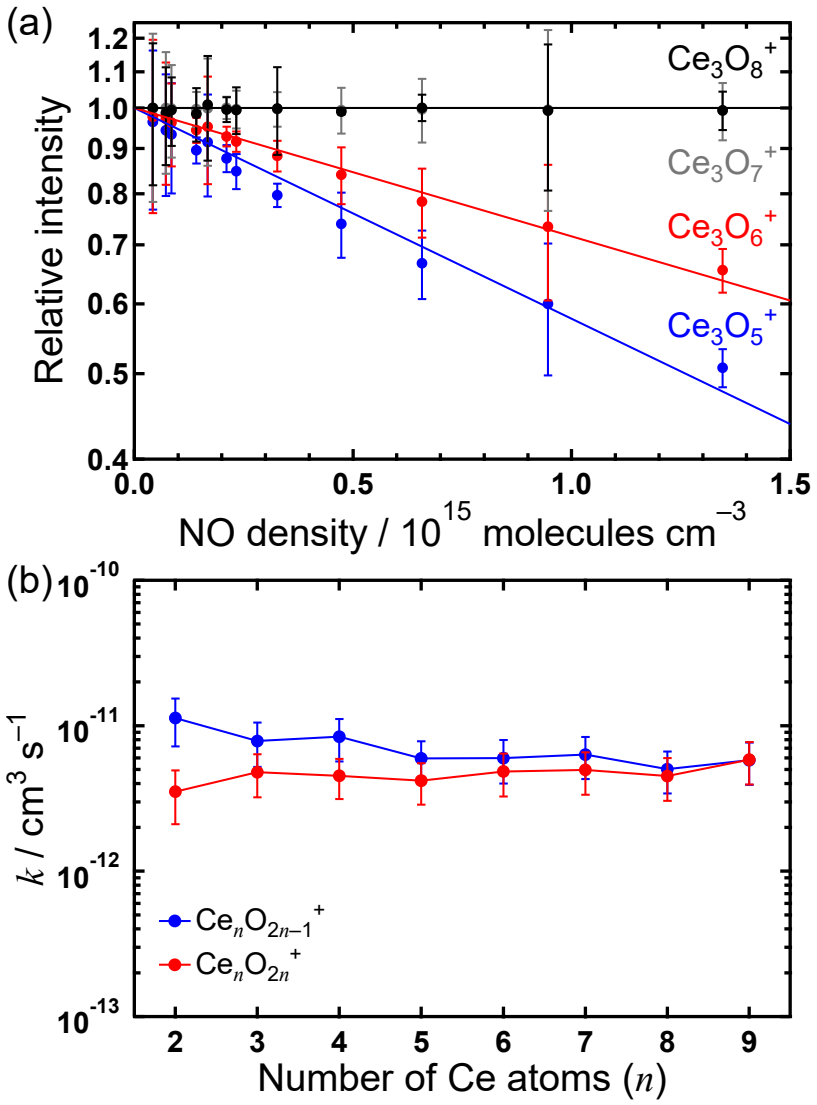

Figure 4.5. (a) Semi-logarithmic plot of relative intensities of $Ce_3O_{5-8}^+$ after exposure to NO_2 in a reaction gas cell as a function of the concentration of NO_2. (b) Rate constants for NO_2 adsorption, $Ce_nO_{2n+x}^+ + NO_2 \rightarrow Ce_nO_{2n+x}(NO_2)^+$, for $x = -1$ and 0 as a function of the cluster size, n.

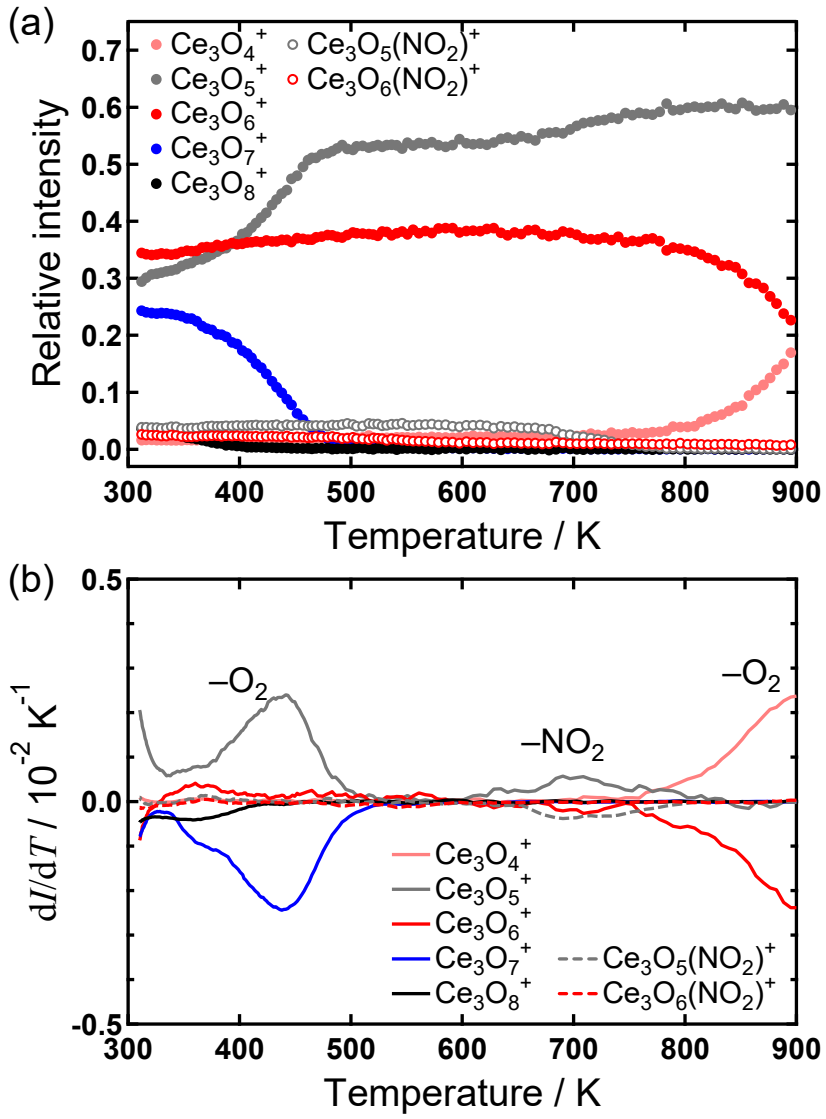

Figure 4.6. (a) Relative intensities of $Ce_3O_{4-8}(NO_2)_{0,1}^+$ cluster ions during TPD. (b) Differential of relative intensities of $Ce_3O_{4-8}(NO_2)_{0,1}^+$ cluster ions by temperature.

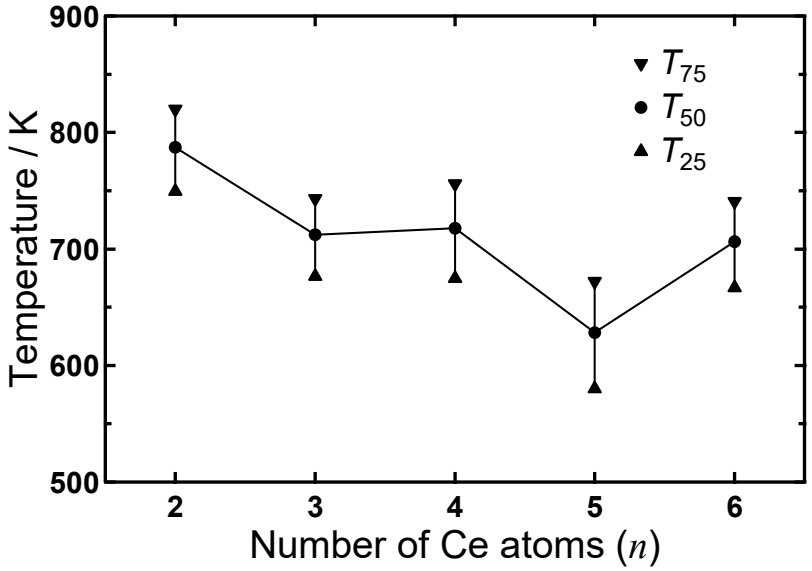

Figure 4.7. Temperature for the NO_2 release, $Ce_nO_{2n-1}(NO_2)^+ \rightarrow Ce_nO_{2n-1}^+ + NO_2$, as a function of the cluster size, n. T_{25}, T_{50}, and T_{75} are the temperature at which 25%, 50%, and 75% of $Ce_nO_{2n-1}(NO_2)^+$ had released NO_2, respectively.

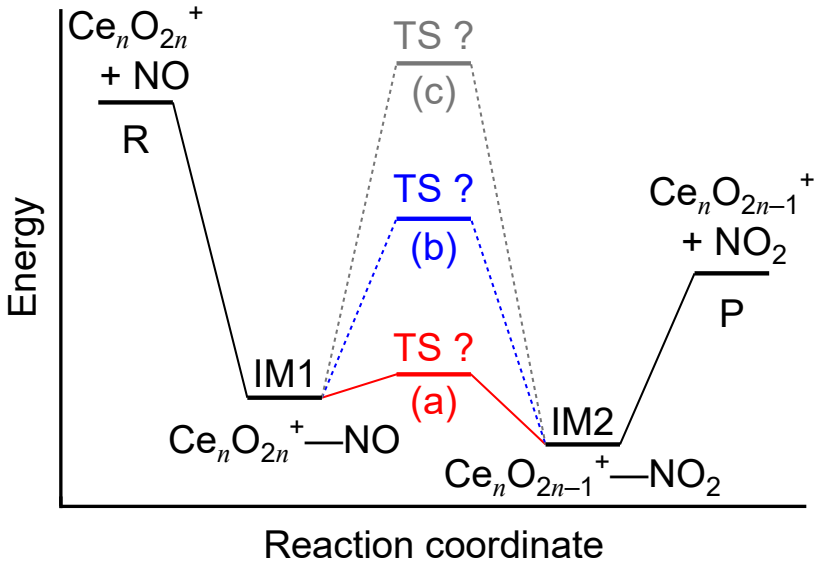

Figure 4.8. Schematic diagram of a possible reaction pathway of NO oxidation by a $Ce_nO_{2n}^+$ cluster. R, P, IM, and TS are the reactant, product, intermediate, and transition state, respectively.

Chapter 5

Conclusion

5.1. Summary of this thesis

In this thesis, I investigated the stability and redox reactivity of cerium oxide cluster cations. The present studies were performed by using a time-of-flight mass spectrometer (TOF-MS) combined with a newly developed gas-phase temperature- programmed desorption (TPD) device.

Heating experiments revealed the stable stoichiometry of cerium oxide clusters to be $Ce_nO_{2n-1}^+$ and $Ce_nO_{2n}^+$ for each size, n, indicating that the stability is mainly determined by the valence rather than the structure of cerium oxide clusters. The gas-phase TPD measurement showed oxygen-rich species released O_2 molecules by heating. The activation energy of the O_2 release was successfully estimated based on a simple model, the Arrhenius equation. In addition, reactions with carbon monoxide molecules were examined. The stoichiometric cerium oxide clusters, $Ce_nO_{2n}^+$, oxidized CO to form CO_2 and $Ce_nO_{2n-1}^+$, and the reactivity was significantly size dependent: $Ce_5O_{10}^+$ showed a particular reactivity with CO. The size dependence is likely to originate from a structural factor. Further investigations including computational studies are required to reveal it.

Reactivity of oxygen-deficient cerium oxide clusters was also investigated. They extracted oxygen atoms from reactants because the oxygen affinities of the oxygen-deficient clusters were large enough. Oxygen-deficient species, $Ce_nO_{2n-2}^+$, were able to be generated from stoichiometric cerium oxide clusters, $Ce_nO_{2n}^+$, by heating over 800 K. Combining the results that the oxygen-rich and stoichiometric cerium oxide clusters lost oxygen by heating and the oxygen-deficient ones extracted oxygen from other molecules, it can be concluded that the oxygen storage capacity (OSC) of cerium oxide surely works even in the small clusters.

In addition, I investigated a detailed mechanism of a redox reaction, the oxidation of nitric oxide by $Ce_nO_{2n}^+$ clusters. Using the thermalized condition, I succeeded in trapping and

analyzing the reaction intermediates. Based on the experimental data, I suggested a reaction energy diagram of the NO oxidation. Generally, such energy diagrams have been suggested based on theoretical studies. Therefore, the experimental approach presented in this thesis is important.

Throughout the present thesis, I have investigated the redox behavior of cerium oxide clusters from several aspects. I believe that these results provide useful insights into the redox reactions of cerium oxide clusters, which are a model system for ceria-based catalysts.

5.2. Perspectives

In this thesis, I have investigated the chemical properties of cerium oxide clusters. A next stage of the study is how to modify the properties of clusters as desired. One strategy is combining another element to cerium oxide clusters. As mentioned previously, cerium oxide is widely used as a supporting material of catalysts. Hence, composite clusters of cerium oxide with other components are a natural extension of investigations on cerium oxide clusters (see Figure 5.1). The group which I belong to has a technique to generate such composite clusters by a dual or triple laser ablation method.[1-3] One of the candidate for the combined component is a precious metal element. Precious metals are used in practical catalysts as active centers, thus they are expected to affect reactivity of clusters. Indeed, some reports suggested the role of precious metal atoms supported on cerium oxide clusters. For instance, a computational study on $Pt_8Ce_{21}O_{42}$ and $Pt_8Ce_{40}O_{80}$ clusters predicted an oxygen spillover phenomenon, in which one oxygen atom is transferred from the cerium oxide moiety to the platinum aggregation.[4] As another example, $AuCeO_2^+$ cluster cation was reported to activate H_2 based on an experimental and computational study.[5] In spite of such high interest, investigations of the metal-ceria composite clusters are currently limited. According to my preliminary results, gold atoms supported on cerium oxide clusters much affect the stable stoichiometry and reactivity of the clusters. The methodology presented in this thesis is believed to be applicable and useful to investigations on such complex systems.

5.3. References

(1) Miyajima, K.; Himeno, H.; Yamada, A.; Yamamoto, H.; Mafuné, F. Nanoalloy Formation of Ta-Containing Trimetallic Small Clusters. *J. Phys. Chem. A* **2011**, *115*, 1516-1520.

(2) Himeno, H.; Miyajima, K.; Yasuike, T.; Mafuné, F. Gas Phase Synthesis of Au Clusters

Deposited on Titanium Oxide Clusters and their Reactivity with CO Molecules. *J. Phys. Chem. A* **2011**, *115*, 11479-11485.

(3) Miyajima, K.; Sobhan, M. A.; Hardy, R. A.; Metha, G. F.; Mafuné, F. Structural Rearrangement in Gas Phase Niobium Carbide Clusters, Nb_nC_3 and Nb_nC_6. *Chem. Phys. Lett.* **2015**, *634*, 261-265.

(4) Vayssilov, G. N.; Migani, A.; Neyman, K. Density Functional Modeling of the Interactions of Platinum Clusters with CeO_2 Nanoparticles of Different Size. *J. Phys. Chem. C* **2011**, *115*, 16081-16086.

(5) Meng, J.; He, S. Thermal Dihydrogen Activation by a Closed-Shell $AuCeO_2^+$ Cluster. *J. Phys. Chem. Lett.* **2014**, *5*, 3890-3894.

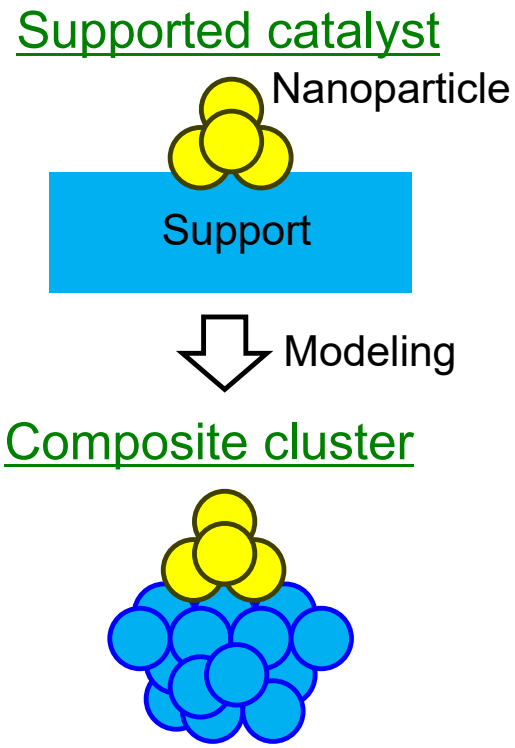

Figure 5.1. Concept of modeling a supported catalyst by a composite cluster.

Acknowledgements

The present thesis is the summary of my work from 2013 to 2015 at Professor Fumitaka Mafuné's group, Department of Basic Science, Graduate School of Arts and Sciences, the University of Tokyo.

I would like to express my deepest appreciation to Professor Fumitaka Mafuné. He has been guiding, supporting, and encouraging my studies continuously during my doctoral course. Thanks to him, I have accomplished this thesis, and I feel that I have grown up as a researcher and a human in the three-year course. I am really pleased to join his group.

I would particularly like to thank Dr. Ken Miyajima. He made a great contribution to the experiments and data analysis in my investigation. Without his support, this thesis would not have been possible. He also gave much valuable suggestions and ideas on my studies.

I have greatly benefited by discussions with Prof. Gregory F. Metha and Mr. Robert Allan Hardy in the University of Adelaide, Australia. The results presented in Chapter 3 are a part of the fruits of a collaborated study with them.

I am grateful to Dr. Philippe Dugourd, Prof. Driss Rayane, Mr. Marin Vojkovic, and the members of Dr. Dugourd's group in Université Lyon 1, France. I stayed their laboratory for one month in my doctoral course. I had learned a lot there.

I would like to thank the members of Prof. Mafuné's group: Dr. Satoshi Kudoh, Mr. Kohei Koyama, Mr. Masato Takenouchi, Ms. Yuki Tawaraya, Mr. Hodaka Kurokawa, Mr. Eima Yoshinouchi, and Ms. Naoko Suzuki. I am also grateful to the former members of that group: Dr. Michał Piotr Kwiatkowski, Dr. Rumi Levi, Mr. Keisuke Morita, Mr. Daisuke Shigeta, and Mr. Yusuke Kobayashi. They are good co-workers, and my life in the university has been supported by them.

I would like to express my gratitude to Prof. Shin-ichi Ohkoshi and the members of his group in Department of Chemistry, School of Science, the University of Tokyo. I completed my bachelor and master courses in Prof. Ohkoshi's group. I owe what I am to their supports.

Lastly, I am grateful to my family and my friends for their hearty support and encouragement.

Tokyo, Japan, December 2015

Toshiaki Nagata